2015

Impacts of Urban Areas on Vegetation Development Along Rural-Urban Gradients in the Upper Midwest: 2003-2012

Cole Krehbiel
South Dakota State University, cole.krehbiel@jacks.sdstate.edu

IMPACTS OF URBAN AREAS ON VEGETATION DEVELOPMENT ALONG RURAL-URBAN GRADIENTS IN THE UPPER MIDWEST: 2003-2012

BY

COLE KREHBIEL

A thesis submitted in partial fulfillment of the requirements for the

Master of Science

Major in Geography

South Dakota State University

2015

IMPACTS OF URBAN AREAS ON VEGETATION DEVELOPMENT ALONG RURAL-URBAN GRADIENTS IN THE UPPER MIDWEST: 2003-2012

This thesis is approved as a creditable and independent investigation by a candidate for the Master of Science in Geography degree and is acceptable for meeting the thesis requirements for this degree. Acceptance of this does not imply that the conclusions reached by the candidate are necessarily the conclusions of the major department.

Xiaoyang Zhang, Ph.D.
Major Advisor Date

Geoffrey Henebry, Ph.D.
Thesis Advisor Date

George White, Ph.D.
Head, Department of Geography Date

Dean, Graduate School Date

ACKNOWLEDGEMENTS

I would like to thank my thesis advisor, Dr. Geoffrey Henebry, for patiently guiding an undergraduate who had never heard of remote sensing through the scientific research process to become a published remote sensing scientist. Thank you to my undergraduate advisor, Dr. Bob Watrel, for helping me through my Bachelor's degree and encouraging me to do undergraduate research. I would like to acknowledge Dr. Trisha Jackson for her early guidance in my graduate studies and thesis proposal, and to my current major advisor Dr. Xiaoyang Zhang for "adopting" me during the difficult thesis writing and revising period. To the faculty of the Geography department: thank you for providing me with the geographical perspective, tools, and expertise necessary for geospatial research.

I am indebted to my family and friends for their support while pursuing my degree. To my parents, Cindy and Randy, whose love and support has enabled me to pursue higher education. My parents encouraged me to follow my passion as a geographer and demonstrated the invaluable virtue of hard work, and to them I am forever grateful. I am likewise thankful for my older brother and sister. To all of my friends, thank you for always being by my side when the stresses of graduate school were weighing me down.

I would like to thank the SDSU Honors College for kick starting my research career through an undergraduate research grant. Thank you to the South Dakota Space Grant Consortium and the NASA Interdisciplinary Research in Earth Science program (grant #NNX12AM89G to Dr. Geoffrey Henebry) for funding my research endeavors, to the Geospatial Sciences Center of Excellence for equipping me with the resources necessary to undertake this project, and of course to SDSU for proving that a kid from South Dakota really can go anywhere from here. Go Jacks!

CONTENTS

LIST OF FIGURES

LIST OF TABLES

ABBREVIATIONS

AGDD	Accumulated Growing Degree-Days
AVHRR	Advanced Very High Resolution Radiometer
CONUS	Conterminous United States
CxQ LSP	Convex Quadratic Model of Land Surface Phenology
DGS_{AGDD}	Duration of Growing Season in Accumulated Growing Degree-Days
DOY	Day of Year
EOS	End of Season
ETM+	Enhanced Thematic Mapper Plus
GCA	Green Core Area
GDD	Growing Degree-Days
Half-TTP_{NDVI}	NDVI at half Thermal Time to Peak
IDL	Interactive Data Language
ISA	Impervious Surface Area
LCT	Land Cover Type
LSP	Land Surface Phenology
NDVI	Normalized Difference Vegetation Index
LST	Land Surface Temperature
MODIS	Moderate Resolution Imaging Spectroradiometer
NASA	National Aeronautics and Space Administration
NLCD	National Land Cover Database
PH_{NDVI}	Peak Height in NDVI
SD	Scientific Dataset
SOS	Start of Season

ABSTRACT

IMPACTS OF URBAN AREAS ON VEGETATION DEVELOPMENT ALONG RURAL-URBAN GRADIENTS IN THE UPPER MIDWEST: 2003-2012

COLE KREHBIEL

2015

Between one-third and one-half of Earth's land surface has been directly altered by humans, with the remainder comprised of "human-dominated ecosystems" (Vitousek et al. 2008). Earth's population has surpassed seven billion, projected to increase by 2.5 billion by 2050 in urban areas alone (United Nations 2014). The rapid urbanization of our planet drives global environmental changes in hydrosystems, biodiversity, biogeochemical cycles, land use and land cover, and climate (Grimm et al. 2008). Urban areas alter local atmospheric conditions by modifying surface albedo and consequently evapotranspiration, releasing energy through anthropogenic heat sources, and increasing atmospheric aerosols, leading to increased temperatures in cities compared with surrounding rural areas, known as the "urban heat island" effect (Arnfield 2003). Recent urbanization of our planet has generated calls for remote sensing research related to the impacts of urban areas and urbanization on the natural environment (Herold 2009; Seto, Güneralp, and Hutyra 2012). Spatially extensive, high spatial resolution data products are needed to capture phenological patterns in regions with heterogeneous land cover and external drivers such as cities, which are comprised of a mixture of land cover/land uses and experience microclimatic influences, namely the UHI effect (Fisher, Mustard, and Vadeboncoeur 2006; Melaas, Friedl, and Zhu 2013). Here I use the normalized difference vegetation index (NDVI) product provided by the Web-Enabled Landsat Data (WELD) project to analyze the impacts of urban areas and urban heat islands on the

seasonal development of the vegetated land surface on an urban-rural gradient for six regions located in the Upper Midwest of the United States. I fit NDVI observations from 2003-2012 as a convex quadratic function of thermal time as accumulated growing degree-days (AGDD) calculated from the Moderate-resolution Imaging Spectroradiometer (MODIS) land surface temperature product to model decadal land surface phenology metrics. In general, duration of growing season measured in AGDD in green core areas is equivalent to duration of growing season in urban extent areas, but significantly longer than duration of growing season in regions outside of the urban extent. I found an exponential relationship in the difference of duration of growing season between urban and surrounding rural regions as a function of distance from urban core areas in perennial vegetation land cover types, with an average magnitude of 669 AGDD and the influence of urban areas extending over 11 km from urban core areas. A linear relationship exists between the modeled rate of vegetation green up and maximum NDVI for perennial forests, but not for annual croplands. At the regional scale, relative change in duration of growing season does not appear to be significantly related to total area of urban extent, population, or latitude, with the distance and magnitude that urban areas influence vegetation in and near cities being relatively uniform, although larger urban areas have a greater impact on duration of growing season in terms of total area.

Keywords: *land surface phenology, land surface temperature, MODIS, NDVI, remote sensing, Upper Midwest, urbanization, urban environmental change, urban heat island, Web-Enabled Landsat Data*

INTRODUCTION

Humans have altered and modified Earth's surface for thousands of years, beginning with the use of fire, speech, and tools, which led to the development of agriculture and consequently large concentrations of people living together (Sauer 1956; Childe 1950). Beginning around 300 years ago, humans entered a new era, characterized by large increases in population and the harnessing of fossil fuels for energy, leading to unprecedented rates of earth surface transformation and subsequent environmental change (Kates, Turner II, and Clark 1990). Recent increases in population have largely been concentrated in urban areas, with global urban areas increasing from only 13% of total global population in 1900 to 54% by 2014 (United Nations 2006; United Nations 2014). Urban areas alter local climatic conditions by modifying surface albedo and consequently evapotranspiration, releasing energy through anthropogenic heat sources including building materials, and increasing atmospheric aerosols, leading to increased temperatures in cities compared with surrounding rural areas, a phenomenon known as the "urban heat island" (UHI) effect (Arnfield 2003). Future climate change and urbanization is projected to increase UHI temperatures by around 1 °C per decade (Voogt 2002). The combination of urban population growth, urbanization, and climate change warrants the need for enhanced remote sensing research on the environmental impacts of urban areas and urbanization on the natural environment (Herold 2009; Seto, Güneralp, and Hutyra 2012). Specifically, there have been calls for urban remote sensing research of small to medium sized cities and their associated impacts on vegetation (Seto and Christensen 2013).

In this study, I analyze the impacts of urban areas and UHIs on the seasonal development of vegetation on an urban-rural gradient at the local to regional scale for six regions encompassing 19 small to medium sized cities located in the Upper Midwest region of the United States. I use satellite remote sensing time series data to investigate the impacts of urban areas on the seasonal development of vegetation using model-derived land surface phenology (LSP) metrics. I explore the spatial arrangement of urban areas in order to understand the influence of regions of highly concentrated impervious surfaces and large areas of urban vegetation on microclimatic conditions within cities. I analyze the distance and magnitude of urban alteration of local atmospheric conditions in and around cities. I compare the results from all 19 cities in order to analyze the influences of city size, land cover, spatial arrangement, and latitude on the seasonal development of vegetation.

Problem Identification and Description

There is no doubt that humans modify Earth's terrestrial surface. But what are the consequences of man-made alteration of our planet? In the 19th century, scientists were hypothesizing that human modification of the Earth altered temperature and atmospheric humidity based on direct observation (Marsh 1864). In 1833, Luke Howard provided evidence that cities experienced higher temperatures than the surrounding rural areas (Howard 1833). By the 20th century, questions related to the understanding of human disturbance, displacement, and domination of organic ecosystems—including how urban areas alter Earth's atmosphere—were being developed (Sauer 1956). Around the mid-20th century, humanity entered the "Great Acceleration", characterized by rapid increases in global population, consumption, scientific knowledge, and technological advances

(Costanza et al. 2007). It is estimated that between one-third to one-half of Earth's land surface has been directly altered by humans during the "Great Acceleration", with the remaining regions of our planet being classified as "human-dominated ecosystems" (Vitousek et al. 2008).

One major driver of Earth's "Great Acceleration" is global urban population growth. In 1950, global urban population was 746 million, accounting for 30% of Earth's total population. By 2014, global urban population increased to 3.9 billion, with over half of global population residing in urban areas. Future projections estimate that Earth will add an additional 2.5 billion urban inhabitants by 2050, 66% of total global population (United Nations 2014). From 1970 to 2000, global urban land area increased by 58,000 km^2, projected to increase by 1,527,000 km^2 by 2030 (Seto et al. 2011). Although global urban land cover extent is estimated to cover 0.24–2.74% of total global land area (Schneider, Friedl, and Potere 2009), the impacts of urban areas likely encompass a larger area, with one study finding the ecological footprint of urban areas to extend 10 km from urban land cover, impacting an area 2.4 times greater than urban land cover extent alone (Zhang et al. 2004a).

Consequences and Implications of the Problem

A recent study found four major urban land teleconnections that linked various land cover conversions to changes in urban consumption (Seto et al. 2012). Most relevant to my research is the teleconnection between increases in urban population leading to land cover conversion for residential development (Seto et al. 2012). Gross Domestic Product and other economic factors also drive urban land expansion (Bettencourt et al. 2007; Bettencourt 2013; Seto et al. 2011). Global increases in urban population and economic

output will inevitably lead to future urban land expansion. The rapid urbanization of our planet drives global environmental changes in hydrosystems, biodiversity, biogeochemical cycles, land cover/land use, and climate (Grimm et al. 2008). Urban land expansion has irreversible impacts on the natural environment, including the loss of agricultural lands, fragmentation of ecosystems, reduction of biodiversity, and alteration of local climate (Seto et al. 2011). Urban land cover/land use and change can potentially alter local to regional climate on daily, seasonal, and even annual scales (Seto 2009). Possibly the clearest example of urban climate modification is the phenomenon where urban temperatures are generally higher than the surrounding countryside, or the UHI effect (Oke 1987). UHI intensity is related to patterns of land use/land cover changes, including the composition of water, vegetation, and built-up areas (Chen et al. 2006). The effects of the UHI and land use/land cover change are linked to modified surfaces that affect the transfer and storage of airflow, water, and heat (Hartmann et al. 2013).

UHI-related impacts on vegetation ultimately have consequences for humans. Global climate models project that future climate change and urbanization will increase the UHI effects by as much as 30% with a doubling of atmospheric CO_2 (McCarthy, Best, and Betts 2010). Released in 2013, the Intergovernmental Panel on Climate Change report (AR-5) concluded with medium confidence that the duration and frequency of heat waves has increased since 1950 (Hartmann et al. 2013). The IPCC report from Working Group II concluded with "very high confidence" that projected climate change will exacerbate health problems, including a greater chance of disease, injury, or death related to more intense heat waves (IPCC 2014). UHIs are linked to grave health-related consequences for humans, including decreased quality of living conditions and increased heat-related

injuries and mortality (Changnon, Kunkel, and Reinke 1996; Patz et al. 2005). It is estimated that anthropogenic atmospheric carbon dioxide concentrations have doubled the risk of heat waves occurring in Europe (Stott et al. 2004). The internationally recognized European Heat Wave of 2003 was linked to over 70,000 deaths (Robine et al. 2008). In the U.S., heat waves are the highest cause of human mortality related to weather (Changnon, Kunkel, and Reinke 1996). The human-environment interaction of UHI-related impacts on vegetation comes full circle when we consider UHI mitigation strategies, including the widely researched idea of increasing vegetation cover, or "urban greening", within cities in order to ameliorate the UHI effect (Bowler et al. 2010).

The Knowledge Gap

Despite (1) the recent and ongoing urbanization of our planet, (2) the likelihood that UHI-related heat waves are increasing, (3) the known negative health impacts on humans, and (4) studies linking urbanization and climate change to increased UHI intensity, current climatological and meteorological models do an inadequate job of predicting the influence of urban areas on atmospheric conditions (Best 2006). The majority of global climate models that are used for climate change assessment do not include urban surfaces, and there have been calls for more accurate information of urban areas for weather forecasting (Best 2006). More recently, the first international urban land surface model comparison project aimed to identify the processes, complexity, and parameters necessary to improve urban land surface models (Best and Grimmond 2014). In the comparison, models that included a representation of urban vegetation performed better than models that did not include vegetation (Best and Grimmond 2014). Moreover, the project found that representation of vegetation was the most critical process in the

accuracy of urban land surface model behavior related to seasonality (Best and Grimmond 2013). The project concluded that in order to understand the impacts of urban vegetation, research on the seasonality of vegetation is needed (Best and Grimmond 2013). One reason why urban vegetation is excluded from urban land surface models is related to the spatially heterogeneous nature of the urban land surface, comprised of a mixture of impervious and vegetated land covers.

Urban land surface phenology observes the seasonal development of vegetation in and nearby cities. The majority of urban land surface phenology studies have used surface observation networks (Schwartz, Betancourt, and Weltzin 2012) or coarse spatial but high temporal resolution satellite data from sensors including the Advanced Very High Resolution Radiometer (AVHRR) (White et al. 2002) and more recently, the Moderate Resolution Imaging Spectroradiometer (MODIS) (Zhang et al. 2004a; Zhang et al. 2004b; Walker, de Beurs, and Henebry 2015). Surface observation networks and high temporal/coarse spatial resolution remote sensing studies are useful. However, spatially extensive, higher spatial resolution data products are needed to capture phenological patterns in areas with heterogeneous land cover and external drivers such as urban areas, which are a mixture of land cover/land uses that result in distinct microclimates, via the UHI effect (Fisher, Mustard, and Vadeboncoeur 2006; Melaas, Friedl, and Zhu 2013). Using Landsat data for phenology studies allows for local to regional scale analyses, offering a spatial resolution that is useful for exploring factors that influence phenology including land use and urban heat islands (Melaas, Friedl, and Zhu 2013).

My research project addresses this knowledge gap by analyzing the impacts of urban areas and subsequent UHIs on the seasonal development of vegetation in and around

cities on a local to regional scale using spatially extensive, high spatial resolution data, leveraged over a decade of observations to alleviate problems associated with coarse temporal resolution. This project provides much needed and currently lacking information on (1) the differences in the seasonal development of vegetation between urban and rural areas of the Upper Midwest, (2) the magnitude and extent of UHI effects on the seasonal development of vegetation in small to medium sized cities, and (3) the differences in land surface phenology between annual croplands and perennial urban vegetation. More importantly, this project provides a procedural framework to deal with the difficult issue of spatial heterogeneity of the urban land surface as well as differences in local land surface phenology arising from microclimatic factors. This information can be used to inform a variety of interests, including scientists interested in performing urban land surface phenology analyses in other regions as well as urban land surface modelers, urban ecologists, urban policy-makers, city planners and developers, meteorologists, and climatologists.

LITERATURE REVIEW

Human Environment Interactions

During the Paleolithic period, fire, speech, and tools led to human modification and alteration of Earth's land surface at local to regional scales (Sauer 1956). Humans began developing agriculture during the Neolithic period approximately 10,000 years ago, leading to large increases of people living in permanent settlements, known as the urban revolution (Childe 1950). By the 19th century, scientists hypothesized that human alteration of the planet was changing local temperature and atmospheric humidity based on empirical observation (Marsh 1864). In the 20th century, scientists knew that humans were disturbing, displacing, and dominating Earth's various ecosystems, and began to question how urban areas altered Earth's atmosphere (Sauer 1956). Today, we know that the rapid urbanization of our planet is driving global environmental changes in hydrosystems, biodiversity, biogeochemical cycles, land use and land cover, and climate (Grimm et al. 2008). Urban land cover/land use and change can potentially alter local to regional climate on daily, seasonal, and even annual scales (Seto 2009). Urbanization has been linked to increased intensity of the urban heat island effect (Lo and Quattrochi 2003; Chen et al. 2006).

Urban Heat Islands

In early 19th century England, Luke Howard observed that London experienced higher temperatures than the surrounding countryside (Howard 1833). The "urban effect" was described as a "heat island" in the 1940's, leading to the term "urban heat island" (Balchin and Pye 1947). The urban heat island (UHI) effect is the phenomenon where urban areas exhibit generally higher temperatures than in neighboring rural areas (Oke 1987). The UHI effect results from urban/rural differences in the surface energy budget

(Oke 1982; Arnfield 2003). During the daytime, impervious surfaces in densely built up areas of cities absorb more incoming solar radiation than areas of dense green vegetation in rural areas. Building materials have higher heat storage capacity than vegetation and re-radiate part of that stored energy at night in the form of longwave thermal infrared radiation. Impervious surfaces are drier than vegetation resulting in more net radiation being converted to sensible heat flux (heating of the air) than to latent heat flux (evapotranspiration) (Avissar 1996; Arnfield 2003; Patz et al. 2005). The geometry of the urban canopy (street canyons with limited skyview) decreases outgoing longwave radiation and increases its re-absorption in nearby buildings (Oke 1982; Oke et al. 1991). The radiative, thermal, moisture, and aerodynamic characteristics of various urban surfaces also influence the spatial, temporal, and intensity patterns of the UHI (Oke 1982; Jackson et al. 2010). Anthropogenic heat sources in cities (HVAC, vehicles, industry, lighting) also contribute to the UHI effect (Oke 1982).

Calculations of UHI intensity consider the difference between urban maximum temperature and the corresponding background rural temperature (Oke 1987). Under stable conditions, the UHI is more pronounced during the overnight hours due to reduced cooling rates from late afternoon into the evening, and may even be negative around midday, resulting in the urban center being cooler than the surrounding landscape (Oke 1987). The increased heat stored during the day from urban surfaces is released into the urban environment at night, leading to warmer overnight minimum temperatures in cities (Oke 1987). Consequently, the diel (24 hour) temperature range is smaller in urban areas than surrounding rural areas (Oke 1982). Seasonally, the UHI is weakest in summer and strongest in autumn and winter (Kim and Baik 2002). UHI studies have also found that

cities can act as both heat and moisture islands during the overnight hours (Deosthali 2000).

Studies of Urban Heat Islands

Early studies of the UHI used stationary in-situ temperature measurements from weather instruments at meteorological stations (Howard 1833; Balchin and Pye 1947). In the 1960's and 1970's, UHI studies began combining weather station network measurements with mobile temperature measurement readings using automobiles and aircraft (Bornstein 1968, Kopec 1970, Chandler 1976, Landsberg 1981, Oke 1982). The advent of satellite data in the 1970's gave rise to the use of satellite-derived surface temperature data for UHI research beginning with a study that used thermal infrared data to identify urban areas (Rao 1972). Roth, Oke, and Emery (1989) described the difference between air temperature studies of UHIs and satellite remote sensing-based studies of *surface* urban heat islands (SUHIs), finding that SUHI intensity is related to land cover/land use and intensity is greater during the daytime compared to at night (Roth, Oke, and Emery 1989). A study in 1993 evaluated the relationships between (1) NDVI and (2) surface temperature to the UHI effect using data from the National Oceanic and Atmospheric Administration's (NOAA) AVHRR satellite (Gallo et al. 1993). A 1995 review of the use of satellite data for UHI assessment found that remotely sensed data provides an objective method for analyzing UHIs (Gallo et al. 1995). More recently, studies have used land surface temperature (LST) data provided by MODIS to monitor the UHI (Streutker 2003; Imhoff et al. 2010; Tomlinson et al. 2012; Hu and Brunsell 2013).

In summary, studies of the UHI generally use air temperature data from in situ weather station measurements or LST derived from satellite remote sensing instruments.

Streutker (2003) explains that in situ air temperature observations have higher temporal resolution spanning a longer record, but suffer from poor spatial coverage. In contrast, satellite data have better spatial distribution however lower temporal resolution and a much shorter period of observation (Streutker 2003).

Impacts of UHIs on Vegetation Phenology

Early studies analyzing the impacts of urban areas on vegetation focused on observations of phenology, or the biological cycle of living organisms. Notably, urban areas impact plant phenology via the UHI effect. The UHI effect has been attributed to earlier budding and blooming of flowers and trees in the city and generally longer growing seasons (Oke 1987). There are two main approaches to collecting phenological observations, including observation networks (Schwartz, Betancourt, and Weltzin 2012) and coarse spatial but high temporal resolution satellite data from sensors such as AVHRR (White et al. 2002) and MODIS (Zhang et al. 2004a; Zhang et al. 2004b; Walker, de Beurs, and Henebry 2015). Jochner et al. (2012) provide an overview of observational studies from European, North American, and Asian cities that all found earlier vegetation development in urban areas (Jochner et al. 2012), beginning with a study in Hamburg, Germany in 1955 (Franken 1955). Additional studies have used species composition (Gödde and Wittig 1983) and plant specific phenology (Bechtel and Schmidt 2011) in order to characterize the influence of UHIs on vegetation development in cities.

Land Surface Phenology and the Normalized Difference Vegetation Index

Studies have also used satellite data to study the UHI effects on land surface phenology in urban and surrounding rural areas. Land surface phenology (LSP) is defined

as the spatio-temporal development of the vegetated land surface as revealed by satellite sensors (de Beurs and Henebry 2004). LSP metrics are often calculated from time series data of vegetation indices (de Beurs and Henebry 2010). There are four main methods used to calculate LSP metrics, including (1) thresholds, (2) derivatives, (3) smoothing functions, and (4) fitting models (de Beurs and Henebry 2010). I use a convex quadratic regression model that describes the normalized difference vegetation index (NDVI) as a function of accumulated growing degree-days (AGDD), which has been used successfully in the past to analyze LSP dynamics in temperate regions (de Beurs and Henebry 2004; Walker, de Beurs, and Henebry 2015). This linear model requires estimation of only three model parameter coefficients that admit relevant ecological interpretation (de Beurs and Henebry 2005). The significance of the model is dictated by its ability to explain the temporal variation of NDVI, summarized as the coefficient of determination, or R^2 (de Beurs and Henebry 2005).

The normalized difference vegetation index uses a band ratio of the difference between red and near-infrared reflectance divided by their sum (Tucker 1979). NDVI is used to capture vegetation "greenness" and is the most extensively used vegetation index in satellite remote sensing (Myneni et al. 1995). One limitation of NDVI is that loss of sensitivity occurs in densely vegetated areas (Wang, Liu, and Huete 2002, 979): moderate to high levels of leaf area index (LAI) lead to decreased NDVI sensitivity (Viña, Henebry, and Gitelson 2004). However, I use the NDVI as a *relative* measure of green vegetation during the growing season rather than an *absolute* measure of the biophysical properties of vegetation such as biomass or leaf area index.

UHI influence on Urban LSP Studies

One study found that, on average, urban areas expanded the growing season of vegetation by 7.6 days in the eastern United States using time series of the NDVI derived from AVHRR data (White et al. 2002). More recently, studies have used a combination of LST and Enhanced Vegetation Index (EVI) data time series derived from MODIS to analyze the effects of the UHI on vegetation phenology (Zhang et al. 2004a; Zhang et al. 2004b). Important findings from these studies include the following: the length of growing season for forests is strongly related to mean annual LST (Zhang et al. 2004a), earlier green-up and later dormancy occurs in urban areas (Zhang et al. 2004a; Zhang et al. 2004b), and urban climate influences on vegetation phenology extend up to 10 km beyond the urban land cover extent of cities in eastern North America (Zhang et al. 2004a). The UHI effects were found to be stronger in North America than in Asia or Europe (Zhang et al. 2004b). The ecological footprint of urban climates in 70 cities in eastern North America was found to be 2.4 times greater than the extent of urban land use, which was determined as the distance where 95% of asymptotic values were reached in the exponential model of differences in green-up onset and dormancy onset vs. distance from the urban perimeter (Zhang et al. 2004a). Here I use a similar method to calculate the difference in duration of growing season between urban and surrounding rural areas and determine the magnitude and extent of urban influence on the seasonal development of vegetation.

UHI influence on Urban LSP Studies using Landsat

While surface observation networks and high temporal/coarse spatial resolution remote sensing studies are useful, there exists a need for more spatially extensive, higher

spatial resolution data products to capture phenological patterns in areas with heterogeneous land cover and external drivers such as urban areas that are a mixture of land cover/land uses and experience microclimatic influences, namely the UHI effect (Fisher, Mustard, and Vadeboncoeur 2006; Melaas, Friedl, and Zhu 2013). Using Landsat data for phenology studies allows for local to regional scale analyses, offering a spatial resolution that is useful for exploring factors that influence phenology including land use and urban heat islands (Melaas, Friedl, and Zhu 2013). One study used Landsat 5 Thematic Mapper (TM) and Landsat 7 Enhanced Thematic Mapper Plus (ETM +) time series to model phenology in eastern United States deciduous forests and found a significant relationship between distance from urban core and green-up onset, suggesting that UHI impacts are reflected in the phenological characteristics of surrounding vegetation (Fisher, Mustard, and Vadeboncoeur 2006).

Knowledge Gap, Introduction to Study Area, and Data

To date, no Landsat-resolution studies have investigated UHI impacts on LSP in the Upper Midwest region of the United States. There are multiple reasons why the Upper Midwest is an ideal location for studying the impacts of urban areas on LSP within and surrounding cities. The region is a relatively flat, continental, temperate plain that is distant from confounding meteorological influences such as major mountain ranges or large water bodies. Cities in the region are relatively isolated and embedded in a vegetated landscape (Figure 1). The cities span size (area, population) and latitudinal gradients but precipitation is relatively uniform over the region.

The Web-Enabled Landsat Data (WELD) project generated 30 meter composited mosaics of Landsat 7 ETM+ SLC-off data over the Conterminous United States

(CONUS) from 2003-2012 (Roy et al. 2010). WELD was designed to provide consistent Landsat data to develop land cover, bio-physical, and geo-physical products in order to study Earth system science and regional land-cover dynamics (Roy et al. 2010). MODIS, or Moderate Resolution Imaging Spectroradiometer, is a scientific instrument aboard the Aqua and Terra satellites. Aqua and Terra are National Aeronautics and Space Administration (NASA) Earth Science satellites that operate as a part of the Earth Observing System. The MODIS-Aqua/Terra products used in this study (MYD11A2, MOD11A2) included level-3 global Land Surface Temperature and Emissivity 8-day data with 1 km spatial resolution, and are provided in Sinusoidal grid format as the mean clear-sky LST values during the 8-day time frame (NASA LP DAAC 2001). The National Land Cover Database (NLCD) provides 30 meter resolution land surface characteristics over the United States that can be used for applications including assessment of ecosystem health and ecosystem status (Homer, Fry, and Barnes 2012). The NLCD includes Percent Developed Imperviousness (ISA) (Xian et al. 2011) and Land Cover Type (LCT) (Jin et al. 2013) products from 2001, 2006, and 2011.

Literature Review Conclusion

Human alteration and modification of Earth's land surface is not a new phenomenon. Knowledge and observation of the impacts of human settlements on Earth's land surface and surrounding environment is not a recent discovery either. Scientists have observed urban microclimatic influences such as the UHI effect for nearly 200 years. The advent of remote sensing data from satellite instruments in the 1970's provided enhanced opportunities to study human-environment interactions such as the impacts of urban areas and UHIs on the seasonal development of vegetation. A multitude of research in the past

has been dedicated to this important topic. The combination of WELD-derived NDVI, MODIS LST-derived AGDD, and NLCD LCT and ISA data, all freely available, spanning at least a decade, at a spatial resolution that is appropriate for urban areas, provides an opportunity to investigate the UHI-related impacts on land surface phenology at the local to regional scale, over a region where no previous studies of UHI effects on LSP have been conducted at 30 meter spatial resolution.

FRAMING THE TOPIC WITHIN THE GEOGRAPHIC METHOD

Location of the problem and the study area

Urban areas are widespread across the planet. The top five countries with the greatest areal extent of urban land cover are the United States, China, The Russian Federation, Brazil, and India—with the U.S. accounting for 18.5% of total global urban land cover at the start of the 21st century (Angel et al. 2011). From 1970-2000, the highest rates of urban land expansion occurred in India, China, and Africa, however the greatest change in total urban extent was in North America (Seto et al. 2011). A global study of the Northern Hemisphere (35°N to 70°N) found the urban heat island-related influence on vegetation phenology to be stronger in North America than in Europe and Asia (Zhang et al. 2004b).

I have chosen to analyze remotely sensed vegetation dynamics at multiple scales: regionally for six selected regions in the Upper Midwest of the United States, and locally for 19 cities located within the six greater urban regions. My region of interest is between 47.5°N, 99°W and 40.5°N, 92°W (Figure 1). An early study of urban climate characterized the nature of UHIs under "ideal" conditions, described as a city situated on flat terrain with population greater than 100,000 and a temperate climate (Oke 1982). I chose the Upper Midwest and six greater urban regions for multiple reasons, including that (1) there are a number of useful, relatively high resolution (spatial & temporal) remote sensing datasets freely available for the CONUS (Roy et al. 2010; Xian et al. 2011; Jin et al. 2013), (2) the region is characterized as a temperate plain with relatively isolated urban areas situated within a largely vegetated landscape that experiences distinct annual seasonality, (3) five of the six regions contain at least one city with population > 100,000 and (4) the regions represent population, urban area, land cover

type, thermal regime and latitudinal gradients. Figure 2 demonstrates the southwest to northeast gradient in annual accumulated growing degree-days, a measure of thermal time that dictates perennial vegetation growing season length.

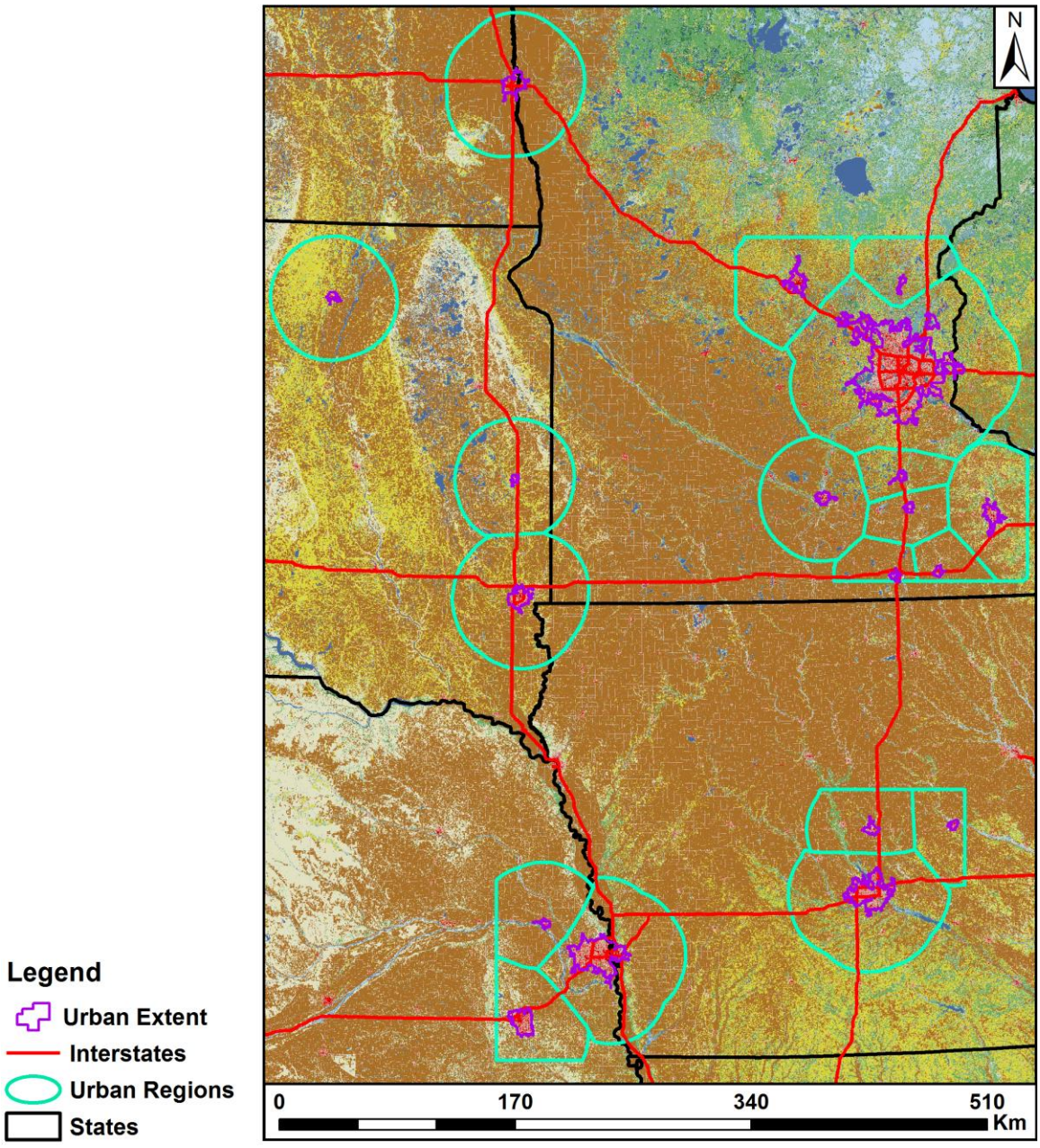

Figure 1. 2011 NLCD LCT product over the Upper Midwest region showing the 19 selected study cities in purple and corresponding urban regions in cyan.

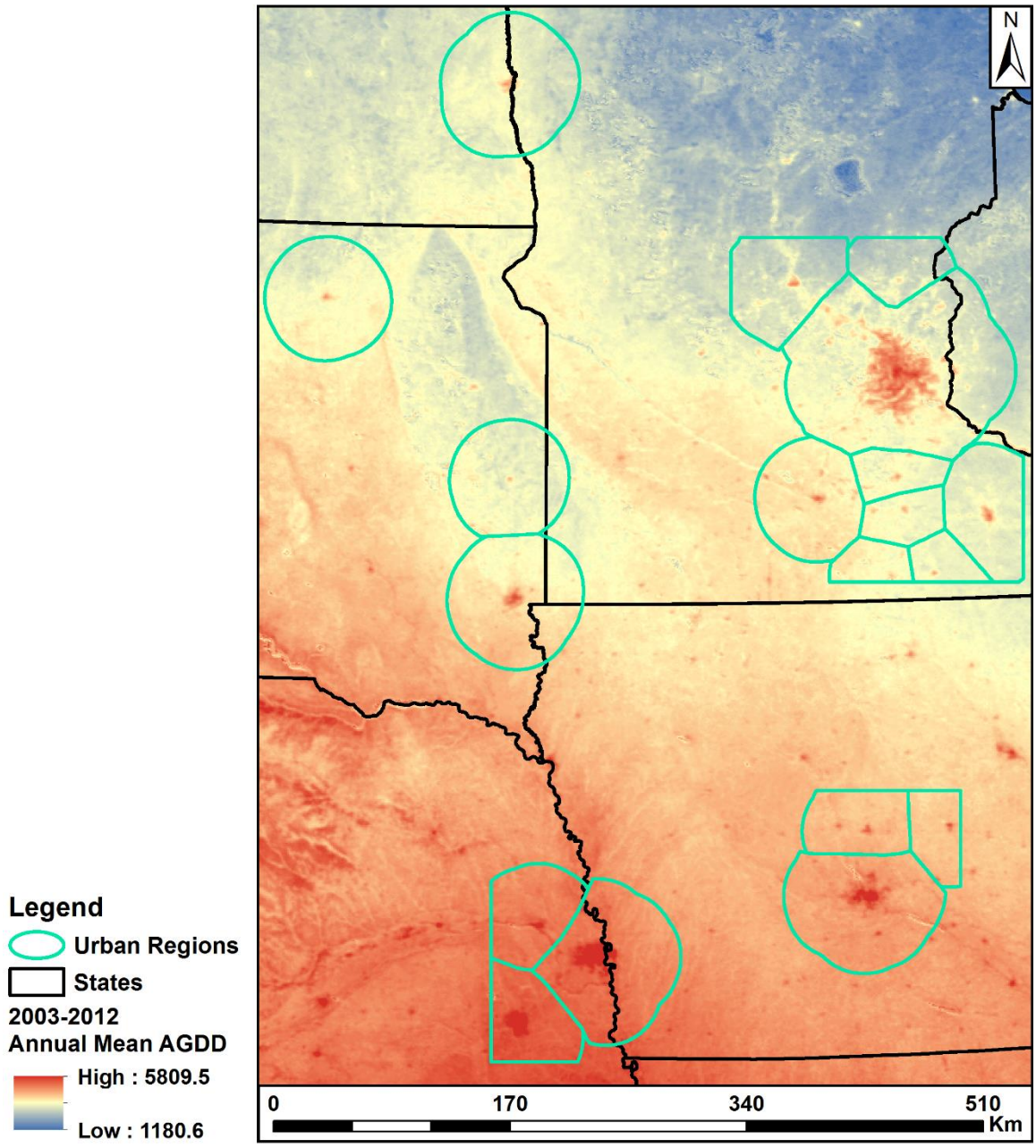

Figure 2. MODIS LST-derived decadal (2003-2012) mean annual AGDD over the Upper Midwest showing the southwest (shades of red; higher AGDD) to northeast (shades of blue; lower AGDD) gradient of thermal time in the Upper Midwest region.

I selected 19 cities as defined by the United States Census Bureau "Urban Areas" (U.S. Census Bureau 2010a) located within the bounds of the study region that represent a small to medium sized city gradient in terms of population and urban extent. I chose the six greater urban regions on the basis that each included an urban area that experienced a relative increase in urban extent > 12% from 2001-2011, as calculated using the 2001 and 2011 NLCD ISA datasets. The six greater urban regions are: (1) Minneapolis-St. Paul-Bloomington, MN-WI; (2) Omaha, NE-Council Bluffs, IA; (3) Des Moines-West Des Moines, IA; (4) Sioux Falls-Brookings, SD; (5) Fargo, ND-Moorhead, MN; and (6) Aberdeen, SD. All 19 individual urban regions analyzed can be found in Table 1. My study time period spans 2001-2012, which covers the 2001-2006-2011 NLCD LCT and ISA archive (Xian et al. 2011; Jin et al. 2013), as well as the ten-year (2003-2012) time series available from the CONUS WELD project (Roy et al. 2010).

How much is there

The 19 cities that I selected span three orders of magnitude in population, from ~15,000 in the Cambridge, MN region to 3.4 million in the Minneapolis-St. Paul metropolitan statistical area (Bureau of Economic Analysis 2011). The urban areas also cover three orders of magnitude in terms of urban extent, ranging from ~25 km^2 in Brookings, SD to 2,773 km^2 in Minneapolis-St. Paul, MN in 2010 (U.S. Census Bureau 2010b). Total urban extent for the six greater urban regions increased by almost 40,000 hectares (18.2 %) from 2001-2011 (Xian et al. 2011). Table 1 contains information on the size, location and thermal regime for each of the 19 urban regions included in the analysis.

Table 1. Characteristics of the 19 study cities: 2011 population (Bureau of Economic Analysis 2011), area of the urban extent (U.S. Census Bureau 2010b), latitude, longitude, decadal mean annual AGDD calculated from the MODIS LST-derived AGDD product, and percentage of pixels with LSP model fit (R^2) > 0.5 in each of the 19 urban regions.

City	2011 Pop.	2010 UE (km^2)	Lat	Lon	2003-2012 AGDD	LSP Model (%)
MSP, MN	3,388,716	2773.3	44.98	-93.28	4318	66.2
Omaha, NE	876,836	702.4	41.23	-96.03	5129	72.2
Des Moines, IA	580,779	519.5	41.62	-93.66	4889	88.4
Lincoln, NE	306,443	229.1	40.81	-96.68	5161	62.9
Sioux Falls, SD	232,553	166.2	43.53	-96.74	4428	56.5
Fargo, ND	212,695	182.1	46.86	-96.82	3819	28.6
Rochester, MN	208,446	131.0	44.02	-92.48	4157	75.9
St. Cloud, MN	189,980	130.1	45.57	-94.19	3918	63.8
Mankato, MN	97,280	68.3	44.17	-93.99	3867	73.6
Ames, IA	90,834	59.8	42.03	-93.63	4435	80.4
Faribault, MN	64,908	29.5	44.29	-93.28	3996	82.7
Marshalltown, IA	40,967	29.7	42.04	-92.91	4576	77.6
Aberdeen, SD	40,902	33.1	45.46	-98.47	3780	37.8
Austin, MN	39,320	31.7	43.67	-92.98	3920	83.2
Fremont, NE	36,943	28.2	41.44	-96.49	4804	73.1
Owatonna, MN	36,551	33.0	44.09	-93.22	4035	81.2
Brookings, SD	32,109	24.6	44.30	-96.78	4008	58.3
Albert Lea, MN	31,111	25.5	43.65	-93.37	3898	67.1
Cambridge, MN	15,155	25.7	45.54	-93.23	3833	76.3

RESEARCH QUESTIONS AND OBJECTIVES

Here I investigate the impacts of urban areas and UHIs on the seasonal development of the vegetated land surface along an urban-rural gradient. I use satellite remote sensing data and products from 2001-2012 to explore spatio-temporal variation in the seasonal development of vegetation in the urban and peri-urban environment for 19 cities along size, land cover, thermal regime, and latitudinal gradients located within the Upper Midwest region of the United States. In order to conduct this research, I define different spatial urban regions (Figure 3), including urban extent (UE), urban core areas (UCAs), which I define as a spatially contiguous area of pixels (> 10 hectares) located within the UE classified as "Developed, High Intensity" based on the 2011 LCT dataset, green core areas (GCAs), defined as a spatially contiguous area of pixels (> 60 hectares) located within the UE classified as "Developed, Open Space", "Forest", "Shrub/Scrub", "Grassland/Herbaceous", "Pasture/Hay", or "Wetlands" based on the 2011 LCT dataset, and areas outside of the UE but within the 40 km region of interest, classified as "Outside of the Urban Extent". Additionally, the parameters used to define each urban spatial region are defined in Appendix I. This project aims to answer the overarching question: What are the impacts of urban areas and UHIs on the seasonal development of the vegetated land surface as seen via satellite remote sensing? The project includes three hypotheses:

Urban Spatial Arrangement Hypothesis (A1):

I hypothesize that Duration of Growing Season in Green Core Areas is shorter than in Urban Extent areas, but longer than regions outside of the Urban Extent.

Urban-Rural Gradient Hypothesis (A2):

I hypothesize that Duration of Growing Season decreases with distance from nearest Urban Core Area for perennial vegetation LCTs.

Land Cover Type Hypothesis (A3):

I hypothesize that a positive linear relationship exists between the model-derived rate of vegetation green-up and maximum NDVI for perennial vegetation LCTs but not for annual croplands.

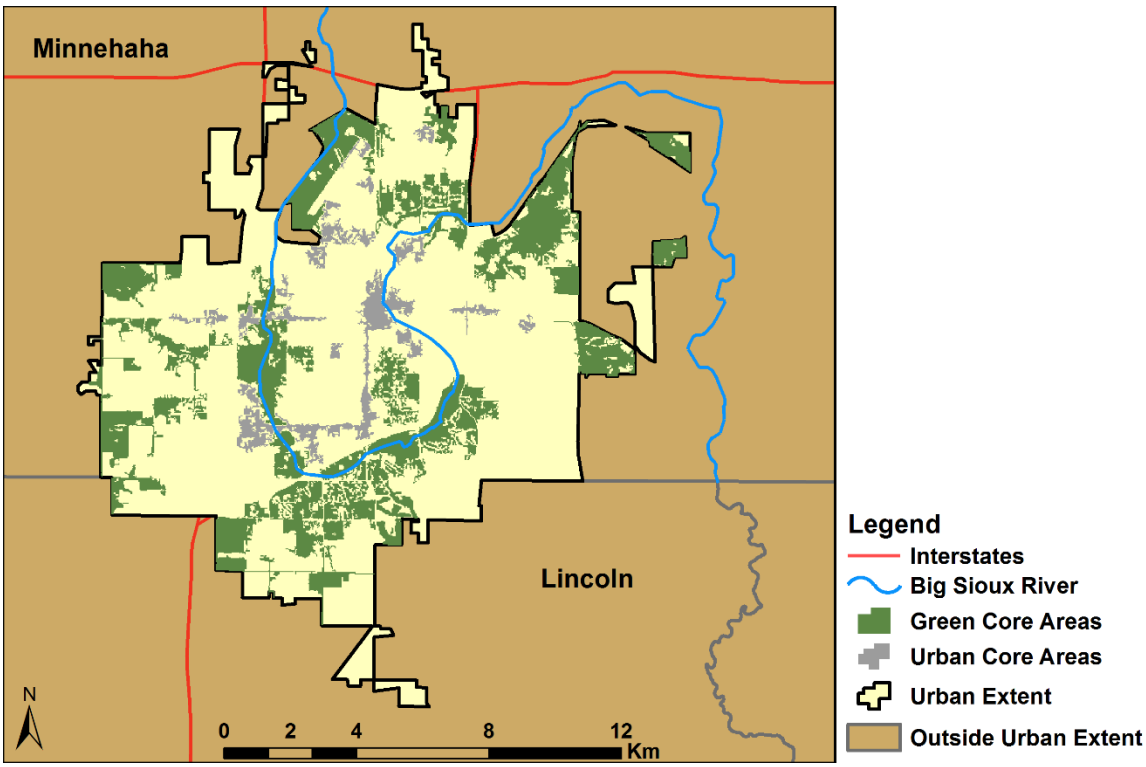

Figure 3. Example of the four urban spatial regions used in the analysis including: urban extent (UE), urban core areas (UCAs), green core areas (GCAs), and areas outside of the UE over Sioux Falls, SD.

METHODOLOGY

Data Collection: Web-Enabled Landsat Data

Web-Enabled Landsat Data (WELD) is a NASA funded project that generates 30 meter composited mosaics of Landsat 7 ETM+ over the United States from 2003-2012 (Roy et al. 2010). WELD was designed to make consistent Landsat data readily available to develop land cover, biophysical, and geophysical products in order to study Earth system science and regional land-cover dynamics (Roy et al. 2010). One advantage of WELD is that the weekly composites include a pre-calculated NDVI band as well as additional quality control flags (saturation, clouds) (Roy et al. 2010). I developed a Perl script using the Linux Operating System that bulk downloads the ten-year archive of WELD files via http. I selected all WELD tiles within 40 km of the UE for each of the 19 urban regions. I used the Perl script to call the "WELDtiletogeotif" tool that converts WELD tile products from HDF to GeoTIFF format (Roy et al. 2010). From there, the Perl script invokes multiple Interactive Data Language (IDL) procedures that (1) georeference each composited mosaic and (2) filter out saturated and cloudy observations using the "Saturation_Flag", "DT_Cloud_State", and "ACCA_State" bands (Roy et al. 2010). I used an additional filter based on a threshold value of NDVI > 0.2 to exclude non-vegetated observations. Ultimately I compiled ten-year time series of the georeferenced and filtered NDVI weekly composites covering each urban region. Figure 8 provides an outline of the aforementioned processing steps.

Data Collection: MODIS Land Surface Temperature Data

MODIS, or Moderate-resolution Imaging Spectroradiometer, is a scientific instrument aboard the Aqua and Terra satellites (Maccherone and Frazier 2015). Aqua and Terra are NASA Earth Science satellites that operate as a part of the Earth Observing

System (Graham and Parkinson 2015). Here I use the MODIS-Aqua (MYD11A2) and MODIS-Terra (MOD11A2) products, which are the level-3 global Land Surface Temperature and Emissivity 8-day composites with 1 km resolution, and are provided in Sinusoidal grid format as the mean clear-sky LST values during an 8-day time frame (NASA LP DAAC 2001). The specific Scientific Datasets (SD) that I extracted from the product include "LST_Day_1km" and "LST_Night_1km", with units in Kelvin (NASA LP DAAC 2001). I developed a Perl script using the Linux Operating System that bulk downloads all observations from 2003-2012 (46 annually; 460 total). I used the MODIS Conversion Toolkit to select and georeference the desired SDs for MODIS tiles H10V04 and H11V04 (NASA LP DAAC 2001).

I also downloaded the MODIS Aqua (MYD10A2) and Terra (MOD10A2) Snow Cover products, which contain level-3 global "Maximum Snow Extent" 8-day composites at 500 meter resolution (Hall et al. 2006). I resampled the 500 meter resolution data to 1 km using the nearest neighbor method provided by the Environment for Visualizing Images (ENVI) software in order to align each pixel with the corresponding MODIS LST 1 km pixel. I used the maximum snow extent product to exclude MODIS LST observations when snow cover was present. The MODIS LST observations were additionally filtered to exclude observations that were below freezing (273.15 K), or unreasonably high (330 K).

Next, I developed an algorithm that converts the two daytime and two nighttime LST observations from Kelvin to degrees Celsius. The algorithm also calculates the mean daytime and nighttime LST for each day of year (DOY) (using the 10 years available for each date), which is later used to fill data gaps from missing values. However, the mean

LST by DOY is only calculated when 8 or more years have available data. From there, the script calculates growing degree-days (GDD).The traditional calculation of GDD is to take the mean of the daily maximum and minimum temperature and subtract from a set base temperature. My GDD calculation used the mean of the mean daily (maximum temperature) and mean nightly (minimum temperature) LST values and a base of 0 °C:

$$\mathrm{GDD} = \frac{\mathrm{mean}(\mathrm{mean}(\mathrm{LST_{day}}) + \mathrm{mean}(\mathrm{LST_{night}}))}{2} - 0\ ^{\circ}\mathrm{C}. \qquad (1)$$

Next, the script filters the data to exclude observations where GDD < 0, which signifies that no GDDs were accumulated for that particular compositing period. The next step creates annual time series of GDD multiplied by 8 to account for the 8-day compositing period of the MODIS products and accumulates each observation (GDD in °C) by year. The final product is a ten-year time series of accumulated growing degree-days (AGDD in °C). Figure 4 shows the workflow for the MODIS LST to AGDD conversion process.

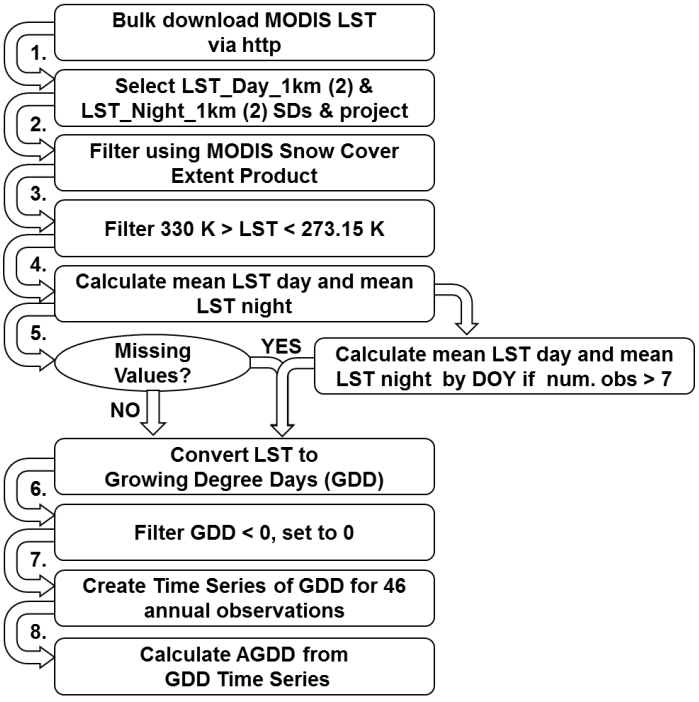

Figure 4. Processing outline for MODIS LST to AGDD algorithm that converts MODIS LST 8-day composites into annual time series of AGDD.

Data Collection: National Land Cover Database Datasets

The National Land Cover Database (NLCD) provides 30 meter resolution land surface characteristics over the United States that can be used for applications including assessment of ecosystem health and ecosystem status (Homer, Fry, and Barnes 2012). I use the Percent Developed Imperviousness (Xian et al. 2011) and Land Cover Type (Jin et al. 2013) products from 2001, 2006, and 2011 for my research. The Impervious Surface Area product is determined using IKONOS and Landsat 7 ETM+ data and describes the percentage of each 30 m pixel covered by anthropogenic (concrete, asphalt, etc.) surfaces (Yang et al. 2003). The Land Cover Type product is derived from unsupervised classification of Landsat 5 TM and Landsat 7 ETM+ at a spatial resolution of 30 m (Jin et al. 2013). The datasets are freely available for download from the Multi-Resolution Land Characteristics Consortium website: (http://www.mrlc.gov) (Jin et al. 2013; Xian et al. 2011).

Data Analysis: Identifying Urban Land Cover Types and Change

I began by characterizing each of the six greater urban regions based on the 2001, 2006, and 2011 LCT and ISA datasets. I identified the LCT and ISA for each corresponding 30 m WELD pixel located in each region. I used a decision tree classification scheme to aggregate the 16-class LCT data into nine classes for my research. Table 2 shows the class groupings used for my study. I also performed change detection from 2001-2006-2011 to identify pixels that experienced a change in LCT, ISA, or both. I classified pixels with ISA change into two classifications based on time period: (1) “2001-2006” and (2) “2006-2011” change (Table 2). Pixels classified as “Water”,

"Barren", "2001-2006 Change" and "2006-2011 Change" were excluded from the analysis. Figure 5 shows an example of the LCT classification over Sioux Falls, SD.

Table 2. Summary of LCT groupings used for classification of pixels in the study.

NLCD Class	ID	My Class
Open Water, Perennial Ice/Snow	1	Water
Developed: Open Space, Low/Medium Intensity	2	Developed
Developed: High Intensity	3	Urban Core Area
Barren Land (Rock/Sand/Clay)	4	Barren Land
Deciduous, Evergreen, Mixed Forest, Woody Wetlands	5	Forest
Shrub/Scrub, Grassland/Herbaceous, Pasture/Hay, Emergent Herbaceous Wetlands	6	Herbaceous
Cultivated Crops	7	Cropland
Change in Impervious Surface Area: 2001-2006	8	2001-2006 Change
Change in Impervious Surface Area: 2006-2011	9	2006-2011 Change

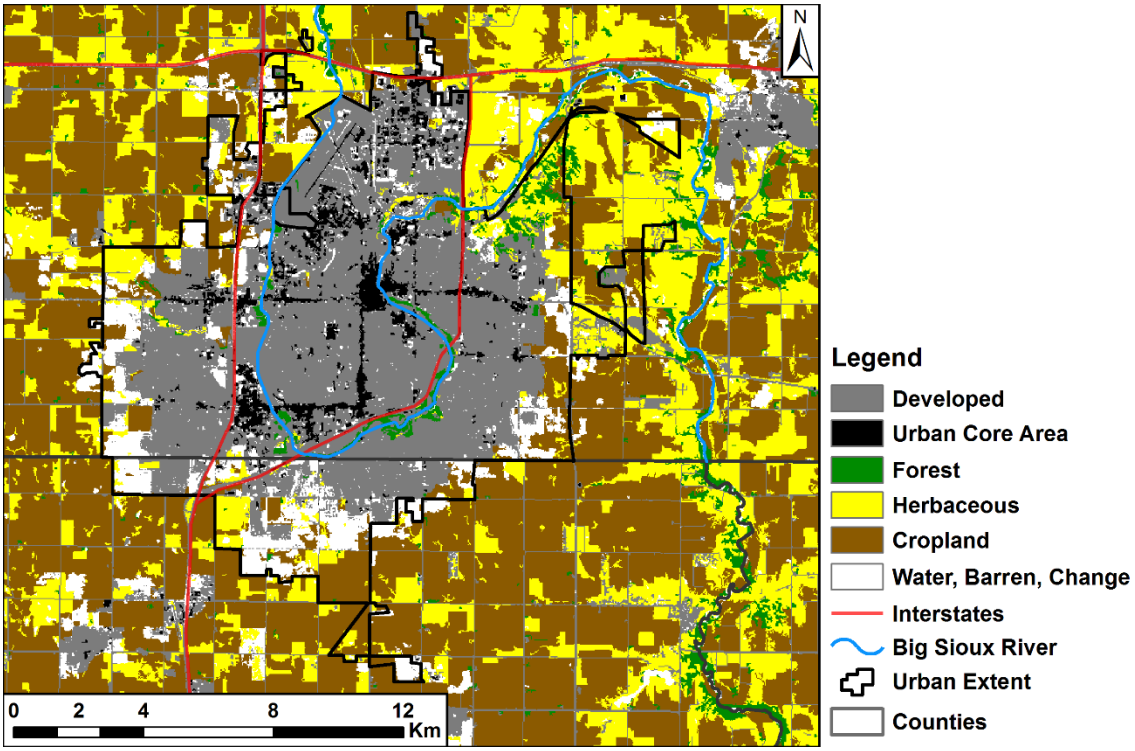

Figure 5. Example of LCT classification (derived from the 2011 NLCD LCT product) over Sioux Falls, SD. "Water", "Barren", and "Change" pixels (white) were excluded from the analyses.

Data Analysis: Spatial Arrangement of Urban Areas

In order to characterize the spatial arrangement of heterogeneous urban landscapes, I defined four specific urban spatial regions of interest. I used the 2010 U. S. Census Bureau delineated "urban areas" cartographic boundary shape files to define Urban Extent (UE) for each urban area in my analysis (U. S. Census Bureau 2010b). Next, I identified urban core areas (UCA), which I define as a spatially contiguous area of pixels (> 10 hectares) located within the UE of each city classified as "Developed, High Intensity" based on the 2011 LCT dataset. I identified green core areas (GCA), defined as a spatially contiguous area of pixels (> 60 hectares) located within the UE of each city classified as "Developed, Open Space", "Forest", "Shrub/Scrub", "Grassland/Herbaceous", "Pasture/Hay", or "Wetlands" based on the 2011 LCT dataset. The UCA and GCA size thresholds were determined so that each city contained at least one of each urban spatial region. Pixels located outside of the UE but within the 40 km region of interest are simply classified as "Outside of the Urban Extent".

In order to draw conclusions on the spatiality of the influences of the six greater urban regions' influence on the surrounding environment, it is necessary to control for the compounding factors of nearby towns and cities. Thus, I chose to expand my study region to include all urban areas with area > 24.6 km, the area of my smallest originally selected city, Brookings, SD. There were 22 cities identified by this threshold. However, 3 of the 22 urban areas (Forest Lake, MN, Monticello-Big Lake, MN, and Hudson, WI) were located < 10 km from the Minneapolis-St. Paul UE, and consequently were added to the Minneapolis-St. Paul urban region. Thus, 19 total urban areas are used for analysis (Table 1). After identifying the boundaries for (1) UE, (2) UCAs, (3) GCAs, and (4) areas

outside of the UE, I calculated Euclidean distance from each pixel to the nearest UCA. Distance is rounded to the nearest kilometer. Figure 6 shows the distance gradient used for the analysis. Each individual urban areas' region of interest was reconfigured after Euclidean distance calculation to group pixels by distance to nearest UCA by city. Figure 6 shows an example of the final boundaries used to define the 9 individual urban regions within the greater Minneapolis-St. Paul, MN urban region.

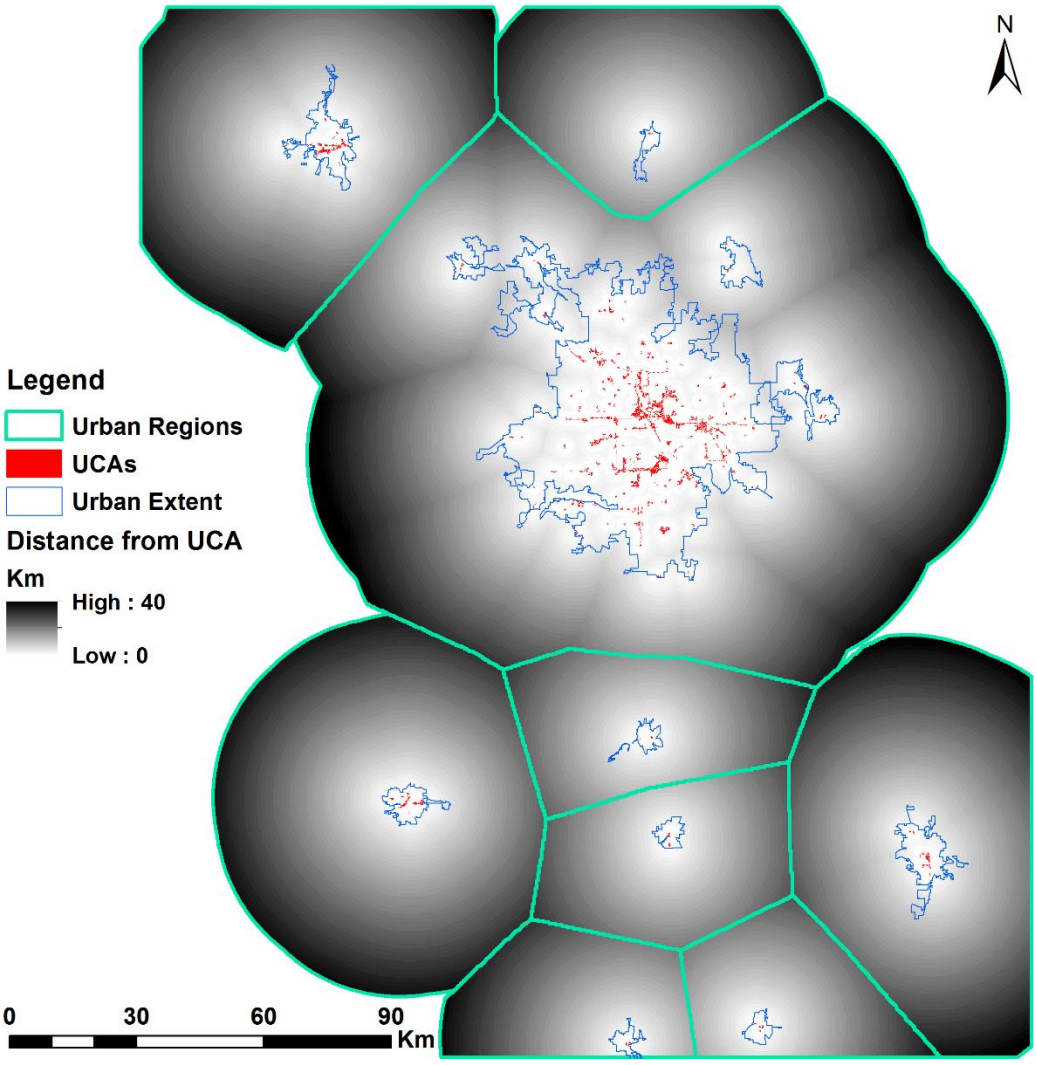

Figure 6. Distance from nearest UCA (red) for nine study cities in the greater Minneapolis-St. Paul urban region. In cyan are the boundaries used for grouping analysis results by city.

Data Analysis: Modeling Land Surface Phenology Metrics

I used a convex quadratic regression model that describes NDVI as a function of AGDD, which has been used successfully in the past to analyze LSP dynamics in temperate regions (de Beurs and Henebry 2004; Walker, de Beurs, and Henebry 2015). The convex quadratic model of LSP (CxQ LSP) is defined as:

$$NDVI = \alpha + \beta AGDD - \gamma AGDD^2 \quad (2)$$

where NDVI contains all NDVI values (unitless; -1 to 1) for a specific period and AGDD (°C) contains all AGDD values for the corresponding period (de Beurs and Henebry 2005). The CxQ LSP model requires only three model parameter coefficient estimates with relevant ecological interpretations (de Beurs and Henebry 2005). The significance of the model is dictated by its ability to explain the variance in NDVI, expressed as the coefficient of determination, or R^2 (de Beurs and Henebry 2005). I applied the CxQ LSP model to the decadal time series of NDVI and AGDD observations for each pixel and derived the following LSP metrics:

$$\text{Peak Height in NDVI } (PH_{NDVI}) = \alpha - \beta^2/4\gamma \quad (3)$$

$$\text{Thermal Time to Peak NDVI (TTP)} = -\beta/2\gamma \quad (4).$$

I derived NDVI at half-thermal time to peak (half-TTP_{NDVI}) from PH_{NDVI} and TTP. I used a threshold of NDVI = 0.3 to determine Start of Season (SOS) and End of Season (EOS) for a given pixel. This threshold was chosen because all NDVI values are filtered to select observations where NDVI > 0.2, and thus once NDVI = 0.3, vegetation has increased in NDVI. $NDVI_{sos}$ is then input and solved for in eq. 2 for both sides of the convex quadratic parabola (i.e., SOS and EOS). This provides AGDD at SOS and EOS, from which I take the difference of (EOS-SOS) to calculate Duration of Growing Season

(DGS_{AGDD}). I used a coefficient of determination threshold of $R^2 < 0.5$ to exclude ill-fitting models. Figure 7 demonstrates the fitting of the CxQ LSP model to a decade of NDVI vs. AGDD observations and the associated LSP metrics derived from the model. Figure 8 shows the data, methods, and parameters involved in executing the model. Figure 9 depicts the model fit (R^2) over the greater Minneapolis-St. Paul, MN region.

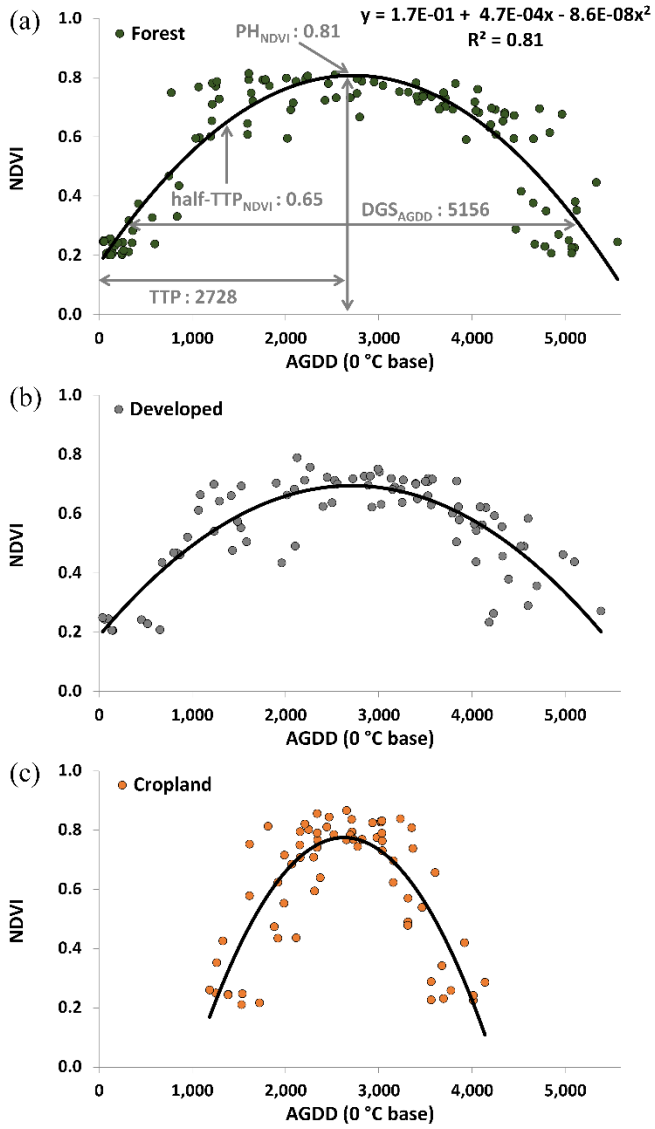

Figure 7. CxQ LSP model fit to the 2003-2012 time series of WELD NDVI vs. MODIS LST-derived AGDD for (a) forest, (b) developed, and (c) cropland pixels selected from Omaha, NE. (a) Shows the LSP metrics derived from the model.

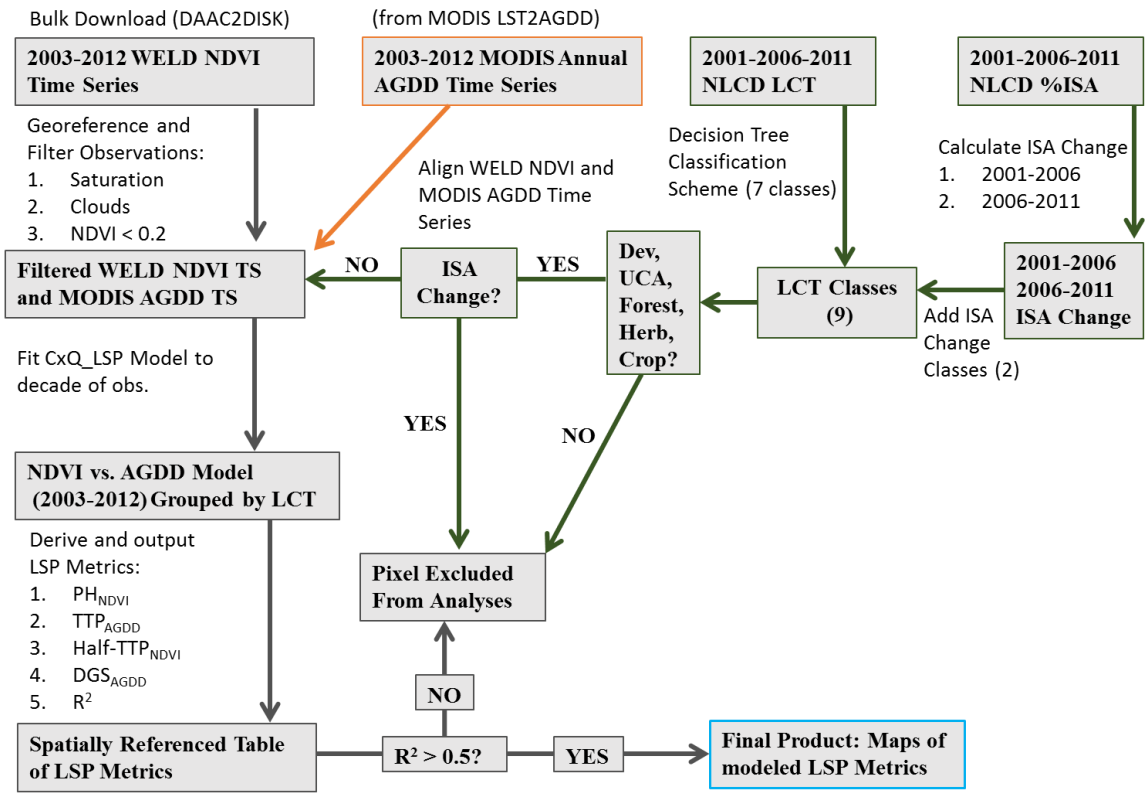

Figure 8. Processing outline of data, methods and parameters used to execute the CxQ LSP model. In grey are the steps performed on the WELD NDVI dataset, in orange is the output from the MODIS LST to AGDD conversion process (Figure 4), and in green are the steps demonstrating the urban LCT scheme.

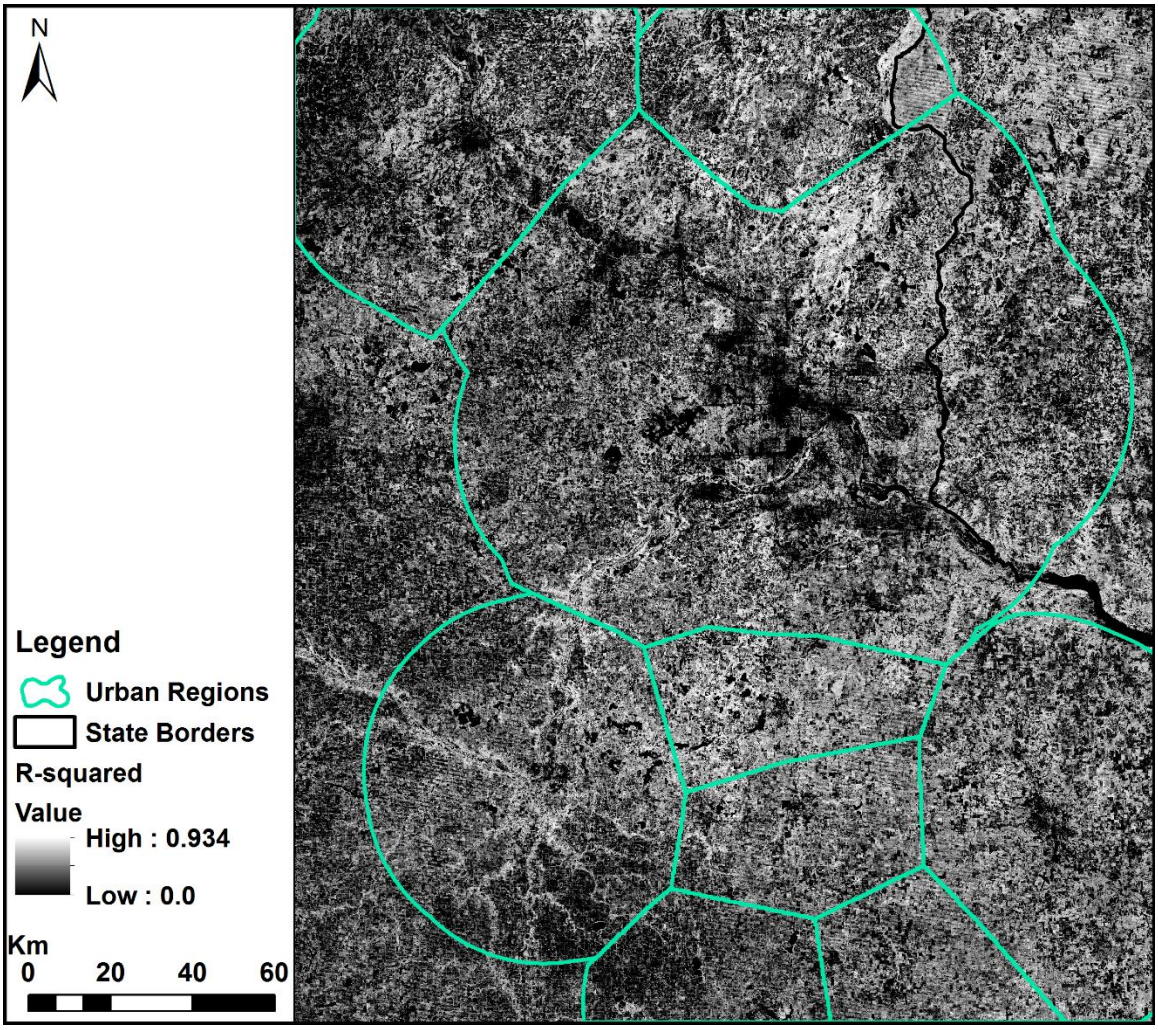

Figure 9. Coefficient of determination (R^2) values from the CxQ LSP Model fit for nine study cities within the greater Minneapolis-St. Paul urban region.

Data Analysis: Equivalence Testing of Urban Spatial Regions

In order to address hypothesis A1 and determine if significant differences exist in DGS_{AGDD} between GCAs, UE areas, and areas outside of the UE, I performed a statistical analysis known as equivalence testing. I use the two one-sided tests (TOST) approach to test for equivalence between group means (Schuirmann 1987). Tests of equivalence evaluate the similarity between two groups rather than the more commonly used tests of

difference or inequality (Foody 2009). There are multiple reasons why equivalence tests are more appropriate for my study than more traditional tests of significant differences between two groups. First, when sample size *n* is extremely large (~10M pixels in the Minneapolis-St. Paul urban region), difference tests may prove statistically significant for any non-zero difference in group means (Goodman 1999; Foody 2009). Moreover, remote sensing data suffer from high positive spatial autocorrelation and it is difficult to correct for positive spatial autocorrelation in difference testing (de Beurs et al. 2015). Another benefit of equivalence testing is that it allows for interpretation of the *magnitude* of differences between two groups (Carlin and Doyle 2002; Foody 2009). Contrary to tests of difference, the null hypothesis in an equivalence test is that two groups are significantly different (Foody 2009). In order to test for equivalency, a zone of indifference is specified which identifies the upper and lower bounds to test for a difference in means between two groups. This leads to the hypothesis:

$$H_{0a}: \mu_1 - \mu_2 > \delta \text{ and } H_{0b}: \mu_1 - \mu_2 < -\delta. \quad (5)$$

If we reject both of these hypotheses, we conclude that the difference in means between two groups falls within the zone of indifference. Figure 10 graphically illustrates a test of equivalence between group means showing the zone of indifference in blue. If the difference in group means falls within the blue region in Figure 10, we can conclude that the groups are statistically equivalent.

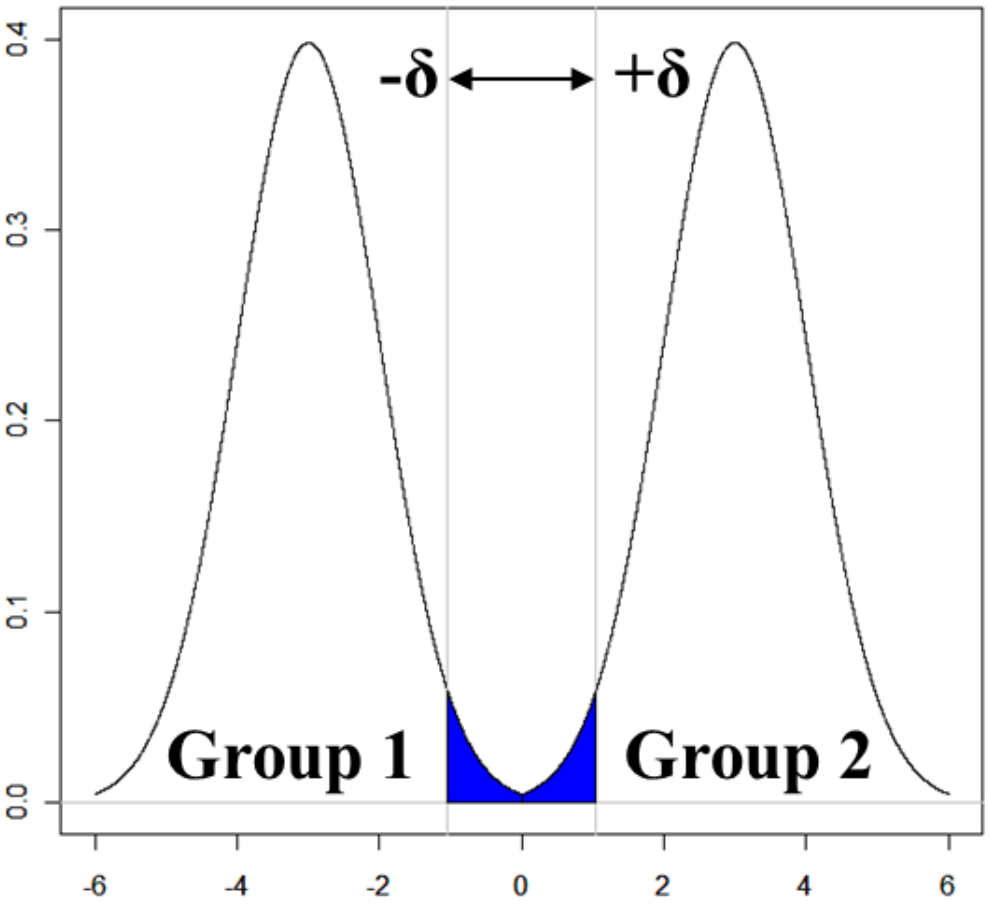

Source: http://www.unt.edu/rss/class/mike/5700/Equivalence%20testing.ppt

Figure 10. Example of the conceptual approach to equivalence testing (University of North Texas 2015). In order to conclude that two groups are equivalent, the difference in group means must fall within the zone of indifference in blue, which is bounded by the specified ±δ.

I performed equivalence tests on the difference between group means of LSP metrics for GCAs, UE areas, and areas outside of the UE. I adjusted for multiple comparisons using the Bonferroni correction method (Bland and Altman 1995). The LSP metrics

tested include: PH_{NDVI}, half-TTP_{NDVI}, TTP, and DGS_{AGDD}. To objectively determine the zone of indifference, or δ, I took 10% of the mean for each LSP metric for each of the 19 study cities. For example, the mean DGS_{AGDD} in the St. Cloud, MN region for perennial LCTs is 3234.9 AGDD * 0.1 = 323.5 AGDDs. If we then test for equivalence between DGS_{AGDD} within the UE and all pixels outside of the UE, we can either (a) reject the null hypothesis, concluding that means between these groups are statistically equivalent, or (b) fail to reject the null hypothesis, concluding that mean DGS_{AGDD} between these groups is different, and by at least 10%.

Figure 11 shows the multiple comparisons tested and the four possible outcomes of the equivalence tests. That is, when testing for equivalence between group means of LSP metrics between GCAs, UE areas, and areas outside of the UE, it is possible for (1) all three groups to be statistically equivalent, (2) all groups to be different (hypothesis A1 for DGS_{AGDD}), (3) one pair of group means to be equivalent, while two pairs are different, or (4) two pairs of group means equivalent, with one pair different. In the analysis, the letters are ranked descending. Thus, the letter “A” symbolizes the highest value, and the letter “C” the lowest. If the letters are the same, the groups are equivalent.

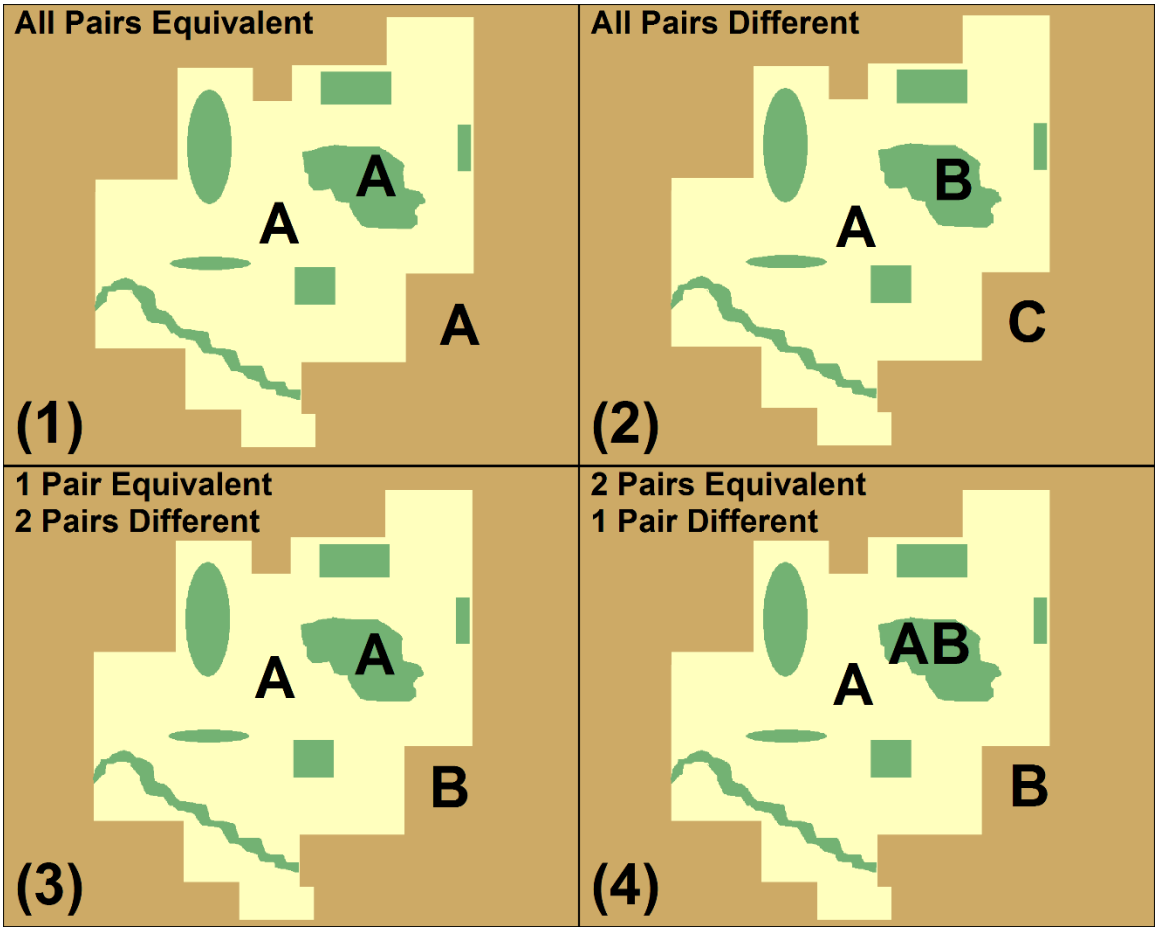

Figure 11. Examples of the four possible outcomes of equivalence tests between GCAs (green), UE areas (tan) and areas outside of the UE (brown). Outcome (1) symbolizes statistical equivalence between all group means and (2) shows statistical difference between all group means. In case (3) group means between GCAs and UE areas are equivalent but both are different and higher than areas outside of the UE. In example (4) group means are equivalent between GCAs and UE areas, and between GCAs and areas outside of the UE, but not equivalent between UE areas and areas outside of the UE. Letter symbols rank group means from highest (A) to lowest (C). This graphical representation will be used in the analysis section to demonstrate the most common results obtained from equivalence testing between group means of LSP metrics.

Data Analysis: Exponential Trend Model: DGS_{AGDD} vs. Distance from UCAs

In order to address Hypothesis A2 (DGS_{AGDD} decreases with distance from UCAs), I based my methods off of a study by Zhang et al. 2004a, which investigated differences in LST and phenological transition dates for urban areas in eastern North America (Zhang et al. 2004a). I began by calculating the mean DGS_{AGDD} for all pixels with $R^2 > 0.6$ within each cities' UE. Next, I calculated the mean DGS_{AGDD} grouped by distance from nearest UCA at 1 km intervals. Then I took the difference between mean UE DGS_{AGDD} and the mean DGS_{AGDD} for each 1 km distance grouping. I then plotted the mean difference in DGS_{AGDD} (ΔDGS_{AGDD}) as a function of distance from UCA for each urban region (Figure 12). From there, I fit an exponential function

$$\Delta DGS_{AGDD} = a(1-ue^{-b*distance}) \qquad (6)$$

where a is the horizontal asymptote, u is the relative amount the curve increases from the origin to the horizontal asymptote, and b is a scaling parameter for distance. I assume that the distance from UCAs where impacts on DGS_{AGDD} become insignificant is the distance where each exponential model reaches 95 % of its asymptotic values (Zhang et al. 2004a). This approach provides two very useful values that I use to address hypothesis A2: (1) the extent (distance) of urban influence on LSP, and (2) the magnitude of differences in DGS_{AGDD} between urban and surrounding rural environments.

I chose to limit this part of the analysis to all pixels within 20 km of UCAs, the same distance used in Zhang et al. 2004a. I split this analysis into two parts. The first is limited to perennial vegetation LCTs, whose DGS_{AGDD} is driven largely by local atmospheric conditions and thus allows for conclusions to be made on the impacts of UHIs on DGS_{AGDD}. Second, I performed the same analysis but included annual croplands. It

would be inappropriate to draw conclusions on the influence of urban areas (via the UHI effect) on the DGS_{AGDD} of croplands, because cropland LSP is driven largely by management practices, including the timing of tillage and harvest (Krehbiel, Jackson, and Henebry 2015). However, including croplands allows us to draw conclusions on the difference in the duration of the "green-on" season. That is, the annual time period when the land surface is covered in green vegetation. At the regional level, I compared my results from each urban region to draw conclusions on the influence of city size and latitude in regards to the impacts on the surrounding environment.

$$\mathbf{\Delta DGS_{AGDD} = a(1-ue^{-b*distance})}$$

$$\Delta DGS_{AGDD}(nocrops) = 800.5(1-1.089e^{-0.254*distance})$$

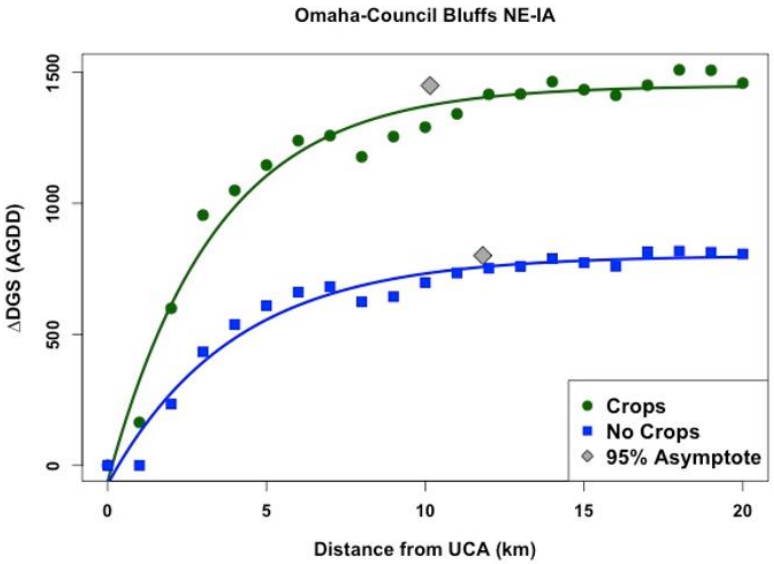

Figure 12. Example of exponential trend model fit to ΔDGS_{AGDD} as a function of distance from nearest UCA for Omaha, NE urban region, with model equation (above) showing a, u, and b parameters. The grey diamonds show where the exponential model reaches 95% of asymptotic values, used to calculate the magnitude of ΔDGS_{AGDD} and the distance at which urban effects become insignificant. In blue is the model fit to strictly perennial vegetation LCTs and in green annual croplands are included.

Data Analysis: Linear Regression of PH_{NDVI} vs. Half-TTP_{NDVI}

I performed linear regression analyses on the relationship between PH_{NDVI} and half-TTP_{NDVI} by land cover type in order to draw conclusions on my third hypothesis (A3). Due to the high volume of observations, I limited this portion of the analysis to pixels with $R^2 \geq 0.8$. In order to determine if the linear model is significant, I used an R^2 threshold of 0.8 in addition to the more traditionally used p-values, again due to extremely large *n* values. I then compared the observed differences between various LCTs. In particular, I am interested in whether or not a significant linear relationship exists for perennial vegetation LCTs but not for annual croplands. Figure 13 shows an example of the linear regression fit by LCT for the Ames, IA urban region.

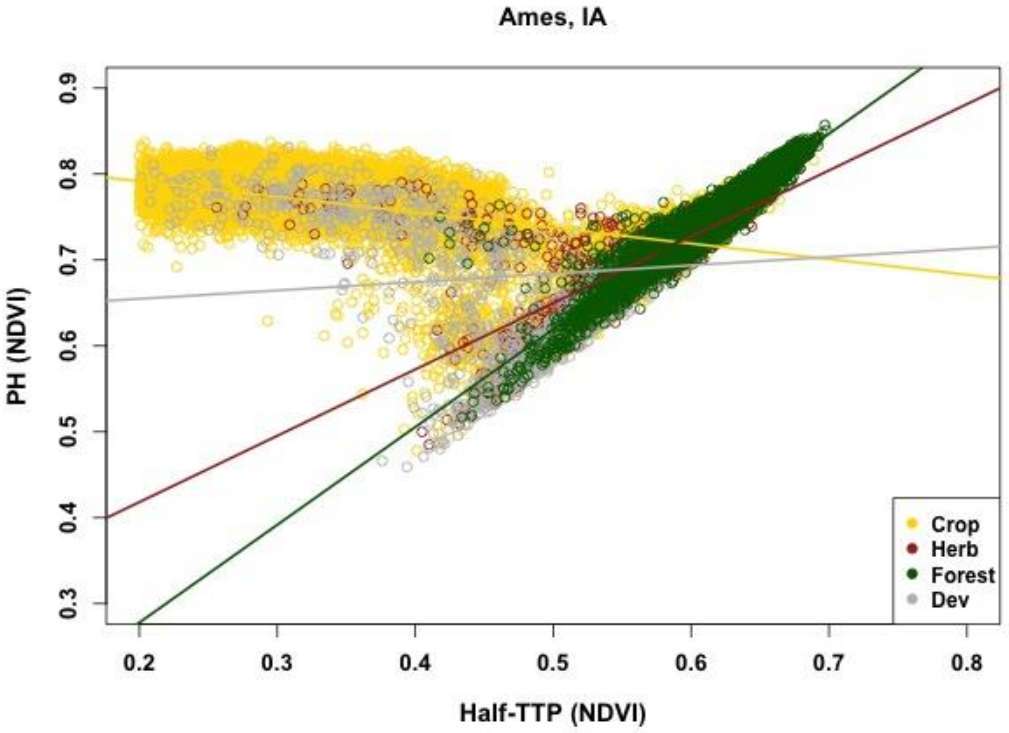

Figure 13. Example of linear regression model fit to PH_{NDVI} vs. Half-TTP_{NDVI} by LCT for Ames, IA urban region. In this example, only the forest LCT (green) exhibits a positive linear relationship that is statistically significant ($R^2 = 0.92$, p-value < 0.0001).

RESULTS

Equivalence Testing: PH_{NDVI}

PH_{NDVI} is statistically equivalent between GCAs and areas outside of the UE and significantly lower in UE areas for 14 of the 19 urban regions (Figure 14; left). Additionally, 3 of the 19 urban regions exhibit statistical equivalency in PH_{NDVI} between two pairs of groups: (1) GCAs and UE areas, and (2) GCAs and areas outside of the UE (Figure 14; right). However, PH_{NDVI} is significantly lower in UE areas than in areas outside of the UE. In summary, 17 of the 19 urban regions have significantly higher PH_{NDVI} in perennial vegetation outside of the UE compared to UE areas. This aligns with results from a similar study that found PH_{NDVI} to decrease with proximity to the center of cities (Krehbiel, Jackson, and Henebry 2015).

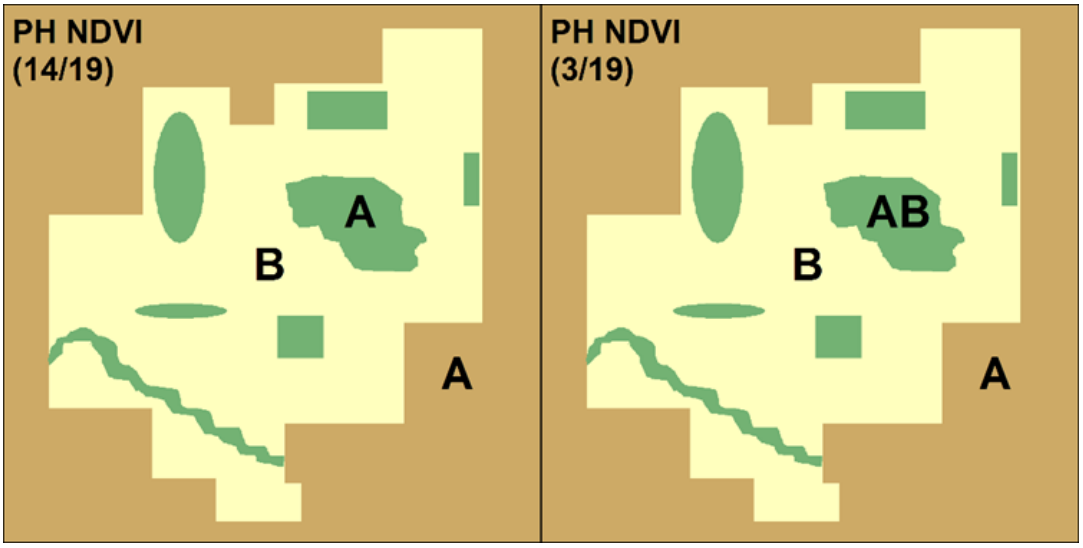

Figure 14. Results from equivalence tests between group means of PH_{NDVI}. PH_{NDVI} is equivalent between GCAs (green) and areas outside of the UE (brown), but significantly lower in UE areas (tan) for 14/19 cities (left). PH_{NDVI} is equivalent between GCAs and UE areas and equivalent between GCAs and areas outside of the UE, but significantly lower in UE areas compared to areas outside of the UE for 3/19 cities (right).

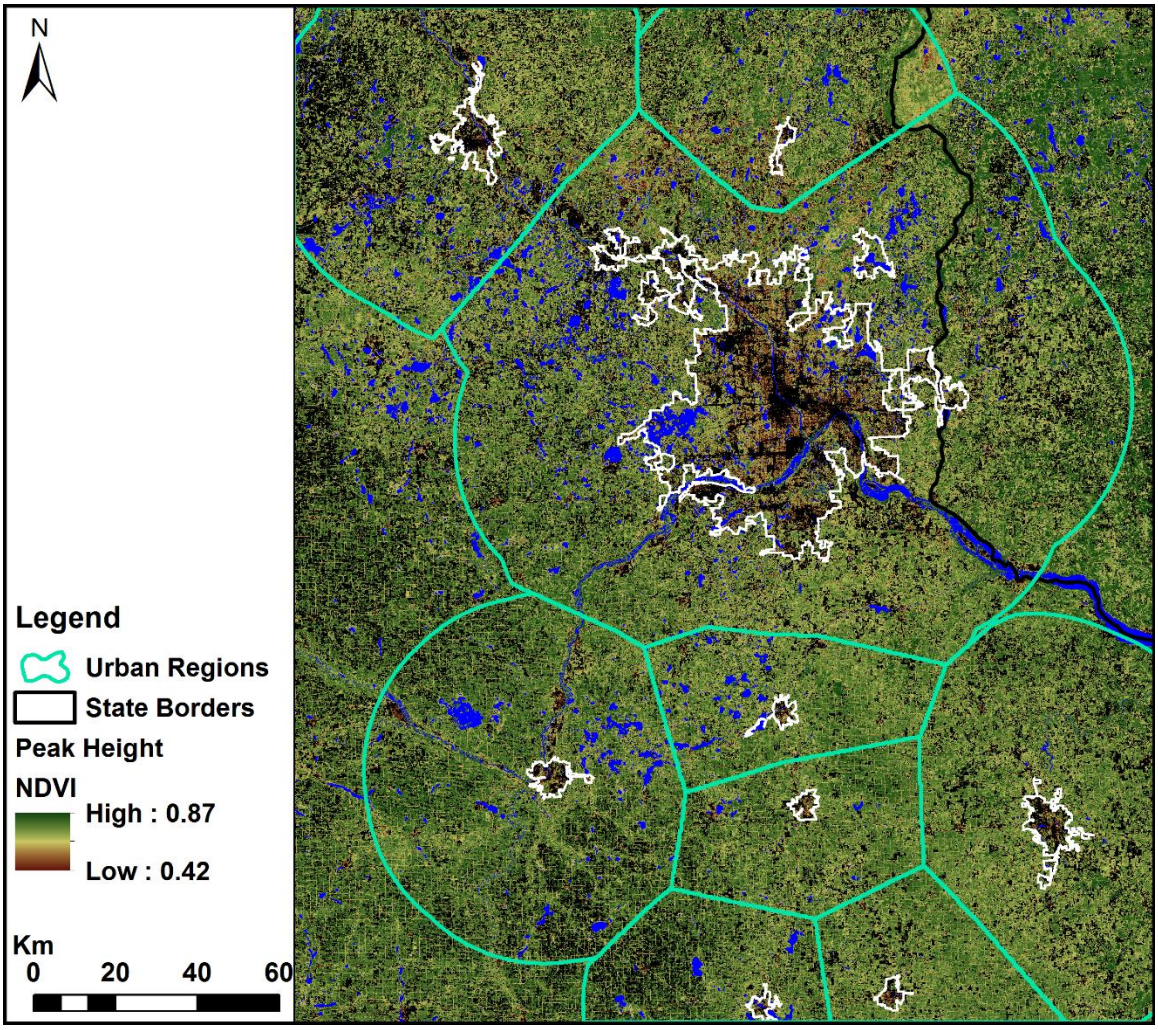

Figure 15. PH_{NDVI} for nine study cities in the greater Minneapolis-St. Paul, MN-WI urban region. Water is masked (blue) and pixels with model fit < 0.5 are in black. Lines are UE (white) and urban regions (cyan) for each of the nine study cities.

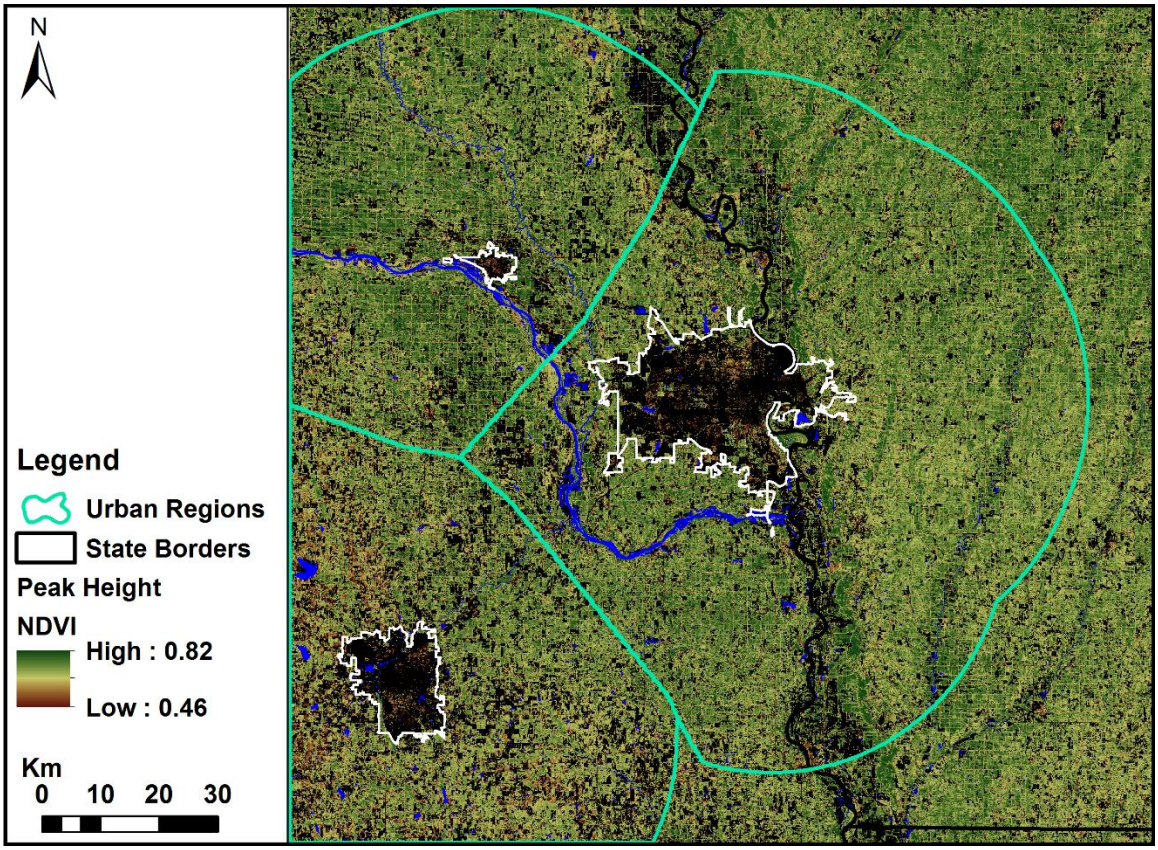

Figure 16. PH_{NDVI} for three study cities in the greater Omaha-Council Bluffs, NE-IA urban region. Water is masked (blue) and pixels with model fit < 0.5 are in black. Lines are UE (white) and urban regions (cyan) for each of the three study cities.

Figures 15-16 show the model results for PH_{NDVI} displayed geographically over the greater Minneapolis-St. Paul (Figure 15) and Omaha-Council Bluffs (Figure 16) study regions. UE is outlined in white. Water has been masked in blue, and pixels with $R^2 < 0.5$ are in black. Both figures show generally decreased PH_{NDVI} within the UE in shades of brown, with darker shades of green indicating higher PH_{NDVI} in the regions outside of the UE. Notice localized regions of higher PH_{NDVI} evident within portions of the UE of Minneapolis-St. Paul (Figure 15; center). This suggests that large urban green spaces contain dense, green vegetation and possibly enhance the health and productivity of

urban vegetation. The two regions that did not exhibit the aforementioned equivalence test results for PH_{NDVI} are Fremont, NE, (Figure 16; Northwest) and Lincoln, NE (Figure 16; Southwest). In Fremont, NE, PH_{NDVI} was different between all areas and highest in regions outside of the UE, followed by GCAs and lastly UE areas. Lincoln, NE, is the only urban region where PH_{NDVI} is equivalent between areas inside the UE and areas outside of the UE. This relationship is evident in Figure 16, with the Lincoln, NE region showing shades of brown (indicating lower PH_{NDVI}) both within and outside of the UE. Lincoln, NE, is the furthest south and warmest city in my study (Figure 2, Table 1), and the absence of higher PH_{NDVI} in the regions surrounding the UE indicates that water availability may be a confounding factor of LSP dynamics in this region in addition to thermal time.

Equivalence Testing: Half-TTP_{NDVI}

Half-TTP_{NDVI} measures the rate of green vegetation development during the start of the growing season. Lower Half-TTP_{NDVI} values indicate a faster rate of green up, which is common in cropland LSP dynamics (Figure 7c). There is no dominant pattern in the spatiality of Half-TTP_{NDVI} for the selected 19 study regions. Half-TTP_{NDVI} is statistically equivalent between UE areas and areas outside of the UE and significantly higher in GCAs for six of the 19 urban regions (Figure 17; left). On the other hand, six of the 19 urban regions are equivalent in Half-TTP_{NDVI} between GCAs and areas outside of the UE, and significantly lower in UE areas. Based on the lack of a dominant spatial pattern between mean half-TTP_{NDVI} by urban region, it appears that urban areas do not significantly alter the rate of vegetation green-up, which is more likely driven by the inherent physiological characteristics of individual vegetation species. This can be

visualized geographically in Figure 18, where it appears that half-TTP_{NDVI} is higher (green) inside the UE (white) of Sioux Falls, SD (south) compared to the surrounding agricultural landscape (brown). This contrast in half-TTP_{NDVI} is caused by differences in LCT, with croplands exhibiting very low half-TTP_{NDVI} compared to the perennial vegetation LCTs within the UE. Lower half-TTP_{NDVI} is associated with a higher rate of green-up, which is characteristic of the soy and maize crops grown in the rural areas surrounding Sioux Falls, SD. However, this relationship is not captured in the equivalence test—which only tested half-TTP_{NDVI} for perennial LCTs within each respective region.

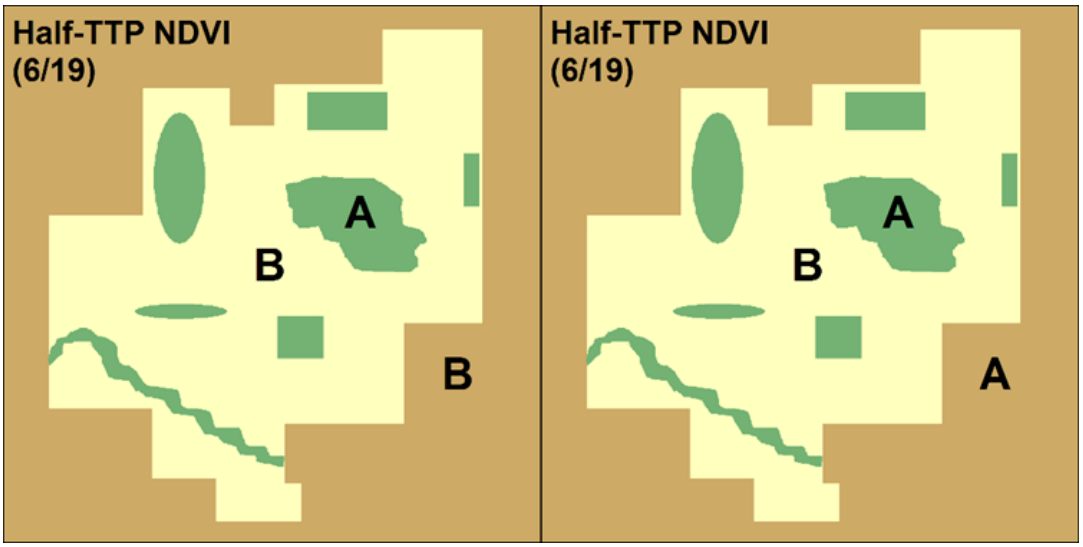

Figure 17. Results from equivalence tests between group means of Half-TTP_{NDVI}. Half-TTP_{NDVI} is equivalent between UE areas (tan) and areas outside of the UE (brown), but significantly higher in GCAs (green) for 6/19 cities (left). Half-TTP_{NDVI} is equivalent between GCAs and areas outside of the UE but significantly lower in UE areas for 6/19 cities (right).

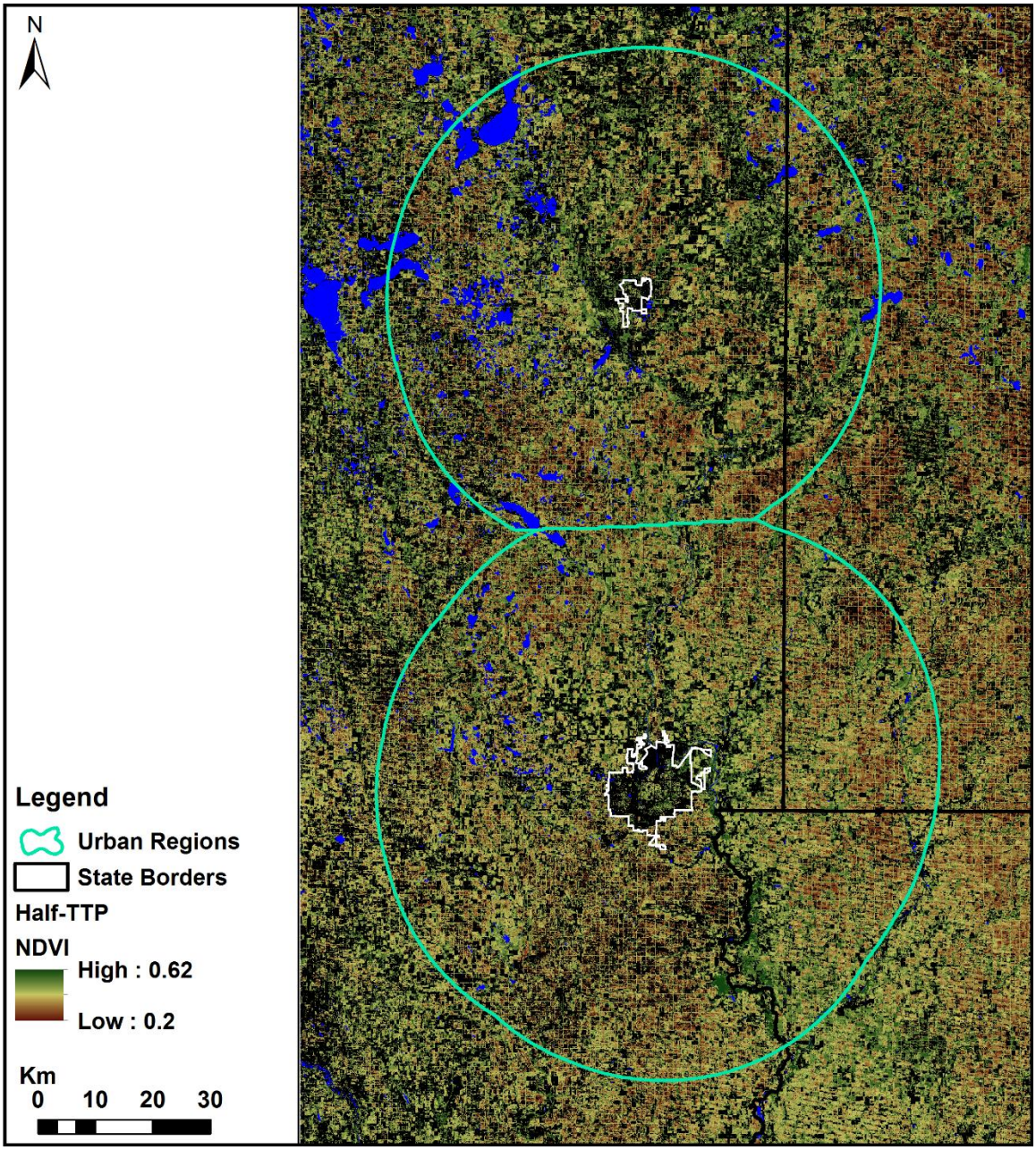

Figure 18. Half-TTP_{NDVI} for the greater Sioux Falls-Brookings, SD urban region. Water is masked (blue) and pixels with model fit < 0.5 are in black. Lines are UE (white) and urban regions (cyan) for the two study cities.

Equivalence Testing: TTP

Thermal time to peak NDVI is statistically equivalent between GCAs, UE areas, and areas outside of the UE for 11 of the 19 study cities (Figure 19; left). This result suggests that urban areas and UHIs do not drastically alter the timing of PH_{NDVI}. However, in five of the 19 cities, TTP is significantly later (higher TTP) in UE areas compared to areas outside of the UE, with TTP equivalent between GCAs and both UE areas and areas outside of the UE (Figure 19; right). Des Moines, IA is an example of one of the five cities with this pattern, evident in Figure 20 (south), where it is clear that TTP occurs later (dark brown) inside of the UE than the surrounding regions, particularly in the less intensely cultivated regions to the south of the city. Both Ames (Figure 20; north) and Marshalltown, IA (Figure 20; Northeast) exhibit the dominant pattern of equivalency in TTP between all three urban spatial regions.

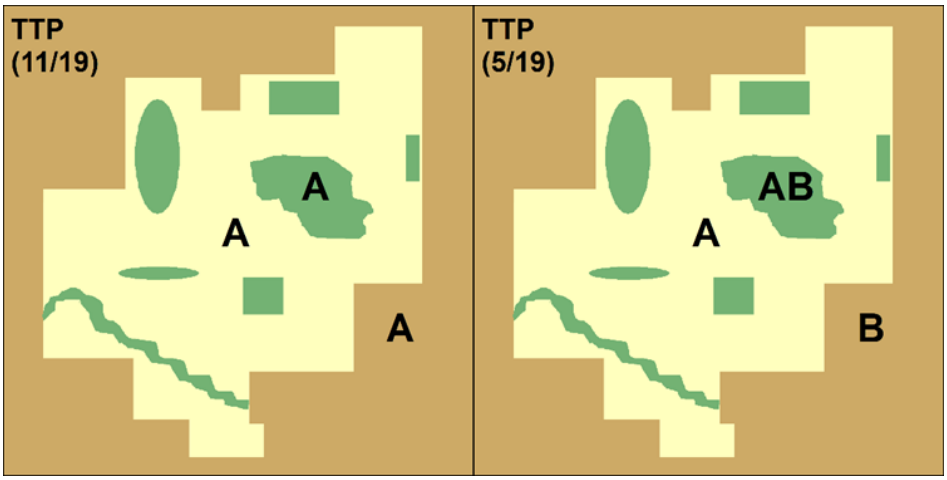

Figure 19. Results from equivalence tests between group means of TTP. TTP is equivalent between GCAs (green), UE areas (tan) and areas outside of the UE (brown) for 11/19 cities (left). TTP is equivalent between GCAs and UE areas and equivalent between GCAs and areas outside of the UE, but significantly higher in UE areas compared to areas outside of the UE for 5/19 cities (right).

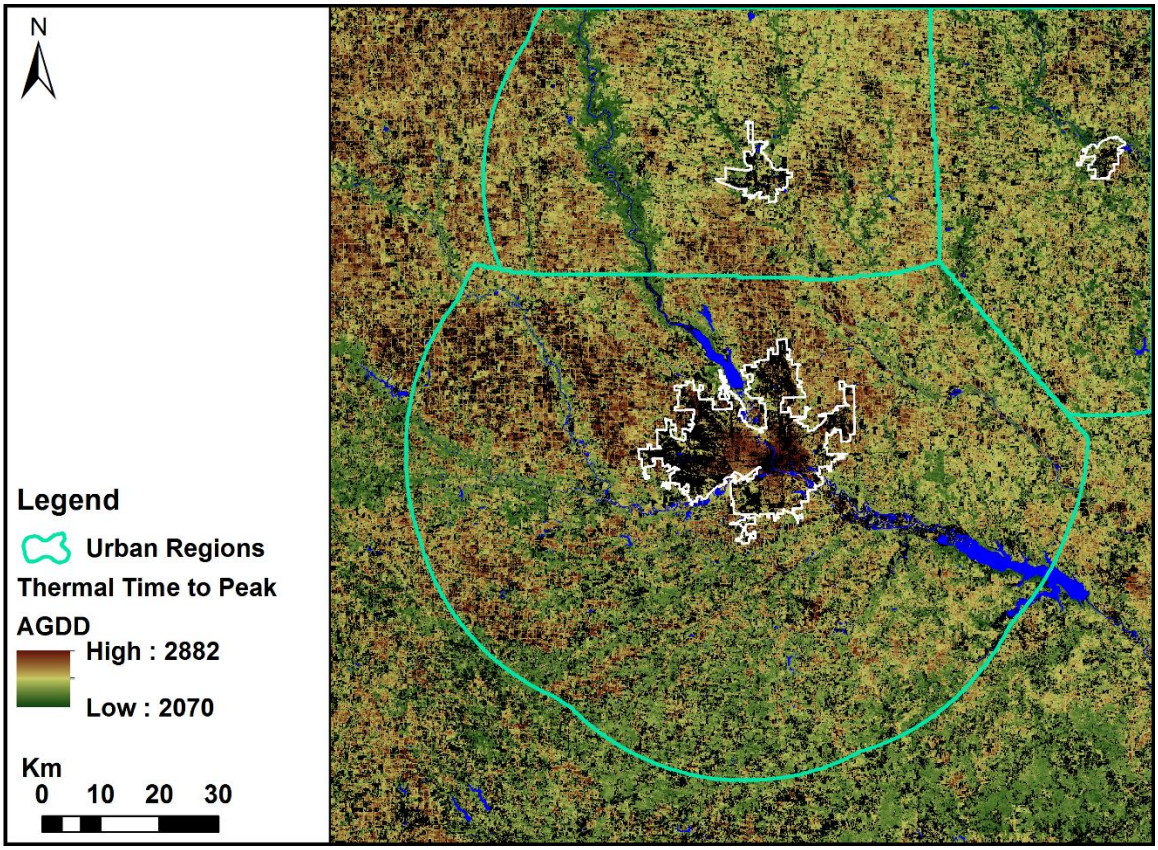

Figure 20. TTP for three study cities in the greater Des Moines, IA urban region. Water is masked (blue) and pixels with model fit < 0.5 are in black. Lines are UE (white) and urban regions (cyan) for each of the three study cities.

Equivalence Testing: DGS_{AGDD}

Hypothesis A1 states that DGS_{AGDD} in GCAs is shorter than in UE areas, but longer than in regions outside of the UE. This hypothesis is based on the premise that vast expanses of urban vegetation could potentially experience shorter growing seasons due to the cooling effects of vegetation. However, only one out of the 19 urban regions exhibits this pattern based on the equivalence testing analysis (Lincoln, NE). DGS_{AGDD} is equivalent between GCAs and UE areas and higher than areas outside of the UE for 17 out of the 19 urban regions (Figure 21). Thus, I reject hypothesis A1 and conclude that in

general, DGS_{AGDD} is longer in both GCAs and UE areas than in areas outside of the UE, but there is not a significant difference between DGS_{AGDD} in GCAs compared to UE areas. This dominant spatial pattern demonstrates the influence of urban areas and UHIs on the seasonal development of perennial vegetation, where vegetation within cities experiences growing seasons that are at least 10% longer than vegetation in the surrounding rural areas. Tables containing all of the results from the equivalence tests for each LSP metric and individual urban regions are found in Appendix II.

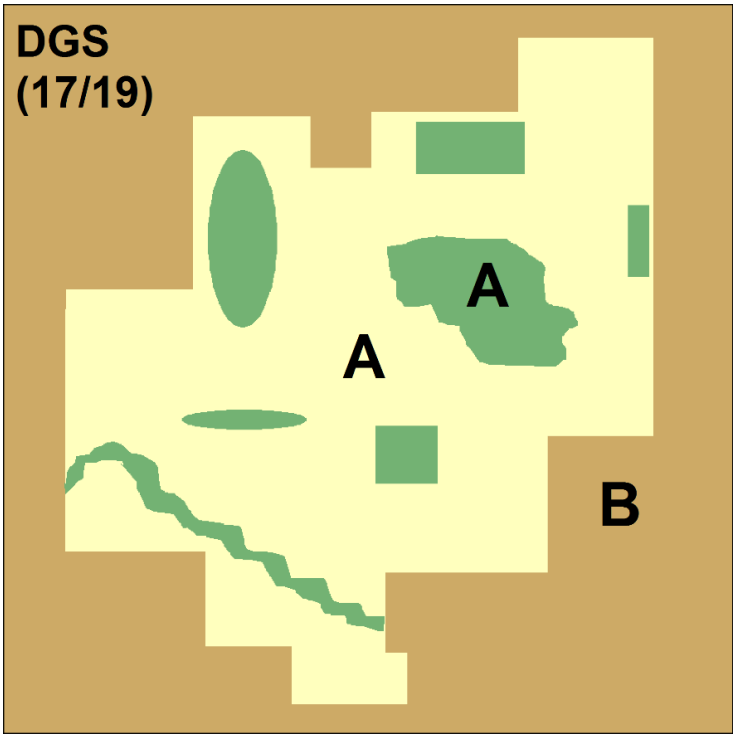

Figure 21. Results from equivalence tests between group means of DGS_{AGDD}. DGS_{AGDD} is equivalent between GCAs (green) and UE areas (tan), but significantly lower in areas outside of the UE (brown) for 17/19 urban regions.

Figures 22-23 show DGS_{AGDD} over the greater Des Moines, IA (Figure 22), and Minneapolis-St. Paul, MN (Figure 23) regions. Darker shades of red relate to longer DGS_{AGDD}, clustered near the densely impervious UCAs of each region. Figure 24 shows

the corresponding LCT over the greater Minneapolis-St. Paul urban region. Notice that significant spatial patterns exist between DGS_{AGDD} and LCT, with higher DGS_{AGDD} in the perennial LCTs (developed, forest, herbaceous) compared to annual croplands. This spatial pattern demonstrates why croplands were omitted from the DGS_{AGDD} analysis: (1) there are little to no cropland areas inside of cities from which to compare, and (2) the seasonal development of annual croplands is dictated by management factors (i.e. field accessibility, timing of tillage, irrigation) rather than by local environmental and atmospheric conditions (i.e. thermal time, the UHI effect).

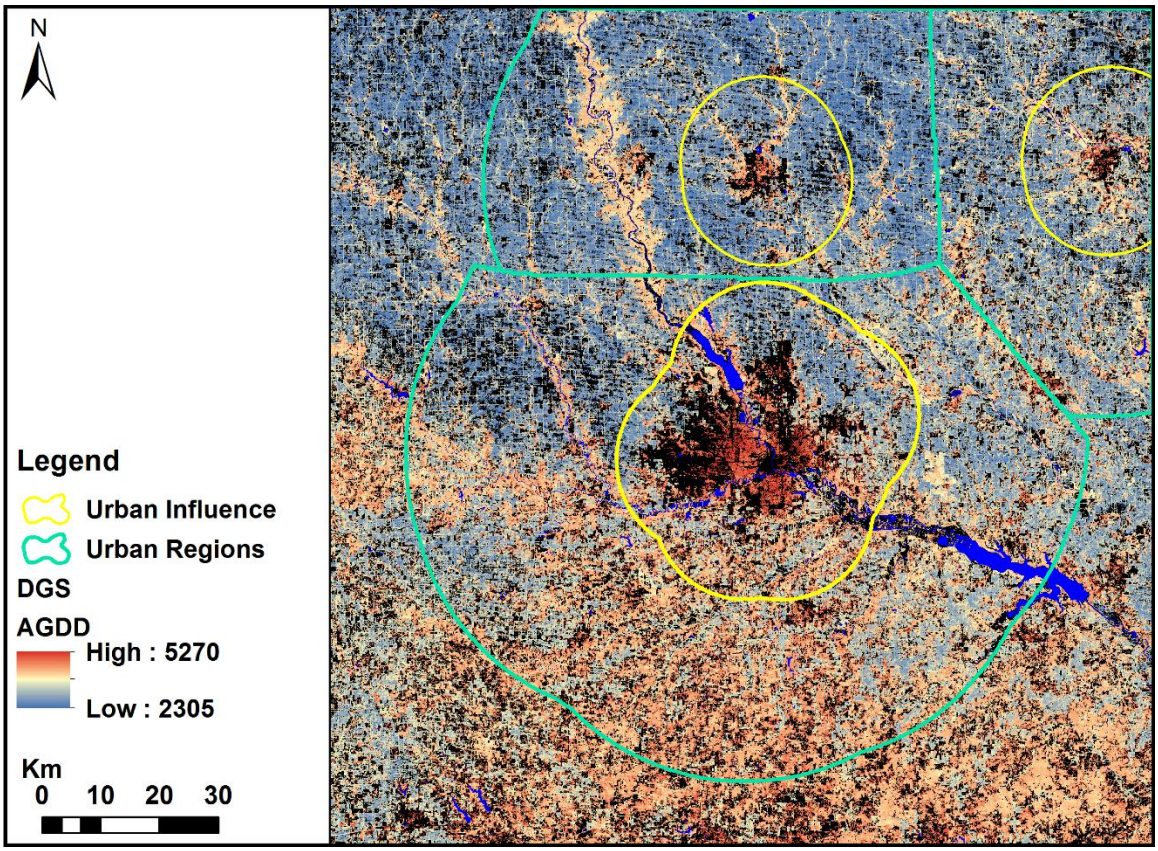

Figure 22. DGS_{AGDD} for three study cities within the greater Des Moines, IA urban region. Water is masked (blue) and pixels with CxQ LSP model fit < 0.5 are in black. Yellow outlines show the distance (extent) of significant urban influence on the surrounding environment, measured from UCAs.

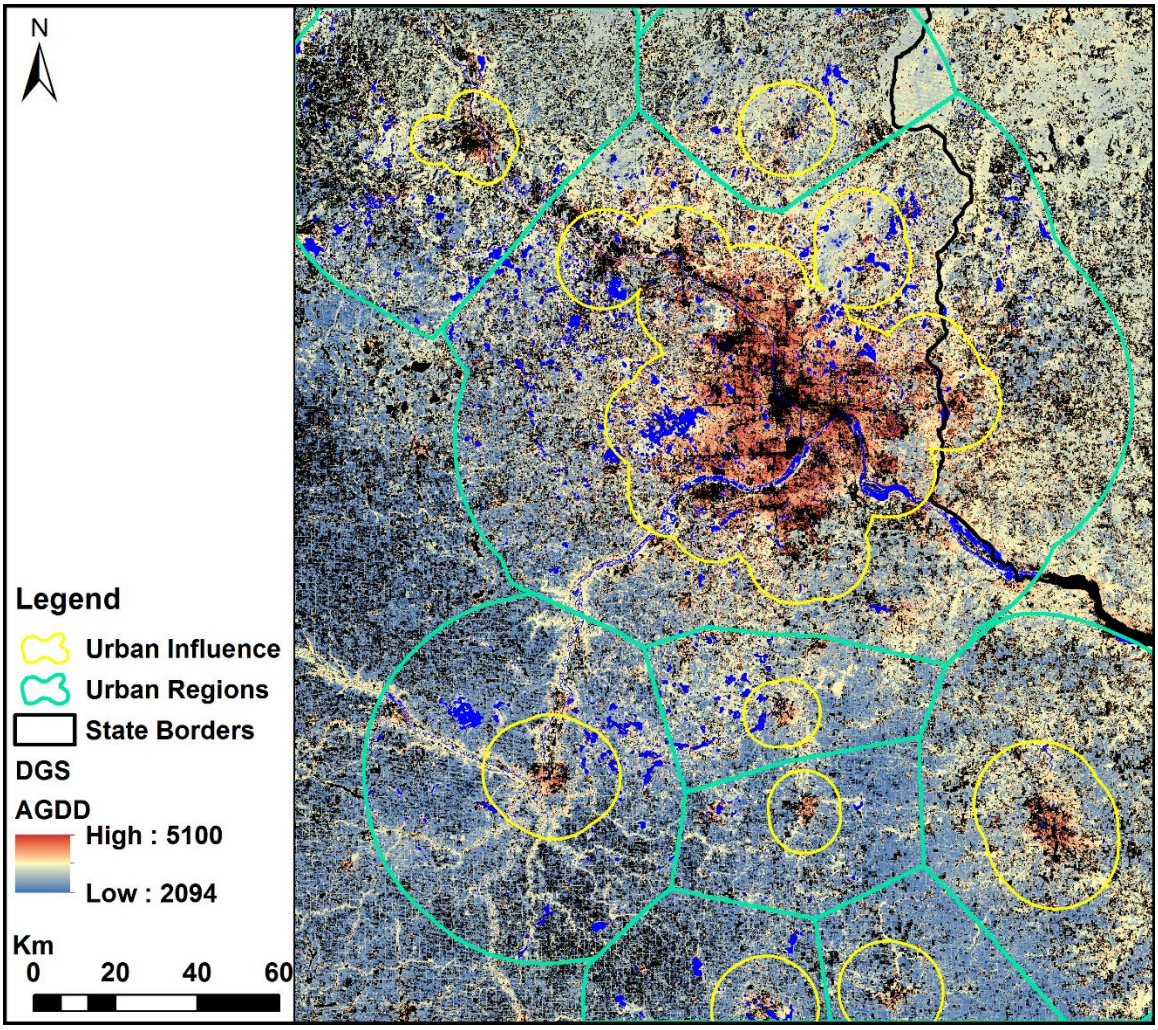

Figure 23. DGS_{AGDD} for nine study cities within the greater Minneapolis-St. Paul, MN-WI urban region. Water is masked (blue) and pixels with CxQ LSP model fit < 0.5 are in black. Yellow outlines show the distance (extent) of significant urban influence on the surrounding environment, measured from UCAs.

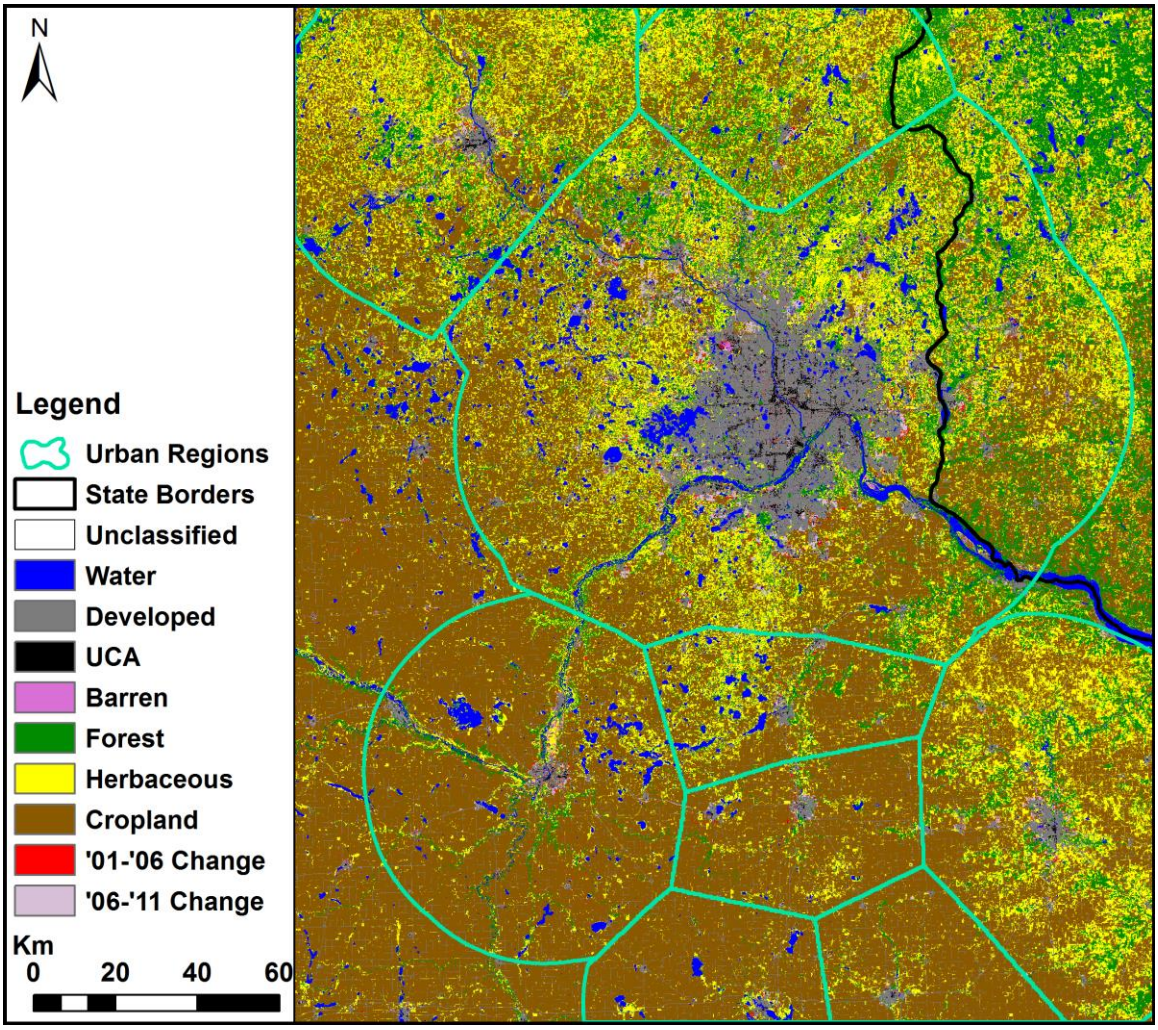

Figure 24. LCT classification scheme for nine study cities within the greater Minneapolis-St. Paul, MN-WI urban region demonstrating regional differences in dominant LCT between the intensely cultivated regions in the southwest (brown) and increasingly forest/herbaceous LCTs (green/yellow) to the north and east, with the large metropolitan area of Minneapolis-St. Paul (grey) lying between the two regions.

Exponential Trend Model: ΔDGS_{AGDD} vs. Distance from UCA

In order to test hypothesis A2, that DGS_{AGDD} decreases with distance from UCAs, I analyzed the difference in DGS_{AGDD} (ΔDGS_{AGDD}) between UE areas and areas grouped by increasing distance from UCAs. ΔDGS_{AGDD} follows an increasing negative exponential trend function of distance from UCAs for all of the 19 study cities. However, the Fargo, ND, region exhibited unreasonable results, likely due to the low R^2 in the study region (28.6% CxQ LSP model fit). Thus, I excluded the Fargo, ND, region from the exponential trend model analysis. I fit the exponential model twice: once for ΔDGS_{AGDD} calculated only from perennial LCTs (developed, forest, herbaceous) (Figure 25; blue) and once incorporating croplands (Figure 25; green). In general, ΔDGS_{AGDD} increases exponentially with distance from nearest UCA (Figure 25). The magnitude of ΔDGS_{AGDD} ranges from 393 AGDD in Mankato, MN, to 855 in Lincoln, NE. The distance at which urban effects are detectable and significant extends from 5.6 km in St. Cloud, MN, to 15.4 km in Des Moines, IA. The results for each individual urban region are found in Table 3. On average, the 18 urban areas experience growing seasons that are 669 AGDD longer than the surrounding rural areas, and the effects of urban areas on the growing season extend 11.4 km into the urban periphery. It is evident that urban areas impact the duration of growing season in perennial LCTs, and that urban effects (namely UHIs) extend beyond the boundaries of cities themselves. Figures 22-23 illustrate the zone of urban influence extending into the urban periphery in yellow.

Analysis of DGS_{AGDD} restricted to perennial vegetation LCTs allows for conclusions on the impacts of UHIs on the seasonal development of vegetation. However, including croplands offers a comparison of the difference between urban and rural duration of

green-on season, or the annual period where the land surface is covered in green vegetation. Figure 25 demonstrates the dramatic difference in ΔDGS_{AGDD} calculated with (green) and without (blue) annual croplands. Notice that the difference in ΔDGS_{AGDD} is greater in regions that are surrounded predominantly by intensive agriculture (Figure 25; Omaha, NE, and Des Moines, IA, regions) compared to areas where there is a greater portion of forest and herbaceous land cover surrounding the urban area (Figure 25; Rochester and Minneapolis-St. Paul, MN). Including croplands into the calculation of ΔDGS_{AGDD} leads to a mean difference between urban and rural DGS_{AGDD} of 1125 AGDD. To reiterate, this result is not demonstrating the influence of urban areas on local atmospheric conditions, but rather highlights the large difference in the duration of *green-on* season between perennial vegetation LCTs and annual croplands. This difference has major implications for the representation of urban vs. rural vegetation in land surface modeling. All of the exponential trend plots for each of the 19 urban regions can be found in Appendix III.

Table 3. Scaling parameters of exponential trend model for ΔDGS_{AGDD} fit with croplands included ("C") and with croplands excluded ("NC") as well as the magnitude of ΔDGS_{AGDD} ("a", in AGDD) and distance where urban influence on the surrounding environment becomes insignificant, measured from nearest UCA.

City	NC b	C b	C u	NC u	C R^2	NC R^2	NC a	C a	Δa	NC Dist (km)	C Dist (km)
Aberdeen, SD	0.233	0.204	0.887	0.848	0.904	0.857	528	836	309	12.9	14.7
Albert Lea, MN	0.243	0.251	1.151	1.174	0.934	0.879	652	1135	482	12.3	12.0
Ames, IA	0.217	0.264	1.097	1.154	0.963	0.899	662	1400	738	13.8	11.4
Austin, MN	0.258	0.374	0.974	0.991	0.953	0.878	689	1203	514	11.6	8.0
Brookings, SD	0.399	0.369	1.069	1.050	0.952	0.964	605	1084	480	7.5	8.1
Cambridge, MN	0.275	0.396	1.003	0.984	0.910	0.951	422	482	60	10.9	7.6
Des Moines, IA	0.195	0.310	1.065	1.109	0.961	0.975	721	1195	474	15.4	9.7
Faribault, MN	0.388	0.419	1.004	1.145	0.966	0.920	545	970	426	7.7	7.2
Fremont, NE	0.253	0.373	0.777	0.970	0.970	0.933	735	1467	732	11.8	8.0
Lincoln, NE	0.276	0.317	0.792	0.900	0.944	0.968	855	1303	448	10.9	9.5
Mankato, MN	0.238	0.312	1.032	1.068	0.946	0.963	393	931	538	12.6	9.6
Marshalltown, IA	0.221	0.178	0.896	1.007	0.987	0.970	804	1428	623	13.6	16.8
MSP, MN	0.289	0.270	1.058	1.094	0.975	0.975	743	929	186	10.4	11.1
Omaha, NE	0.254	0.296	1.042	1.089	0.972	0.963	800	1449	649	11.8	10.2
Owatonna, MN	0.357	0.451	1.101	1.089	0.937	0.937	754	1276	522	8.4	6.6
Rochester, MN	0.201	0.193	1.090	1.124	0.966	0.966	799	1172	374	15.0	15.6
Sioux Falls, SD	0.238	0.340	1.097	1.109	0.960	0.956	832	1375	543	12.6	8.8
St. Cloud, MN	0.532	0.527	1.065	1.085	0.924	0.940	497	611	115	5.6	5.7
Minimum	0.195	0.178	0.777	0.848	0.904	0.857	393	482	60	5.6	5.7
Maximum	0.532	0.527	1.151	1.174	0.987	0.975	855	1467	738	15.4	16.8
Mean	0.281	0.325	1.011	1.055	0.951	0.939	669	1125	456	11.4	10.0

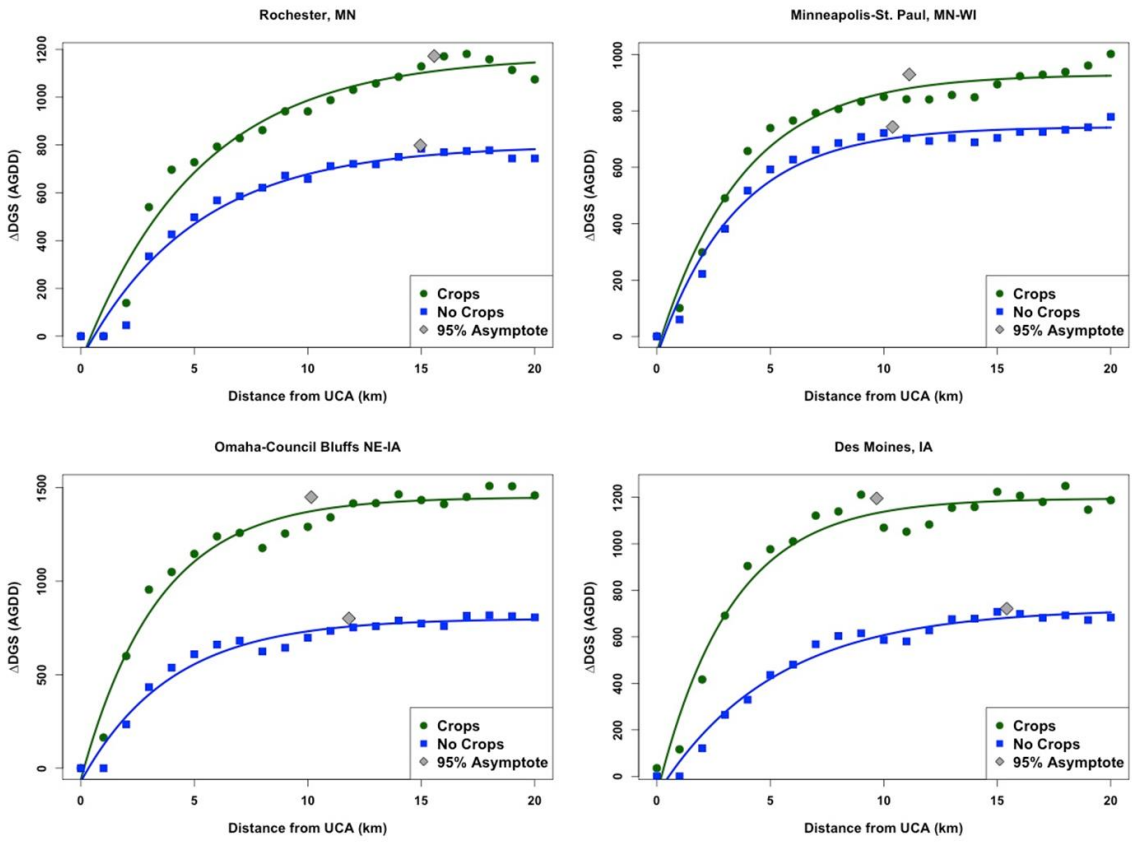

Figure 25. Exponential trend model fit to ΔDGS_{AGDD} as a function of distance from nearest UCA for four selected cities. Differences in ΔDGS_{AGDD} calculated with croplands (green) and without croplands (blue) are evident, particularly in the predominantly agricultural Omaha-Council Bluffs, NE-IA, and Des Moines, IA, regions compared to the Rochester, MN, and Minneapolis-St. Paul, MN-WI, regions where forests and herbaceous land covers are more widely distributed. The grey diamonds show where the exponential model reaches 95% of asymptotic values, used to calculate the magnitude of ΔDGS_{AGDD} and the distance at which urban effects become insignificant.

ΔDGS_{AGDD}: Regional Comparison

It appears that the impacts of urban areas and UHIs on the seasonal development of vegetation are independent of population size, which is congruent with the previous study

from which I used as the methodological basis of the exponential trend model analysis (Zhang et. al 2004a). However, the total area influenced by urban areas is larger in cities with greater area (Figures 22-23, yellow lines). Figure 26 shows the relationship between latitude and ΔDGS_{AGDD}. In orange are ΔDGS_{AGDD} for each city calculated with croplands, and in blue are ΔDGS_{AGDD} calculated without croplands. It appears that ΔDGS_{AGDD} decreases with increasing latitude in Figure 26a, however if we convert ΔDGS_{AGDD} into ΔDGS_{days} (by dividing ΔDGS_{AGDD} by the average daily GDD for each region) the relationship becomes less significant (Figure 26b). If we normalize ΔDGS_{AGDD} as a percentage of the total mean DGS_{AGDD} by urban region, the relationship becomes even less significant (Figure 26c), and the slope is not significantly different from zero for ΔDGS_{AGDD} with croplands excluded (Figure 26c, blue). The trend in the relationship between ΔDGS_{AGDD} as a function of latitude for the analysis including croplands is likely demonstrating the greater *presence* of agriculture in the urban regions located farther south than in the more heavily forested and herbaceous regions surrounding the northern urban cities (Figure 24). This suggests that urban influence on local atmospheric conditions is relatively uniform and proportionally not influenced by latitude. That is, the exponential trend in ΔDGS_{AGDD} found in this study is not caused by differences in latitude, but rather by urban areas and their subsequent UHIs.

Based on the results from the equivalence tests between DGS_{AGDD} in urban areas and surrounding rural regions, and the aforementioned differences in DGS_{AGDD} found with increasing distance from urban core areas, I fail to reject hypothesis A2. I conclude that duration of growing season for perennial vegetation LCTs decreases with distance from urban core areas. I found growing season length to differ by approximately 1 month

between urban areas and their surrounding rural regions. I also found the effects of urban alteration of local atmospheric conditions to extend around 11 km from UCAs.

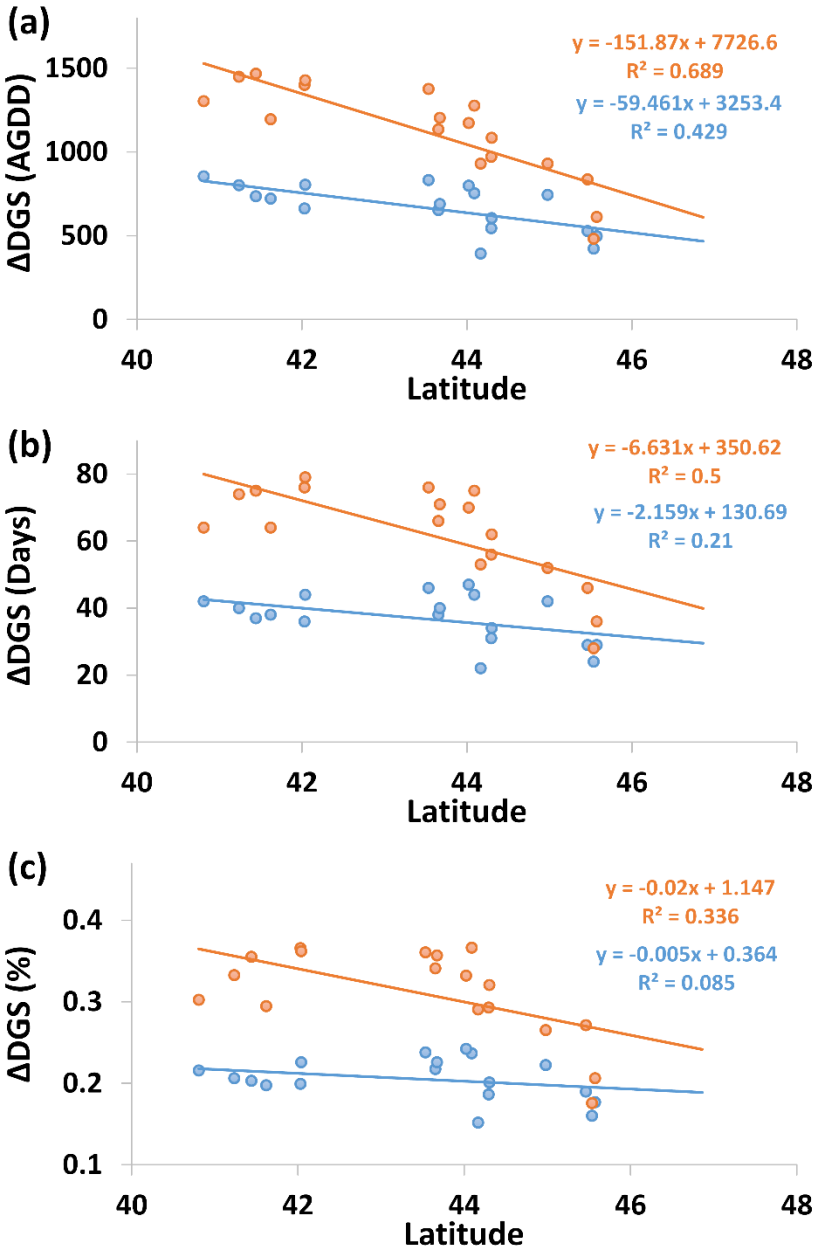

Figure 26. ΔDGS_{AGDD} in terms of (a) AGDD, (b) calendar days, and (c) percentage of mean DGS_{AGDD} for results from model fit with (orange) and without (blue) croplands. Notice that ΔDGS is significantly related to latitude in terms of total AGDD (a), but not relative (%) ΔDGS (c).

Linear Regression: Half-TTP$_{NDVI}$ vs. PH$_{NDVI}$

A previous study (Krehbiel, Jackson, and Henebry 2015) found a linear relationship between half-TTP$_{NDVI}$ and PH$_{NDVI}$ for a sample of forest and developed WELD pixels in Omaha, NE and Minneapolis-St. Paul, MN. The relationship was not found in cropland pixels due to high variation in half-TTP$_{NDVI}$ (Krehbiel, Jackson, and Henebry 2015). I found mixed results in fitting a positive linear model to developed, forest, herbaceous, and cropland pixels in my study (Figure 27). In general, I also found high variation in half-TTP$_{NDVI}$ for cropland pixels. Forest pixels exhibit higher values in both PH$_{NDVI}$ as well as half-TTP$_{NDVI}$ than herbaceous and developed perennial LCTs.

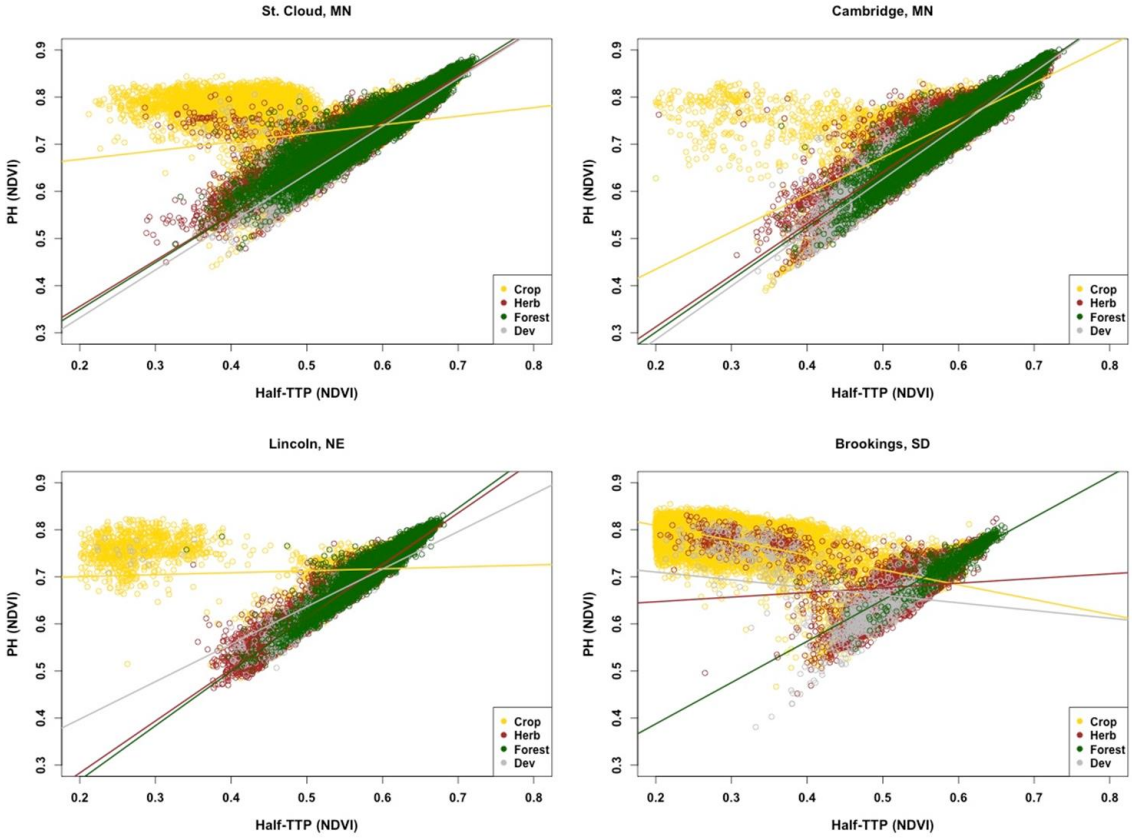

Figure 27. Examples of linear regression model fit to PH$_{NDVI}$ vs. Half-TTP$_{NDVI}$ for four selected urban regions. Note the large variation in Half-TTP$_{NDVI}$ for croplands (yellow) and positive linear relationships seen in the three perennial vegetation LCTs.

Due to the high number of observations, I use a coefficient of determination threshold of 0.8 for each linear regression fit in addition to a significant p-value (< 0.05) to indicate whether or not a significant linear relationship exists between half-TTP_{NDVI} and PH_{NDVI} by land cover type. Table 4 summarizes the results obtained for each individual urban region. All of the plots of half-TTP_{NDVI} vs. PH_{NDVI} by LCT are found in Appendix IV. The model fit crossed the 0.8 threshold for 13 out of the 19 urban regions for forest pixels, followed by 5/19 for herbaceous, and 3/19 for developed LCTs. The positive linear regression model fit was insignificant for cropland pixels in all cases. Three out of the 19 study cities have a significant relationship in all three perennial LCTs: Cambridge, MN, Minneapolis-St. Paul, MN, and St. Cloud, MN (Figure 27, Table 4). Geographically, these three cities are surrounded by a much larger portion of forest and herbaceous LCTs than most of the other urban regions (Figure 24). Based on the inconclusive results, I reject hypothesis A3. A positive linear relationship exists between model-derived half-TTP_{NDVI} and PH_{NDVI} for the majority of cases for forest pixels. A positive linear relationship does not exist for annual croplands in any cases. However, a positive linear relationship was not found in the majority of urban regions for herbaceous and developed LCTs.

Table 4. Linear regression model coefficient of determination (R^2) by LCT for all 19 study cities. $R^2 \geq 0.8$ indicates a significant relationship.

City	Cropland R^2	Forest R^2	Herbaceous R^2	Developed R^2
Aberdeen, SD	0.48	0.90	0.35	0.12
Albert Lea, MN	0.20	0.66	0.38	0.07
Ames, IA	0.27	0.92	0.59	0.02
Austin, MN	0.25	0.68	0.10	0.08
Brookings, SD	0.45	0.76	0.02	0.04
Cambridge, MN	0.58	0.93	0.91	0.90
Des Moines, IA	0.02	0.92	0.81	0.21
Fargo, ND	0.03	0.88	0.70	0.47
Faribault, MN	0.09	0.87	0.71	0.17
Fremont, NE	0.24	0.67	0.45	0.03
Lincoln, NE	0.01	0.90	0.93	0.59
Mankato, MN	0.08	0.81	0.72	0.20
Marshalltown, IA	0.10	0.93	0.77	0.15
MSP, MN	0.02	0.89	0.85	0.86
Omaha, NE	0.24	0.89	0.66	0.16
Owatonna, MN	0.25	0.81	0.45	0.01
Rochester, MN	0.12	0.77	0.08	0.03
Sioux Falls, SD	0.23	0.68	0.18	0.13
St. Cloud, MN	0.07	0.93	0.88	0.85

DISCUSSION

Urban Spatial Arrangement

I expected to find that the duration of growing season in green core areas would be shorter than in urban extent areas, but longer than regions outside of the urban extent. Duration of growing season is significantly longer in urban extent areas compared to regions outside of the urban extent for all of the 19 cities analyzed. However, duration of growing season is not significantly longer in urban extent areas compared to green core areas as expected. I thought that duration of growing season would be lower in green core areas due to the cooling effects of green vegetation. For example, one study reported that urban parks help control urban temperatures due to 300% higher evaporation rates than the surrounding urbanized area (Spronken-Smith, Oke, and Lowry 2000). Another study found that green areas and parks reduce cooling load by 10% (Yu and Hien 2006). An experiment stated that a 600 m^2 park was able to decrease temperatures by 1.5°C (Ca et al. 1998). However, one limitation of my study is the relatively coarse spatial resolution (1,000,000 m^2) of the MODIS-LST product that was used to derive accumulated growing degree-days. However, although this study did not find significant differences between duration of growing season in green core areas vs. urban extent areas, Figure 28 demonstrates that duration of growing season is not spatially uniform throughout cities. It is evident that duration of growing season is longer near urban core areas (Figure 28; purple) than in other regions of the city. Future studies should explore other strategies for dividing cities into spatial regions, perhaps using Local Climate Zones (LCZs) as outlined by the recently launched World Urban Database and Portal Tool project (Mills et al. 2015).

The finding that both green core areas and urban extent areas have significantly higher duration of growing season than areas outside of the urban extent can be attributed to urban areas modulating local atmospheric conditions, namely via increased temperatures and consequently longer growing seasons as a result of the UHI effect. However, there are other factors that may also contribute to the difference in duration of growing season between urban and rural areas, including decreased wind speed, increased water availability as a result of urban irrigation, and differences in urban-rural species composition. However, the finding that maximum NDVI is significantly lower in urban areas than surrounding rural areas suggests that water availability is likely not the main limiting factor in the Upper Midwest, a region that experiences relatively stable precipitation patterns and quantities. If urban irrigation were the main factor contributing to increased duration of growing season, I would expect maximum NDVI to be lower in areas outside of the urban extent, which was not found in this study. As a caveat, it is difficult to draw conclusions on maximum NDVI in cities due to the heterogeneous nature of the urban land surface; pixels that are a mixture of an urban lawn and a rooftop, for example, will exhibit lower maximum NDVI values due to the impervious surface being sensed.

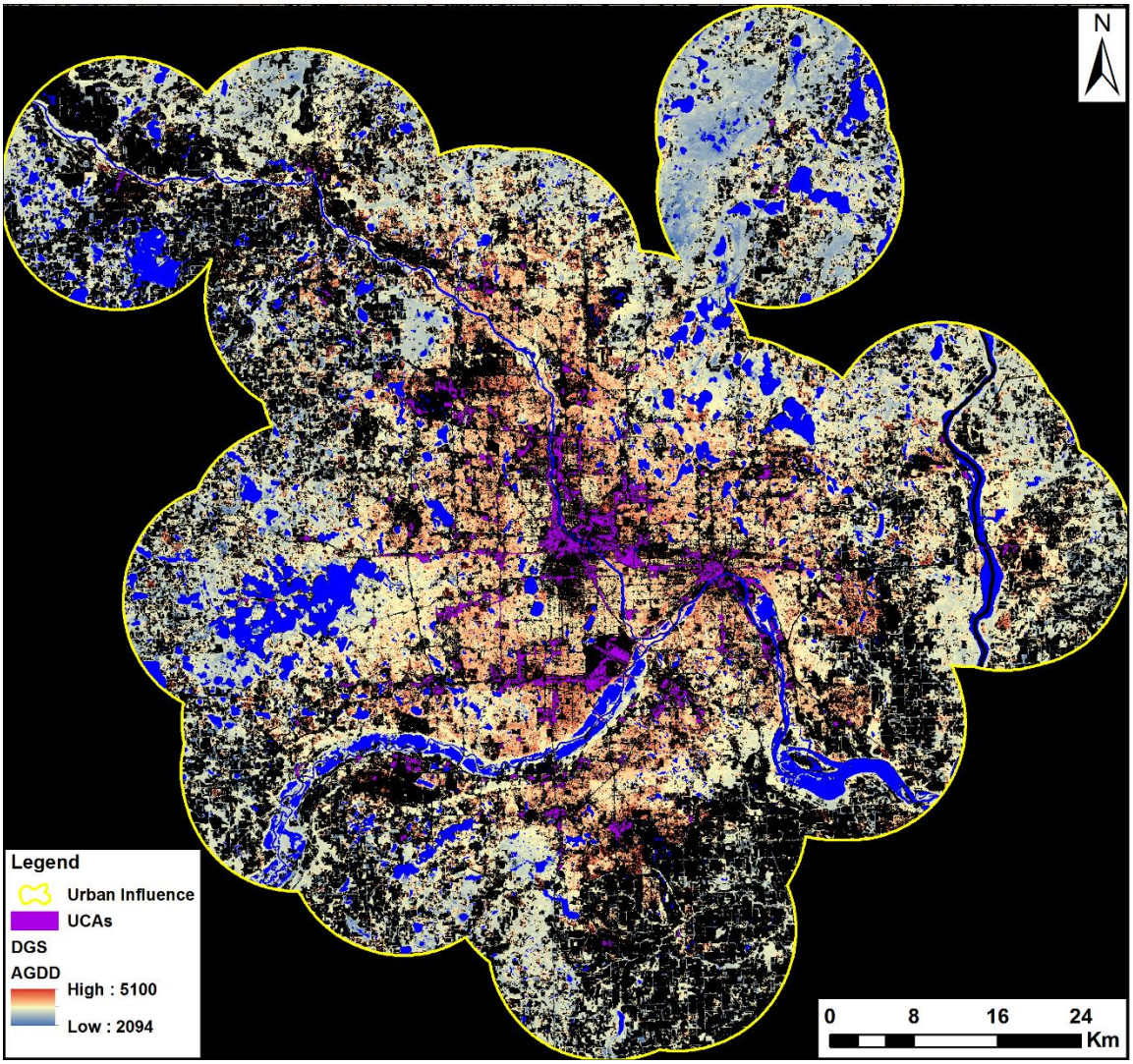

Figure 28. DGS_{AGDD} zoomed into the region of significant urban effects over the Minneapolis-St. Paul, MN-WI, urban region. Notice the spatial variation in DGS_{AGDD}, with local areas of higher DGS_{AGDD} (shades of dark red) concentrated in proximity to UCAs (purple).

Urban Impacts on DGS_{AGDD}: Perennial Vegetation vs. Annual Croplands

The analysis of ΔDGS_{AGDD} demonstrated that urban areas and UHIs influence the local thermal conditions inside of cities and extend into the urban periphery. On average, this study found that UHIs affect growing season length by over 600 AGDD and the

effects extend around 11 km from highly impervious, densely urbanized urban core areas. This finding has major implications on land surface phenology in urban to peri-urban environments. To illustrate, if we say that an average growing season day accumulates 20 growing-degree days, and then divide 600 AGDD by 20, this equates to a difference in the duration of growing season by approximately 1 month between urban areas and surrounding rural areas that are not significantly influenced by local urban atmospheric modification (mainly UHI effects). Note that these results are from the analysis of only perennial vegetation land covers (developed, forest, herbaceous). Perennial vegetation land cover types in this study exhibit a linear trend between peak height in NDVI and NDVI at half-thermal time to peak, suggesting that the seasonal development of perennial vegetation is driven by local atmospheric conditions, namely thermal time. This observation aligns with plant development theory, or the idea that higher temperatures prompt earlier growth in heat-sensitive species (Menzel 2000). Controlling the analysis to strictly perennial vegetation land cover types provides a higher level of confidence that the results are indeed due to the influence of UHI effects rather than differences in land cover type, specifically between annual croplands and perennial vegetation.

Incorporating croplands is, however, useful because it demonstrates the differences in *green-on* season between urban and rural areas, or the time period of the year where the land surface is covered in green vegetation. The addition of annual croplands into the calculation of change in duration of growing season increased the mean difference between urban and rural duration of growing season to around 1100 AGDD. To put it into perspective, that is ~ 2 months difference in the annual time period where the land surface is covered in green vegetation. At first, this may sound like an erroneous result;

however, the major crops grown in the Upper Midwest, namely maize and soybeans, do not begin to develop as soon as the growing season has commenced for perennial vegetation. Rather, the seasonal development of crops such as maize and soybeans is driven largely by external (non-atmospheric) anthropogenic factors including crop management, such as field accessibility, the timing of planting and harvest, and the use of irrigation. This phenomenon is confirmed by the high variation in the rate of vegetation green-up illustrated in cropland pixels in Figure 27. It is not unusual for maize and soybean fields in the Upper Midwest to be mostly bare soil in April-May and either dried-out crops or crop harvest residue in September-October. Meanwhile, perennial vegetation generally begins developing with the commencement of the growing season and ends after the first hard freeze, which are undoubtedly much earlier, and later, respectively, than the duration of green-on season for maize and soybeans. This finding has major implications for urban-rural differences in heat storage and release during different periods of the year. During the summer months when the crop canopy is fully developed, green vegetation redistributes energy absorbed during the day through evapotranspiration, leading to cooler temperatures in the rural regions surrounding cities (Gallo et al. 1993). At the regional scale, relative change in duration of growing season does not appear to be significantly related to urban extent, population, or latitude. This finding suggests that the distance and magnitude that urban areas influence vegetation in and near cities is relatively uniform independent of city size. However, larger urban areas have a greater impact on local atmospheric conditions in terms of area.

The positive linear relationship found in the rate of vegetation green-up vs. maximum NDVI in perennial vegetation land cover types and the high variation in the

rate of green up for annual croplands suggests that studies of urban heat island impacts on urban land surface phenology need to account for differences in urban/rural land cover types. Because annual cropland phenology is driven largely by agricultural planting schedules, it is not appropriate to use annual cropland land surface phenology metrics in order to draw conclusions on the magnitude and extent of urban heat island effects on land surface phenology in and around cities. Vegetation cover/types that exhibit a natural vegetative response, i.e. a positive linear relationship between the rate of vegetation green-up and maximum NDVI, are more appropriate for research aimed at measuring and monitoring the urban heat island effects on land surface phenology.

CONCLUSIONS

There are multiple remote sensing issues that must be accounted for in order to draw conclusions related to the study of UHI impacts on LSP in and around cities. Past studies of UHI effects on urban LSP have centered on surface observation networks and high temporal/coarse spatial resolution remote sensing datasets. Studies of UHIs using air temperature readings from local meteorological stations have higher spatial resolution but are hampered by poor spatial coverage. Studies of UHIs using coarse resolution data for analyzing urban LSP suffer from mixed pixels that make it extremely difficult to account for differences in LSP by LCT. There exists a need for more spatially extensive, higher spatial resolution data products to capture phenological patterns in areas with heterogeneous land cover and external drivers such as urban areas that are a mixture of land cover/land uses and experience microclimatic influences, namely the UHI effect (Fisher, Mustard, and Vadeboncoeur 2006; Melaas, Friedl, and Zhu 2013). Using Landsat data for phenological studies allows for local to regional scale analyses, offering a spatial

resolution that is useful for exploring factors that influence phenology including land use and urban heat islands (Melaas, Friedl, and Zhu 2013).

This regional study leverages multiple datasets from multiple sensors at relatively high spatial resolutions in order to solve the tradeoff between high spatial and temporal resolution, enabling research to be carried out while controlling for LCT, and with full spatial coverage in and around cities. Fitting the CxQ LSP model to the decade of available observations provides a strategy for dealing with the low number of observations that often restrict Landsat studies. This research provides a framework for studying the impacts of urban areas and UHIs on the seasonal development of vegetation at a spatial resolution that is useful and necessary in highly complex, heterogeneous urban areas. The results found in this study highlight the need for future research of UHI-related impacts on urban LSP in order to account for differences in LSP between annual croplands and perennial vegetation covers. Also, DGS_{AGDD} was found to increase with proximity to densely impervious, urban core areas, demonstrating the need to identify local "hotspots" within urban areas that may disproportionately produce warmer atmospheric conditions. The results found in this study demonstrating the drastic difference in the DGS_{AGDD} and the extent of urban influence on DGS_{AGDD} highlights the necessity for urban land surface models to accurately represent the seasonal development of vegetation in and nearby cities. Future urbanization will only increase the amount of Earth's land surface that is significantly impacted by urban areas and subsequent UHI effects. Future studies will model LSP metrics before and after land cover changes as urbanization occurs along the urban periphery. This step should reduce the number of

pixels within cities that were excluded from the analysis due to poor CxQ LSP model fit, and increase our understanding of the impacts of urbanization on LSP.

This study provides much needed and currently lacking information on (1) the differences in the seasonal development of vegetation between urban and rural areas of the Upper Midwest, (2) the magnitude and extent of UHI effects on the seasonal development of vegetation in small to medium sized cities and (3) the differences in land surface phenology between annual croplands and perennial urban vegetation in the Upper Midwest. More importantly, this study provides a framework for alleviating the resolution problems that have restricted studies of UHI effects on urban LSP in the past. This information can be used to inform a variety of interests, including researchers interested in assessing UHI effects on urban LSP in other regions, urban land surface modelers, urban ecologists, urban policy-makers, city planners and developers, meteorologists, and climatologists.

REFERENCES

Angel, S., Parent, J., Civco, D. L., and A. M. Blei. 2011. *Making room for a planet of cities.* Cambridge, MA, USA: Lincoln Institute of Land Policy.

Arnfield, A. J. 2003. Two decades of urban climate research: a review of turbulence, exchanges of energy and water, and the urban heat island. *International Journal of Climatology* 23(1): 1-26.

Avissar, M. 2005. The effects of urban patterns on ecosystem function. *International Regional Science Review* 28(2): 168-192.

Balchin, W. G. V. and N. Pye. 1947. A micro-climatological investigation of bath and the surrounding district. *Quarterly Journal of the Royal Meteorological Society* 73: 297-323.

Bechtel, B. and K. J. Schmidt. 2011. Floristic mapping data as a proxy for the mean urban heat island. *Climate Research* 49: 45–58.

Best, M. J. 2006. Progress towards better weather forecasts for city dwellers: from short range to climate change. *Theoretical and Applied Climatology* 84: 47-55.

Best, M. J., and C. S. B. Grimmond. 2013. Analysis of the seasonal cycle within the first international urban land-surface model comparison. *Boundary-layer Meteorology* 146(3): 421-446.

Best, M. J., and C. S. B. Grimmond. 2014. Key conclusions of the first international urban land surface model comparison project. *Bulletin of the American Meteorological Society*.

Bettencourt, L. M. A. 2013. The Origins of scaling in cities. *Science* 340(6139): 1438-1441.

Bettencourt, L. M. A., J. Lobo, D. Helbing, C. Kühnert, and G. B. West. 2007. Growth, innovation, scaling, and the pace of life in cities. *Proceedings of the National Academy of Sciences* 104(17): 7301-7306.

Bland, J. M., and D. G. Altman. 1995. Multiple significance tests: The Bonferroni method. *British Medical Journal* 310(6973): 170.

Bornstein, R. D. 1968. Observations of the urban heat island effect in New York City. *Journal of Applied Meteorology* 7(4): 575-582.

Bowler, D. E., L. Buyung-Ali, T. M. Knight, and A. S. Pullin. 2010. Urban greening to cool towns and cities: A systematic review of the empirical evidence. *Landscape and Urban Planning* 97: 147-155.

Bureau of Economic Analysis. 2011. Regional economic accounts. U.S. Department of Commerce. Available online at: http://bea.gov/regional/index.htm.

Ca, V. T., T. Asaeda, and E. M. Abu. 1998. Reductions in air-conditioning energy caused by a nearby park. *Energy and Buildings* 29: 83-92.

Carlin, J. B., and L. W. Doyle. 2002. Statistics for clinicians. *Journal of Paediatrics and Child Health* 38: 300-304.

Chandler, T. J. 1976. Urban climatology and its relevance to urban design. World Meteorological Organization 438(149).

Changnon, S. A., K. E. Kunkel, and B. C. Reinke. 1996. Impacts and responses to the 1995 heat wave: a call to action. *Bulletin of the American Meteorological Society* 77(7): 1497-1506.

Chen, X., H. Zhao, P. Li, and Z. Yin. 2006. Remote sensing image-based analysis of the relationship between urban heat island and land use/cover changes. *Remote Sensing of Environment* 104: 133-146.

Childe, V. G. 1950. The urban revolution. *The Town Planning Review* 21(1): 3-17.

Costanza, R., L. Graumlich, W. Steffen, C. Crumley, J. Dearing, K. Hibbard, R. Leemans, C. Redman, and D. Schimel. 2007. Sustainability or collapse: What can we learn from integrating the history of humans and the rest of nature?. *AMBIO: A Journal of the Human Environment* 36(7) 522-527.

de Beurs, K. M., and G. M. Henebry. 2004. Land surface phenology, climatic variation, and institutional change: Analyzing agricultural land cover change in Kazakhstan. *Remote Sensing of Environment* 89(4): 497-509.

de Beurs, K. M., and G. M. Henebry. 2005. A statistical framework for the analysis of long image time series. *International Journal of Remote Sensing* 26(8): 1551-1573.

de Beurs, K. M., and G. M. Henebry. 2010. Spatio-temporal statistical methods for modelling land surface phenology. In *Phenological Research*, eds. I. L. Hudson and M. R. Keatley, 177-208. Netherlands: Springer.

de Beurs, K. M., Henebry, G. M., Owsley, B. C., and I. Sokolik. 2015. Using multiple remote sensing perspectives to identify and attribute land surface dynamics in Central Asia 2001-2013. *Remote Sensing of Environment* 170: 48-61.

Deosthali, V. 2000. Impact of rapid urban growth on heat and moisture islands in Pune City, India. *Atmospheric Environment* 34: 2745-2754.

Fisher, J. I., J. F., Mustard, and M. A. Vadeboncoeur. 2006. Green leaf phenology at Landsat resolution: Scaling from the field to the satellite. *Remote Sensing of Environment* 100(2): 265-279.

Foody, G. M. 2009. Classification accuracy comparison: Hypothesis tests and the use of confidence intervals in evaluations of difference, equivalence, and non-inferiority. *Remote Sensing of Environment* 113: 1658-1663.

Franken E. 1955. Der Beginn der Forsythienbluete in Hamburg 1955. *Meteorologische Rundschau* 8: 113–115

Gallo, K. P., A. L. McNab, T. R. Karl, J. F. Brown, J. J. Hood, and J. D. Tarpley. 1993. The use of a vegetation index for assessment of the urban heat island effect. *International Journal of Remote Sensing* 14(11): 2223-2230.

Gallo, K. P., J. D. Tarpley, A. L. McNab, and T. R. Karl. 1995. Assessment of urban heat islands: a satellite perspective. *Atmospheric Research* 37(1): 37-43.

Gödde, M. and R. Wittig. 1983. A preliminary attempt at a thermal division of the town of Münster (North Rhine-Westphalia, West Germany) on a floral and vegetational basis. *Urban Ecology* 7(3): 255–262.

Goodman, S. N. 1999. Toward evidence-based medical statistics, 1: the P value fallacy. *Annals of Internal Medicine* 130: 995-1004.

Graham, S. and C. Parkinson. 2015. Aqua Project Science. National Aeronautics and Space Administration. Available online at: http://aqua.nasa.gov/.

Grimm, N. B., S. H. Faeth, N. E. Golubiewski, C. L. Redman, J. Wu, X. Bai, and J. M. Briggs. 2008. Global change and the ecology of cities. *Science* 319(5864): 756-760.

Hall, D. K., G. A. Riggs, and V. V. Salomonson. 2006. updated weekly. *MODIS/Terra Snow Cover 8-day L3 Global 500m Grid V005*, [1/1/2003-12/26/2012]. Boulder, Colorado USA: National Snow and Ice Data Center. Digital media. Available online at: http://nsidc.org/data.

Hartmann, D. L., A. M. G. Klein Tank, M. Rusticucci, L. V. Alexander, S. Brönnimann, Y. Charabi, F. J. Dentener, E. J. Dlugokencky, D. R. Easterling, A. Kaplan, B. J. Soden, P. W. Thorne, M. Wild, and P. M. Zhai. 2013. Observations: Atmosphere and Surface. In *Climate Change 2013: The physical science basis*. Contribution of Working Group I to the Fifth Assessment Report of the Intergovernmental Panel on Climate Change, eds. T. F. Stocker, D. Qin, G. K. Plattner, M. Tignor, S. K. Allen, J. Boschung, A. Nauels, Y. Xia, V. Bex, and P. M. Midgley, 161-218. Cambridge, UK and New York, NY: Cambridge University Press.

Herold, M. 2009. Some recommendations for global efforts in urban monitoring and assessments from remote sensing. In *Global mapping of human settlement: experiences, datasets, and prospects,* eds. P. Gamba and M. Herold, 11-27. Boca Raton, FL: Taylor and Francis Group: CRC Press.

Homer, C. H., J. A., Fry, and C. A. Barnes. 2012. The national land cover database. *US Geological Survey Fact Sheet* 3020(4): 1-4.

Howard, L. 1833. *The Climate of London*. Vols I-III, London.

Hu, L., and N. A. Brunsell. 2013. The impact of temporal aggregation of land surface temperature data for surface urban heat island (SUHI) monitoring. *Remote Sensing of Environment* 134: 162-174.

Imhoff, M. L., P. Zhang, R. E. Wolfe, and L. Bounoua. 2010. Remote sensing of the urban heat island effect across biomes in the continental USA. *Remote Sensing of Environment* 114(3): 504-513.

IPCC. 2014. Climate change 2014: Impacts, adaptation, and vulnerability summary for policymakers. Fifth Assessment Report of the Intergovernmental Panel on Climate Change 1-44. Cambridge, UK and New York, NY: Cambridge University Press.

Jackson, T. L., J.J. Feddema, K. W. Oleson, G. B. Bonan, and J. T. Bauer. 2010. Parameterization of urban characteristics for global climate modeling. *Annals of the Association of American Geographers* 100(4): 848-865.

Jin, S., L. Yang, P. Danielson, C. Homer, J. Fry, and G. Xian. 2013. A comprehensive change detection method for updating the National Land Cover Database to circa 2011. *Remote Sensing of Environment* 132: 159-175.

Jochner, S. C., T. H. Sparks, N. Estrella, and A. Menzel. 2012. The influence of altitude and urbanisation on trends and mean dates in phenology (1980–2009). *International Journal of Biometeorology* 56(2): 387-394.

Kates, R. W., B. L. Turner II, and W. C. Clark. 1990. The great transformation. In *The earth as transformed by human action: global and regional changes in the biosphere over the past 300 years,* eds. B. L. Turner II, W. C. Clark, R. W. Kates, J. F.Richards, J. T. Mathews, and W. B. Meyer, 1-18. New York, NY: Cambridge University Press.

Kim, Y. H., and J. J. Baik. 2002. Maximum urban heat island intensity in Seoul. *Journal of Applied Meteorology* 41: 651-653.

Kopec, R. J. 1970. Further observations of the urban heat island in a small city. *Bulletin of the American Meteorological Society* 51(7): 602-606.

Krehbiel, C. P., Jackson, T., and G. M. Henebry. 2015. Web-Enabled Landsat Data time series for monitoring urban heat island impacts on land surface phenology. *IEEE Journal of Selected Topics in Applied Earth Observations and Remote Sensing*, http://dx.doi.org/10.1109/JSTARS.2015.2496951.

Landsberg, H. E. 1981. The Urban Climate. Academic Press, New York, New York, USA.

Lo, C. P. and D. A. Quattrochi. 2003. Land-use and land-cover change, urban heat island phenomenon, and health implications: A remote sensing approach. *Photogrammetric Engineering & Remote Sensing* 69(9): 1053-1063.

Maccherone, B. and S. Frazier. 2015. About MODIS. National Aeronautics and Space Administration. Available online at: http://modis.gsfc.nasa.gov/about/.

Marsh, G. P. [1864] 1965. Introductory. In *Man and nature* (Reprint), ed. by D. Lowenthal, 7-52. Cambridge, MA: The Belnap Press of Harvard University Press.

McCarthy, M. P., M. J. Best, and R. A. Betts. 2010. Climate change in cities due to global warming and urban effects. *Geophysical Research Letters* 37: 1-5.

Melaas, E. K., M. A. Friedl, and Z. Zhu. 2013. Detecting interannual variation in deciduous broadleaf forest phenology using Landsat TM/ETM+ data. *Remote Sensing of Environment* 132: 176-185.

Menzel, A. 2000. Trends in phenological phases in Europe between 1951 and 1996. *International Journal of Biometeorology* 44(2): 76-81.

Mills, G., J. Ching, L. See, B. Bechtel, and M. Foley. 2015. An introduction to the WUDAPT project. In *9th International Conference on Urban Climate, Toulouse*, http://www.wudapt.org/wp-content/uploads/2015/05/Mills_etal_ICUC9.pdf.

Myneni, R. B., F. G. Hall, P. J. Sellers, and A. L. Marshak. 1995. The interpretation of spectral vegetation indexes. *IEEE Transactions on Geoscience and Remote Sensing* 33(2): 481-486.

NASA Land Processes Distributed Active Archive Center (LP DAAC). 2001. MODIS Level 3. USGS/Earth Resources Observation and Science (EROS) Center, Sioux Falls, South Dakota. Available online at: https://lpdaac.usgs.gov/.

Oke, T. R. 1982. The energetic basis of the urban heat island. *Quarterly Journal of the Royal Meteorological Society* 108:1-24.

Oke, T. R. 1987. *Boundary layer climates*. London, UK: Methuen & Co. 2nd edition.

Oke, T. R., G. T. Johnson, D. G. Steyn, and I. D. Watson. 1991. Simulation of nocturnal surface urban heat islands under 'ideal' conditions: Part 2. Diagnosis of causation. *Boundary-Layer Meteorology* 56: 339-358.

Patz, J. A., D. Campbell, T. Holloway, and J. A. Foley. 2005. Impact of regional climate change on human health. *Nature* 438(17): 310-317.

Rao, P. K. 1972. Remote sensing of urban heat islands from an environmental satellite. *Bulletin of the American Meteorological Society* 53(7): 647.

Robine, J. M., S. L. K. Cheung, S. Le Roy, H. Van Oyen, C. Griffiths, J. P. Michel, and F. R. Herrmann. 2008. Death toll exceeded 70,000 in Europe during the summer of 2003. *Comptes Rendus Biologies* 2:171-178.

Roth, M., T. R. Oke, and W. J. Emery. 1989. Satellite-derived urban heat islands from three coastal cities and the utilization of such data in urban climatology. *International Journal of Remote Sensing* 10(11): 1699-1720.

Roy, D. P., J. Ju, K. Kline, P. L. Scaramuzza, V. Kovalskyy, M. Hansen, T. R. Loveland, E. Vermote, and C. Zhang. 2010. Web-enabled Landsat Data (WELD): Landsat ETM+ composited mosaics of the conterminous United States. *Remote Sensing of Environment* 114(1): 35-49.

Sauer, C. O. 1956. The agency of man on the earth. In *Man's role in changing the face of the earth*, ed. by W. L. Thomas, Jr., 2: 49-69. Chicago, IL: The University of Chicago Press.

Schneider, A., M. A. Friedl, and D. Potere. 2009. A new map of global urban extent from MODIS satellite data. *Environmental Research Letters* 4(4): 044003.

Schuirmann, D. J. 1987. A comparison of the two one-sided tests procedure and the power approach for assessing the equivalence of average bioavailability. *Journal of Pharmacokinetics and Biopharmaceutics* 15(6): 657-680.

Schwartz, M. D., J. L. Betancourt, and J. F. Weltzin. 2012. From Caprio's lilacs to the USA National Phenology Network. *Frontiers in Ecology and the Environment* 10(6): 324-327.

Seto, K. C. 2009. Global urban issues: a primer. In *Global mapping of human settlement: experiences, datasets, and prospects,* eds. P. Gamba and M. Herold, 3-9. Boca Raton, FL: Taylor and Francis Group: CRC Press.

Seto, K. C., A. Reenberg, C. G. Boone, M. Fragkias, D. Haase, T. Langanke, P. Marcotullio, D. K. Munroe, B. Olah, and D. Simon. 2012. Urban land teleconnections and sustainability. *Proceedings of the National Academy of Sciences* 109(20): 7687-7692.

Seto, K. C., and P. Christensen. 2013. Remote sensing science to inform urban climate change mitigation strategies. *Urban Climate* 3: 1-6.

Seto, K. C., B. Güneralp, and L. Hutyra. 2012. Global forecasts of urban expansion to 2030 and direct impacts on biodiversity and carbon pools. *Proceedings of the National Academy of Sciences*. 109(40): 16083-16088.

Seto, K. C., M. Fragkias, B. Güneralp, and M. K. Reilly. 2011. A meta-analysis of global urban land expansion. *PLOS One* 6(8): 1-9.

Spronken-Smith, R. A., T. R. Oke, and W. P. Lowry. 2000. Advection and the surface energy balance across an irrigated urban park. *International Journal of Climatology* 20: 1033-1047.

Stott, P. A., D. A. Stone, and M. R. Allen. 2004. Human contribution to the European heatwave of 2003. *Nature* 432: 610-614.

Streutker, D. R. 2003. Satellite-measured growth of the urban heat island of Houston, Texas. *Remote Sensing of Environment* 85(3): 282-289.

Tomlinson, C. J., L. Chapman, J. E. Thornes, and C. J. Baker. 2012. Derivation of Birmingham's summer surface urban heat island from MODIS satellite images. *International Journal of Climatology* 32(2): 214-224.

Tucker, C. J. 1979. Red and photographic infrared linear combinations for monitoring vegetation. *Remote Sensing of Environment* 8(2): 127-150.

U.S. Census Bureau. 2010a. About metropolitan and micropolitan statistical areas. U.S. Department of Commerce. Available online at: http://www.census.gov/population/metro/about.

U.S. Census Bureau. 2010b. Cartographic boundary shapefiles—urban areas. U.S. Department of Commerce. Available online at: https://www.census.gov/geo/maps-data/data/cbf/cbf_ua.html.

United Nations. 2006. World Urbanization Prospects: The 2005 Revision. Department of Economic and Social Affairs, Population Division. (ST/ESA/SER.A/352). http://www.un.org/esa/population/publications/WUP2005/2005WUPHighlights_Final_Report.pdf.

United Nations. 2014. World Urbanization Prospects: The 2014 Revision, Highlights. Department of Economic and Social Affairs, Population Division. (ST/ESA/SER.A/352). http://esa.un.org/unpd/wup/highlights/wup2014-highlights.pdf.

University of North Texas. 2015. Equivalence Testing. [Powerpoint Slides]. Retrieved from: http://www.unt.edu/rss/class/mike/5700/Equivalence%20testing.ppt.

Viña, A., G. M. Henebry, and A. A. Gitelson. 2004. Satellite monitoring of vegetation dynamics: Sensitivity enhancement by the wide dynamic range vegetation index. *Geophysical Research Letters* 31(L04503): 1-4.

Vitousek, P. M., H. A. Mooney, J. Lubchenco, and J. M. Melillo. 2008. Human domination of Earth's ecosystems. In *Urban Ecology*, eds. J. M. Marzluff, E. Shulenberger, W. Endlicher, M. Alberti, G. Bradley, C. Ryan, U. Simon, and C. ZumBrunnen. 3-13. Springer US.

Voogt, J. A. 2002. Urban heat island. In *Encyclopedia of Global Environmental Change*. New York, New York: John Wiley & Sons, 660-666.

Walker, J. J., de Beurs, K. M., & Henebry, G. M. 2015. Land surface phenology along urban to rural gradients in the US Great Plains. *Remote Sensing of Environment* 165: 42-52.

Wang, Z., C. Liu, and A. Huete. 2002. From AVHRR-NDVI to MODIS-EVI: Advances in vegetation index research. *Acta Ecologica Sinica* 23(5): 979-987.

White, M. A., R. R. Nemani, P. E. Thornton, and S. W. Running. 2002. Satellite evidence of phenological differences between urbanized and rural areas of the eastern United States deciduous broadleaf forest. *Ecosystems* 5(3): 260-273.

Xian, G., C. Homer, J. Dewitz, J. Fry, N. Hossain, and J. Wickham. 2011. The change of impervious surface area between 2001 and 2006 in the conterminous United States. *Photogrammetric Engineering and Remote Sensing* 77(8): 758-762.

Yang, L., C. Huang, C. G. Homer, B. K. Wylie, and M. J. Coan. 2003. An approach for mapping large-area impervious surfaces: Synergistic use of Landsat-7 ETM+ and high spatial resolution imagery. *Canadian Journal of Remote Sensing* 29(2): 230-240.

Yu, C., and W. N. Hien. 2006. Thermal benefits of city parks. *Energy and Buildings* 38(2): 105-120.

Zhang, X., M. A. Friedl, C. B. Schaaf, A. H. Strahler, and A. Schneider. 2004a. The footprint of urban climates on vegetation phenology. *Geophysical Research Letters* 31(12): 1-4.

Zhang, X., M. A. Friedl, C. B. Schaaf, and A. H. Strahler. 2004b. Climate controls on vegetation phenological patterns in northern mid- and high latitudes inferred from MODIS data. *Global Change Biology* 10(7): 1133-1145.

APPENDICES

Appendix I: Definitions

Green Core Area— A spatially contiguous area of pixels (> 60 hectares) within the urban extent classified as "Developed, Open Space, Forest, Shrub/Scrub, Grassland/Herbaceous, Pasture/Hay or Wetlands" using the 2011 NLCD LCT product.

Urban Core Area— A spatially contiguous area of pixels (> 10 hectares) within the urban extent classified as "Developed, High Intensity" using the 2011 NLCD LCT product.

Urban Extent—Defined using the cartographic boundary files for urban areas as delineated by the 2010 U. S. Census, provided by the U.S. Census Bureau (U. S. Census Bureau 2010b).

Urban Region—A nominal term for each individual study city and the surrounding rural areas located within the region of interest that are used in the analyses.

Appendix II: Equivalency Test Results

PH_{NDVI}	Outside UE	UE	GCA
MSP, MN	0.721[a]	0.601[b]	0.704[a]
Omaha, NE	0.685[a]	0.608[b]	0.698[a]
Des Moines, IA	0.690[a]	0.602[b]	0.703[a]
Lincoln, NE	0.627[ab]	0.579[b]	0.657[a]
Sioux Falls, SD	0.642[a]	0.540[b]	0.642[a]
Fargo, ND	0.651[a]	0.556[b]	0.684[a]
Rochester, MN	0.729[a]	0.622[b]	0.717[a]
St. Cloud, MN	0.722[a]	0.629[b]	0.695[ab]
Mankato, MN	0.710[a]	0.582[b]	0.704[a]
Ames, IA	0.695[a]	0.589[b]	0.701[a]
Faribault, MN	0.719[a]	0.605[b]	0.731[a]
Marshalltown, IA	0.680[a]	0.584[b]	0.702[a]
Aberdeen, SD	0.614[a]	0.512[b]	0.597[a]
Austin, MN	0.694[a]	0.595[b]	0.707[a]
Fremont, NE	0.657[a]	0.550[c]	0.585[b]
Owatonna, MN	0.697[a]	0.585[b]	0.705[a]
Brookings, SD	0.636[a]	0.553[b]	0.613[ab]
Albert Lea, MN	0.680[a]	0.609[b]	0.677[ab]
Cambridge, MN	0.725[a]	0.583[b]	0.677[a]

Half-TTP$_{NDVI}$	Outside UE	UE	GCA
MSP, MN	0.584^{a}	0.511^{b}	0.582^{a}
Omaha, NE	0.544^{ab}	0.519^{b}	0.586^{a}
Des Moines, IA	0.569^{a}	0.514^{b}	0.591^{a}
Lincoln, NE	0.507^{b}	0.498^{b}	0.551^{a}
Sioux Falls, SD	0.499^{b}	0.464^{b}	0.540^{a}
Fargo, ND	0.523^{a}	0.474^{b}	0.570^{a}
Rochester, MN	0.571^{ab}	0.526^{b}	0.600^{a}
St. Cloud, MN	0.584^{a}	0.528^{b}	0.572^{ab}
Mankato, MN	0.545^{a}	0.483^{b}	0.577^{a}
Ames, IA	0.548^{b}	0.501^{c}	0.591^{a}
Faribault, MN	0.562^{a}	0.511^{b}	0.603^{a}
Marshalltown, IA	0.541^{b}	0.505^{b}	0.593^{a}
Aberdeen, SD	0.482^{a}	0.441^{b}	0.465^{ab}
Austin, MN	0.509^{b}	0.503^{b}	0.591^{a}
Fremont, NE	0.510^{a}	0.471^{b}	0.450^{c}
Owatonna, MN	0.518^{b}	0.493^{b}	0.581^{a}
Brookings, SD	0.503^{ab}	0.476^{b}	0.519^{a}
Albert Lea, MN	0.502^{b}	0.512^{b}	0.560^{a}
Cambridge, MN	0.591^{a}	0.497^{b}	0.560^{a}

TTP	Outside UE	UE	GCA
MSP, MN	2014[b]	2358[a]	2204[ab]
Omaha, NE	2475[a]	2719[a]	2585[a]
Des Moines, IA	2331[b]	2626[a]	2523[ab]
Lincoln, NE	2535[a]	2778[a]	2579[a]
Sioux Falls, SD	2215[b]	2485[a]	2389[ab]
Fargo, ND	1954[b]	2178[a]	2109[ab]
Rochester, MN	2011[b]	2245[a]	2140[ab]
St. Cloud, MN	1912[a]	2167[b]	2098[ab]
Mankato, MN	2153[a]	2286[a]	2237[a]
Ames, IA	2285[a]	2402[a]	2340[a]
Faribault, MN	2070[a]	2210[a]	2137[a]
Marshalltown, IA	2280[a]	2410[a]	2283[a]
Aberdeen, SD	2059[a]	2205[a]	2255[a]
Austin, MN	2102[a]	2165[a]	2053[a]
Fremont, NE	2482[b]	2669[ab]	2681[a]
Owatonna, MN	2121[a]	2256[a]	2160[a]
Brookings, SD	2060[a]	2225[a]	2099[a]
Albert Lea, MN	2192[a]	2163[a]	2087[a]
Cambridge, MN	1878[b]	2133[a]	2107[a]

DGS_{AGDD}	Outside UE	UE	GCA
MSP, MN	3574[b]	4317[a]	4040[a]
Omaha, NE	4267[b]	5128[a]	4903[a]
Des Moines, IA	4251[b]	4889[a]	4800[a]
Lincoln, NE	4315[c]	5160[a]	4742[b]
Sioux Falls, SD	3611[b]	4428[a]	4429[a]
Fargo, ND	3266[b]	3818[a]	3894[a]
Rochester, MN	3428[b]	4157[a]	4070[a]
St. Cloud, MN	3368[b]	3917[a]	3774[a]
Mankato, MN	3498[b]	3866[a]	4019[a]
Ames, IA	3898[b]	4435[a]	4490[a]
Faribault, MN	3464[b]	3995[a]	3940[a]
Marshalltown, IA	3927[b]	4576[a]	4419[a]
Aberdeen, SD	3293[b]	3780[a]	3598[a]
Austin, MN	3251[b]	3920[a]	3872[a]
Fremont, NE	4103[b]	4803[a]	4124[b]
Owatonna, MN	3320[b]	4035[a]	3942[a]
Brookings, SD	3385[b]	4007[a]	3866[a]
Albert Lea, MN	3348[b]	3898[a]	3770[a]
Cambridge, MN	3356[b]	3832[a]	3778[a]

Appendix III: Exponential Model Plots

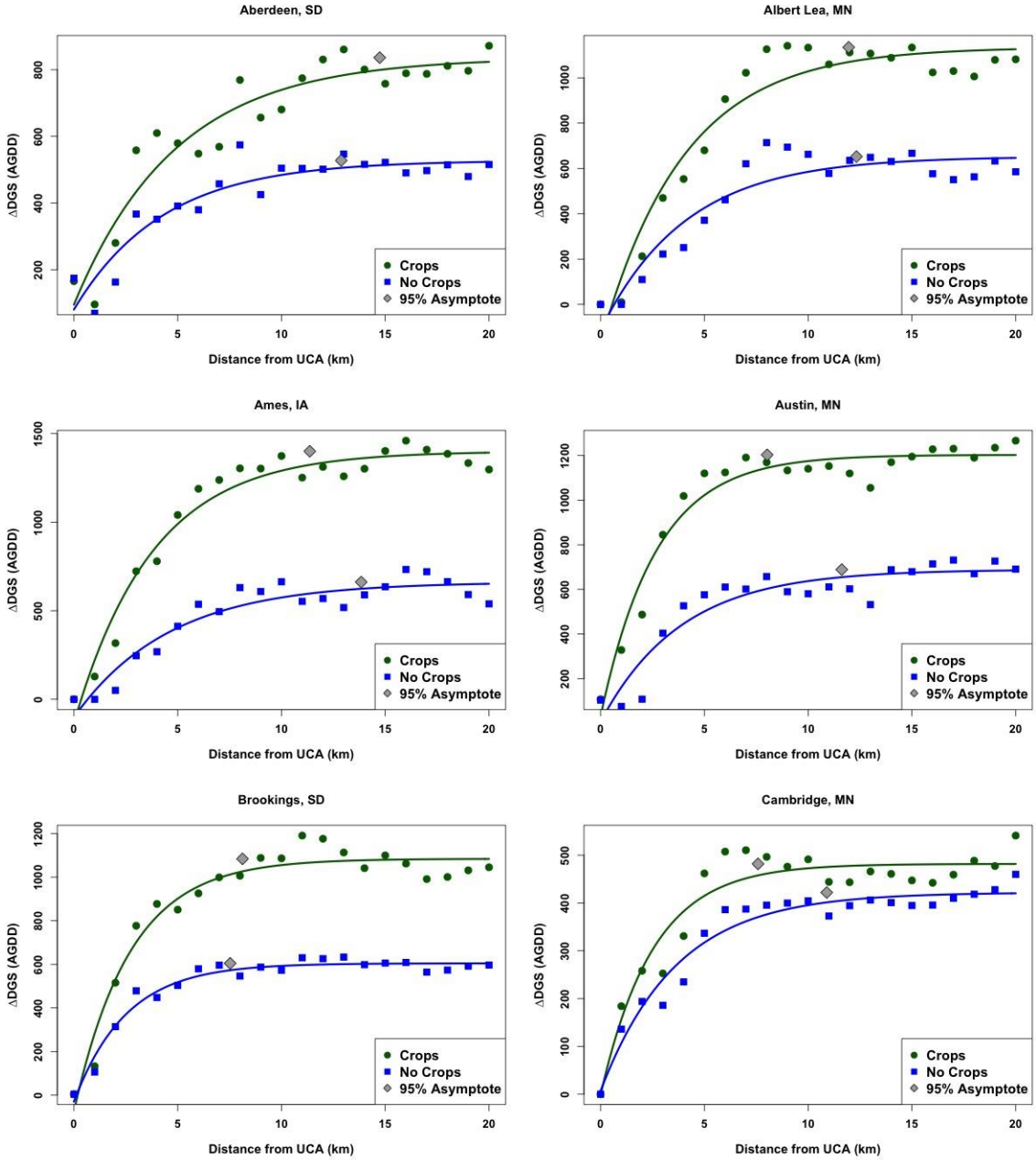

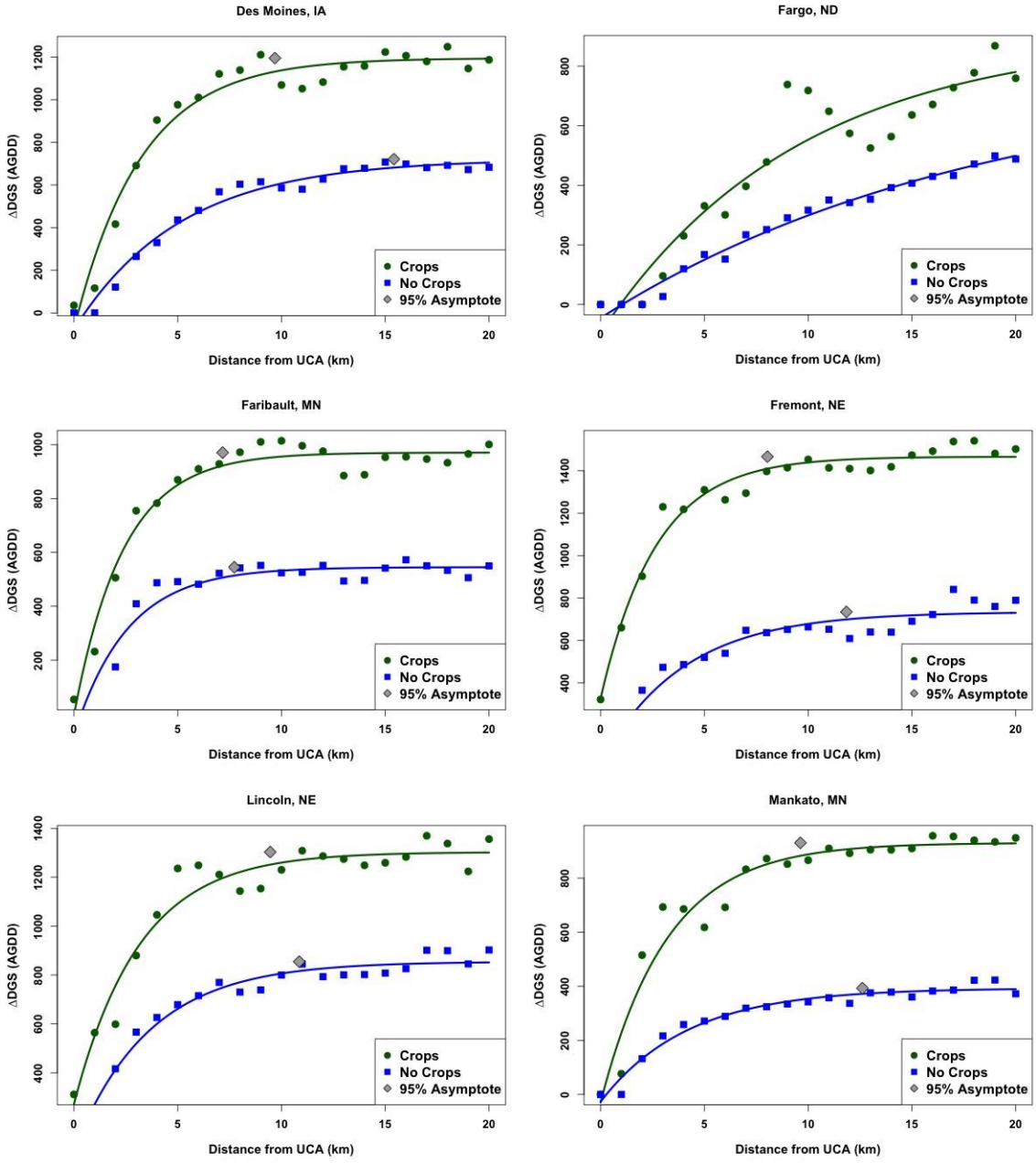
Des Moines, IA
Fargo, ND
Faribault, MN
Fremont, NE
Lincoln, NE
Mankato, MN
ΔDGS (AGDD)
Distance from UCA (km)
Crops
No Crops
95% Asymptote

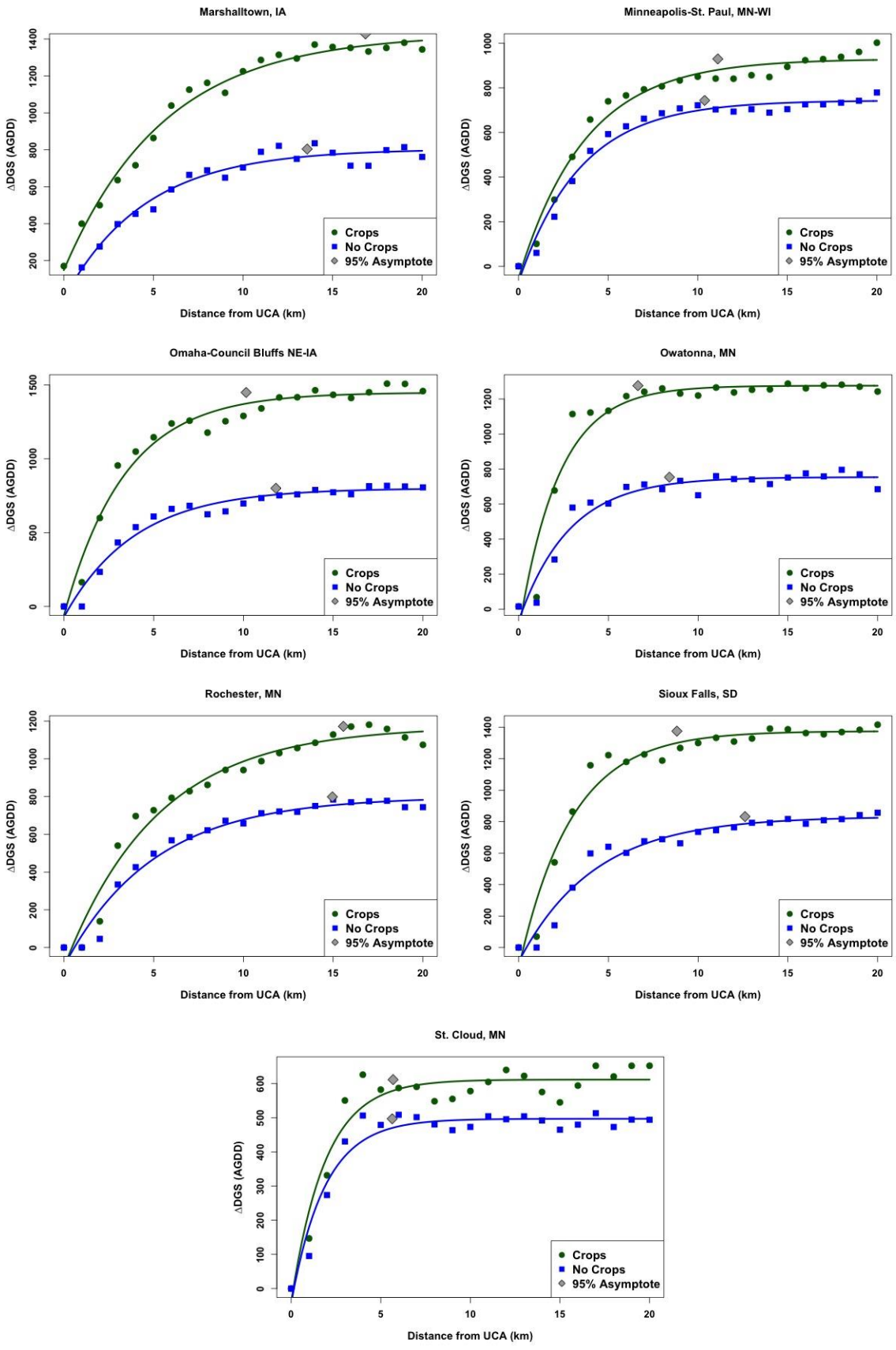
Marshalltown, IA
Minneapolis-St. Paul, MN-WI
Omaha-Council Bluffs NE-IA
Owatonna, MN
Rochester, MN
Sioux Falls, SD
St. Cloud, MN
ΔDGS (AGDD)
Distance from UCA (km)
Crops
No Crops
95% Asymptote

Appendix IV: PH_{NDVI} vs. Half-TTP_{NDVI} Plots

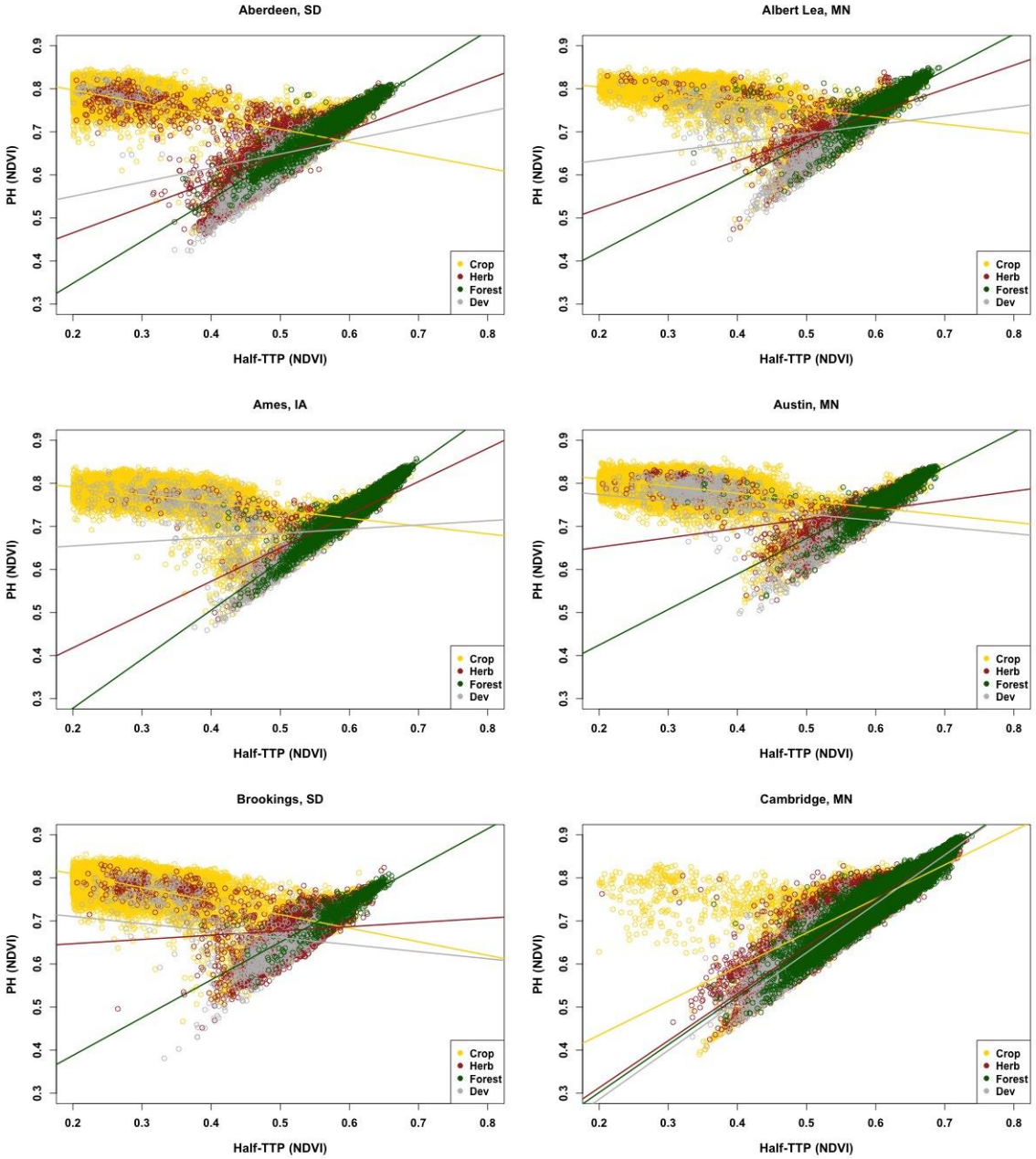

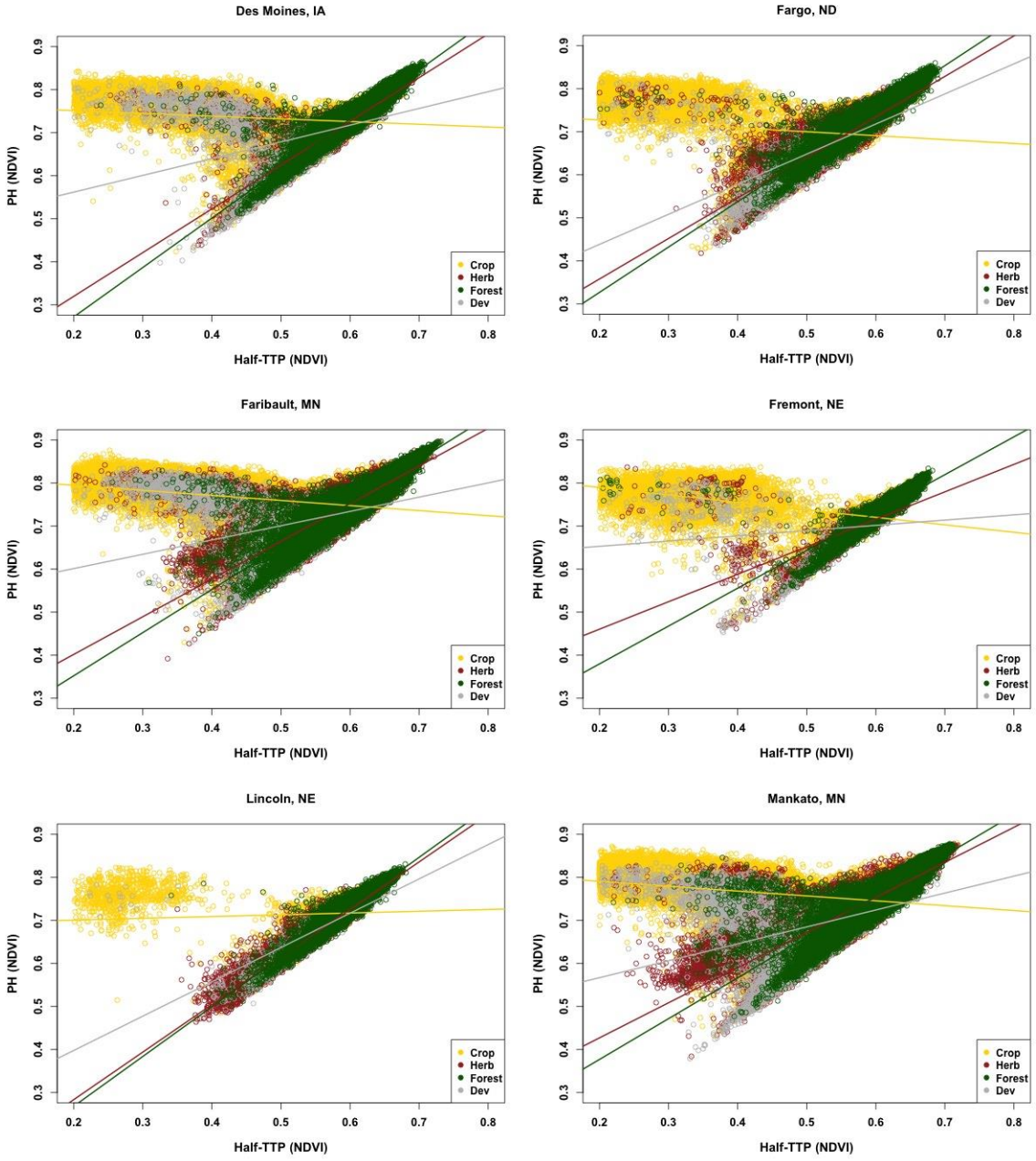
Des Moines, IA
Fargo, ND
Faribault, MN
Fremont, NE
Lincoln, NE
Mankato, MN
PH (NDVI)
Half-TTP (NDVI)
0.3
0.4
0.5
0.6
0.7
0.8
0.9
0.2
Crop
Herb
Forest
Dev

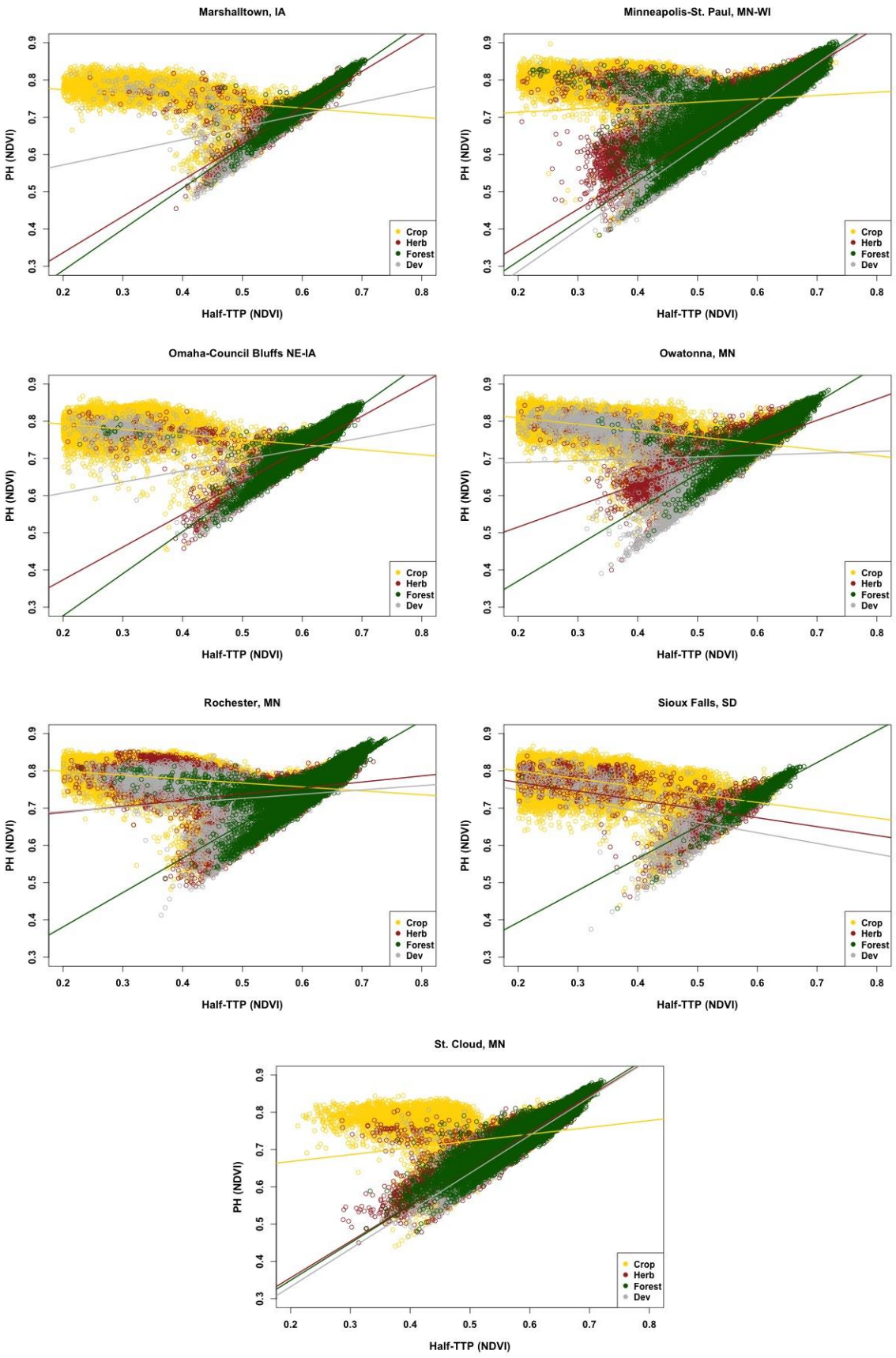
Marshalltown, IA
Minneapolis-St. Paul, MN-WI
Omaha-Council Bluffs NE-IA
Owatonna, MN
Rochester, MN
Sioux Falls, SD
St. Cloud, MN
PH (NDVI)
Half-TTP (NDVI)
Crop
Herb
Forest
Dev